

---

Electronic Thesis and Dissertation Repository

---

10-19-2023 2:00 PM

## Acetylation regulates Thioredoxin Reductase activity and oligomerization

DAVID E. WRIGHT,

Supervisor: Patrick O'Donoghue, *The University of Western Ontario*

A thesis submitted in partial fulfillment of the requirements for the Doctor of Philosophy degree in Biochemistry

© DAVID E. WRIGHT 2023

Follow this and additional works at: <https://ir.lib.uwo.ca/etd>



Part of the [Biochemistry Commons](#)

---

### Recommended Citation

WRIGHT, DAVID E., "Acetylation regulates Thioredoxin Reductase activity and oligomerization" (2023). *Electronic Thesis and Dissertation Repository*. 9721. <https://ir.lib.uwo.ca/etd/9721>

This Dissertation/Thesis is brought to you for free and open access by Scholarship@Western. It has been accepted for inclusion in Electronic Thesis and Dissertation Repository by an authorized administrator of Scholarship@Western. For more information, please contact [wlsadmin@uwo.ca](mailto:wlsadmin@uwo.ca).

## Abstract

The thioredoxin (Trx) system provides the cell with robust defense against oxidative stress and regulates the function of most cellular process through the reduction-oxidation (redox) regulation of proteins. The Trx system is involved in the development of many diseases ranging from cancer to cardiovascular disorders. Thioredoxin reductase (TrxR) is the key enzyme in the Trx system and contains the 21<sup>st</sup> genetically encoded amino acid, selenocysteine (Sec). There were multiple experimentally identified TrxR acetylation sites with an unknown effect on TrxR activity. My thesis tested the hypothesis that programmed protein acetylation will enhance the activity of TrxR1. I used genetic code expansion (GCE) to produce Sec-containing and site-specifically acetylated TrxR variants to biochemically characterize their effect TrxR1 activity.

First, I review GCE and the function of the Trx system and relevance to disease. I combined two GCE systems to produce pure Sec-containing, site-specifically acetylated human TrxR variants from *Escherichia coli* and demonstrate that acetylation increases TrxR activity by reducing the formation of low activity TrxR oligomers. In oxidizing conditions, the TrxR population shifted towards low activity TrxR oligomers resulting from covalent linkages between non-productive TrxR subunits. I demonstrated that site-specific acetylation protects TrxR from oxidative inactivation by reducing the formation of low activity TrxR oligomers and drastically reducing oxidation productions that covalently linked TrxR subunits. I also demonstrate TrxR can be non-enzymatically acetylated by aspirin, which does not stimulate TrxR activity but does protect TrxR from oxidation. I produced and purified Sec-containing TrxR fused to a cell penetrating peptide (CPP). I showed the CPP-linked TrxR was efficiently delivered to mammalian cells. A fluorescent TrxR-specific activity reporter demonstrated cytosolic activity from the CPP-tagged TrxR1. The approach provides a novel route to use GCE in bacteria, and study site-specifically modified human proteins in the homologous context of mammalian cells.

## **Keywords**

Genetic Code Expansion (GCE), thioredoxin reductase (TrxR), Selenocysteine (Sec), thioredoxin (Trx), acetylation, non-canonical amino acids (ncAAs), redox, reactive oxygen species (ROS), oxidation, oxidative stress

## Summary for Lay Audience

Many people have heard of the beneficial effects of antioxidants for health. Antioxidants protect your cells against highly reactive molecules called reactive oxygen species (ROS). ROS can be bad for your health because they ‘steal’ electrons from proteins and deoxyribonucleic acid (DNA) in your cells, causing damage to these important molecules. ROS are generated as your cells produce energy, and can also be generated by other factors, such as exposure to sunlight. Damage caused by ROS can contribute to various diseases such as cancer and heart disease. Antioxidants prevent this damage by providing electrons to ROS before they have a chance to ‘steal’ electrons from your DNA and proteins and provide electrons to molecules in your body that have been damaged by losing an electron to ROS to repair the damage caused by ROS.

Most people think antioxidants come from healthy foods such as fruits and vegetables, but your cells also produce antioxidants of their own. Our cells have a network of proteins that defend the cell against ROS and repairs damage caused by ROS. One of these naturally occurring antioxidant systems in your cells is the thioredoxin (Trx) system, which is largely dependent on a protein called thioredoxin reductase (TrxR). The Trx system transfers electrons to ROS to prevent damage to your cells, and also transfers electrons to proteins and DNA molecules damaged by ROS to repair them.

When TrxR and the Trx system are not functioning properly, damage from ROS can accumulate, leading to the development of many diseases. TrxR and the Trx system are regulated by complex cellular processes to fine-tune the Trx system to defend against ROS. My thesis focuses on understanding how protein modifications regulate TrxR to control its activity and ability to defend itself and the cell against ROS. My thesis developed a new method to produce the TrxR protein in differentially active forms, and I efficiently delivered the TrxR protein to human cells to study the enzyme in its native environment.

## Co-authorship Statement

**Chapter 1:** A portion of this chapter is being prepared for submission to a journal as a review manuscript. Additionally, this chapter contains a single figure (Figure 1.3) from the pre-print version of the published manuscript:

Wright, D.E. and P. O'Donoghue, *The Molecular Architecture of Unnatural Amino Acid Translation Systems*. Structure, 2019. **27**(8): p. 1192-1194.

P. O'Donoghue produced Figure 1.3. All other figures in this chapter were produced by D.E. Wright. D.E. Wright wrote this chapter, with edits by P. O'Donoghue.

**Chapter 2:** This chapter contains the pre-print version of published manuscript:

Wright, D.E., Altaany Z., Bi Y., Alperstein Z., and O'Donoghue P., *Acetylation Regulates Thioredoxin Reductase Oligomerization and Activity*. Antioxid Redox Signal, 2018. **29**(4): p. 377-388.

Y. Bi and Z. Altaany cloned plasmids. Z. Altaany conducted experiments for data in Table S2.1 (ICP-MS) and Figure S2.2 (GFP readthrough reporter). Z. Altaany performed experiments for Figure 2.4 (circular dichroism spectra) with protein produced and purified by Z. Altaany. D.E. Wright produced and purified protein for, and conducted, all other experiments. Y. Bi assisted D.E. Wright with protein production and purification, and with the experiment conducted for Figure 2.5 (deacetylation of TrxR1 variants by HDAC3). P. O'Donoghue and D.E. Wright designed experiments and co-wrote the manuscript.

**Chapter 3:** This chapter contains the pre-print version of published manuscript:

Wright, D.E., N. Panaseiko, and P. O'Donoghue, *Acetylated Thioredoxin Reductase 1 Resists Oxidative Inactivation*. *Front Chem*, 2021. **9**: p. 747236.

D.E. Wright completed all experiments, with the assistance of N. Panaseiko for protein production and purification, and for aspirin incubations (Figure 3.6A, B). D.E. Wright and P. O'Donoghue designed experiments and co-wrote the manuscript.

**Chapter 4:** This chapter contains the pre-print version of published manuscript:

Wright, D.E., Siddika, T., Heinemann, I. U., and O'Donoghue, P. *Delivery of the selenoprotein thioredoxin reductase 1 to mammalian cells*. *Front Mol Biosci*, 2022. **9**: p. 1031756.

D.E. Wright and P. O'Donoghue designed experiments, D.E. Wright and T. Sidiki conducted experiments, and T. Sidiki, I. Heinnemann, and P. O'Donoghue wrote and edited the manuscript.. D.E. Wright cloned plasmids, produced and purified proteins (Figure 4.2A), conducted *in vitro* activity assays (Figure 4.2B, C) and conducted experiments with the TrxRFP1 reporter (Figure 4.3B, 4.5A). T. Sidiki conducted western blot experiments (Figure 4.4) and analyzed data from the TrxRFP1 reporter (Figure 4.5B).

## Acknowledgements

First and foremost, I would like to express my sincere gratitude and thanks to my supervisor Dr. Patrick O'Donoghue for his constant support, kindness, and guidance throughout my graduate studies. You've taught me a lot and I will fondly remember my time in your lab. I would also like to express my sincere gratitude and appreciation for your patience and support during my rather long leave of absence due to medical issues near the ending of my time in your lab.

I would like to thank Yumin Bi for teaching me so many laboratory techniques, and for the constant help throughout her time as a laboratory technician during my graduate studies. She taught me a large portion of the laboratory techniques I used throughout my time as a graduate student, and I am sincerely thankful for that. Another big thank you to Tarana Sidiki for helping me with cell culture work near the ending of my graduate studies.

I would also like to thank Ilka Heinemann, and the past and present members of the O'Donoghue and Heinemann labs that worked alongside me. Specifically, I would like to thank Nileeka Balasuriya, Jeremy Lant, Peter Rozik, Susanna George, Tarana Sidiki, Christina Chung, McShane McKenna, Mallory Frederick, and many more for their friendship and for making my time as a graduate student entertaining and memorable.

## Table of Contents

Abstract .....	ii
Keywords .....	iii
Summary for Lay Audience.....	iv
Co-Authorship Statement.....	v
Acknowledgements.....	vii
Table of Contents.....	viii
List of Figures.....	xiv
List of Tables .....	xvi
List of Abbreviations .....	xvii
Chapter 1 .....	1
1. Natural and Synthetic Genetic Code Expansion.....	1
1.1. Discovery and Evolution of the Genetic Code.....	1
1.1.1. Discovery of the Genetic Code.....	1
1.1.2. Exceptions to the Standard Genetic Code: Selenocysteine .....	3
1.1.3. Exceptions to the Standard Genetic Code: Pyrrolysine.....	5
1.2. Genetic Code Expansion to Produce Recombinant Proteins with non-Canonical Amino Acids .....	6
1.2.1. Archaeal PylRS/tRNA <sup>Pyl</sup> Pairs for Genetic Code Expansion .....	7
1.2.2. <i>Methanocaldococcus jannaschii</i> TyrRS/tRNA <sup>Tyr</sup> Pair for Genetic Code Expansion .....	8
1.2.3. Other Orthogonal aaRS/tRNA Pairs Adapted for ncAA Insertion .....	8
1.3. Genetic Code Expansion Applications.....	9
1.3.1. Translational Control of Gene Expression .....	9



1.3.2. Determining Protein-Protein Interactions .....	10
1.3.3. Controlling Protein Function with Caged ncAAs .....	11
1.3.4. Other Applications of Genetic Code Expansion .....	11
1.4. Genetic Code Expansion to Program Post-Translational Modifications .....	12
1.4.1. <i>N</i> <sub>ε</sub> -acetyl-Lysine (acK) Insertion via Genetic Code Expansion .....	13
1.4.2. Phosphorylated Amino Acid Insertion via Genetic Code Expansion .....	14
1.5. Limitations of Genetic Code Expansion .....	15
1.5.1. Mutual Orthogonality of aaRS/tRNA Pairs.....	15
1.5.2. Codon Availability .....	16
1.5.3. Sense Codon Reassignment Limitations .....	17
1.6. Genetic Code Expansion with Selenocysteine .....	18
1.7. The Mammalian Thioredoxin System Function and Role in Disease.....	20
1.7.1. Thioredoxin Reductase, a Critical Selenoprotein in Redox Biology .....	20
1.7.2. The Mammalian Thioredoxin System.....	21
1.7.3. The Thioredoxin System and Disease .....	23
1.7.4. TrxR and Post-Translational Modifications .....	23
1.8. Thesis Project, Goals, and Hypothesis .....	24
1.9. References .....	25
Chapter 2.....	39
2. Acetylation Regulates Thioredoxin Reductase Oligomerization and Activity.....	39
2.1. Introduction .....	39
2.2. Results .....	40
2.2.1. <i>E. coli</i> Host Strain Alters Expression of TrxR1 with 22 Amino Acids.....	40

2.2.2. Physical Characterization of TrxR1 Variants.....	42
2.2.3. Reversible Activation of TrxR1 .....	44
2.2.4. Acetylation Alters TrxR1 Quaternary Structure.....	47
2.3 Discussion .....	50
2.3.1. Acetylation Controls TrxR1 Structure and Activity.....	50
2.3.2. Relevance to Human Disease .....	51
2.3.3. Impacts of Enhanced TrxR Activity on Cellular Signaling.....	52
2.3.4. Codon Recoding and Codon Reassignment Mechanisms are Mutually Orthogonal.....	52
2.3.5. Innovation.....	54
2.4 Methods and Materials .....	54
2.4.1. Bacterial Strains and Plasmids .....	54
2.4.2. TrxR1 Production and Purification .....	56
2.5.3. <i>In vitro</i> TrxR1 Activity Assay: DTNB.....	57
2.5.4. <i>In vitro</i> TrxR1 Activity Assay: 9,10-phenanthrene Quinone .....	57
2.5.5. Histone Deacetylase 3 (HDAC3) Assays .....	58
2.5.6. Insulin Linked TrxR1 Activity Assays.....	58
2.5.7. Statistical Analysis .....	59
2.5.8. Mass Spectrometry .....	59
2.5.9. Western Blot analysis of TrxR1 Expression .....	60
2.5.10. Size Exclusion Chromatography .....	60
2.5. Acknowledgements .....	61

2.6. References .....	62
2.7. Chapter 2 Appendix – Supplementary Tables and Figures .....	66
2.7.1. Supplementary Tables .....	66
2.7.2. Supplementary Figures .....	67
Chapter 3 .....	72
3. Acetylated Thioredoxin Reductase 1 Resists Oxidative Inactivation .....	72
3.1. Introduction .....	72
3.2. Materials and Methods .....	75
3.2.1. Plasmids and Strains .....	75
3.2.2. TrxR1 and acTrxR1 Protein Purification .....	76
3.2.3. TrxR1 Activity Assays .....	76
3.2.4. Peroxide and Aspirin Incubations .....	77
3.2.5. Western Blotting .....	77
3.2.5. Mass Spectrometry .....	78
3.2.6. Statistical Analysis .....	79
3.3. Results .....	79
3.3.1. Purification of acK and Selenocysteine-Containing TrxR1 Variants .....	79
3.3.2. Resistance of Site-Specifically Acetylated TrxR1 to Oxidative Damage .....	80
3.3.3. Aspirin Acetylates TrxR1 and Provides Robust Resistance to Oxidative Damage .....	84
3.3.4. Location of TrxR1 Acetylation Sites Following Aspirin Treatment .....	87
3.4. Discussion .....	87
3.4.1. Interplay Between Acetylation and Oxidation in the Trx System .....	87

3.4.2. Non-Specific Acetylation of Proteins in the Context of Oxidative Stress .....	90
3.4.3. Relevance of Trx System Acetylation to Disease .....	91
3.5. Conclusion.....	92
3.6. Conflict of Interest .....	92
3.7. Author Contributions.....	93
3.8. Funding.....	93
3.9. Acknowledgements .....	93
3.10. References .....	94
3.11. Chapter 3 Appendix – Supplemental Tables and Figures .....	97
3.11.1. Supplementary Tables .....	97
3.11.2. Supplementary Figures .....	98
Chapter 4.....	102
4. Delivery of the Selenoprotein Thioredoxin Reductase 1 to Mammalian Cells .....	102
4.1. Introduction .....	102
4.2. Materials and Methods .....	105
4.2.1. Plasmids and Molecular Cloning .....	105
4.2.2. TrxR1 Protein Purification .....	106
4.2.3. TrxR1 <i>in vitro</i> Activity Assays.....	106
4.2.4. Endogenous TrxR1 Activity in Live Cells and Fluorescence Microscopy ....	107
4.2.5. TAT-TrxR1 Delivery and Activity in Live Cells .....	108
4.2.6. Western Blotting.....	108
4.3. Results .....	110
4.3.1. Purification and Activity of TrxR1 and TAT-TrxR1 Variants.....	110

4.3.2. Assessing the TrxRFP1 Reporter in Mammalian Cells.....	111
4.3.3. Delivery of TAT-TrxR1 to Mammalian Cells.....	113
4.3.4. TAT-tagged Dependent Uptake and Activity of TAT-TrxR1 in Live Cells..	114
4.4. Discussion .....	117
4.4.1. Genetic Code Expansion and Codon Reassignment .....	117
4.4.2. Delivery of ncAA-Containing Proteins with Cell Penetrating Peptides .....	119
4.4.3. A New System to Study TrxR1-Dependent Activity in Mammalian Cells....	120
4.5. Conclusion.....	121
4.6. Conflict of Interest .....	122
4.7. Author Contributions.....	122
4.8. Funding.....	122
4.9. Acknowledgements .....	122
4.10. References .....	123
4.11. Chapter 4 Appendix – Supplementary Data.....	127
4.11.1. DNA and Protein Sequences for TrxR1 Constructs .....	127
4.11.2. Appendix References.....	131
Curriculum Vitae .....	132

## List of Figures

Figure 1.1. Schematic of protein production by mRNA translation at the ribosome .....	2
Figure 1.2. Schemata of naturally occurring Sec insertion systems .....	4
Figure 1.3. Expanding the genetic code using pyrrolysyl-tRNA synthetase .....	6
Figure 1.4. Electron flow through the thioredoxin system .....	22
Figure 2.1. Schematic for genetically encoding 22 amino acids .....	41
Figure 2.2. Physical identification of acK and Sec in acTrxR1 <sup>K200</sup> .....	44
Figure 2.3. Activity of TrxR1 and acTrxR1 variants.....	45
Figure 2.4. Circular dichroism (CD) spectra of TrxR1 variants .....	46
Figure 2.5. Effect of histone deacetylase on TrxR1 variants .....	47
Figure 2.6. Mechanistic basis for acetylation-dependent enhanced TrxR1 activity .....	48
Figure 2.7. Characterization of WT TrxR1 and acTrxR1 oligomerization.....	49
Figure S2.1. Purified WT and acTrxR1 variants .....	67
Figure S2.2. GFP reporter detecting UAG read-through.....	67
Figure S2.3. MALDI MS analysis confirms acetylation of acTrxR1 variants .....	68
Figure S2.4. Confirmation of Sec incorporation in WT TrxR1 by MALDI MS analysis of the tryptic digested protein.....	69
Figure S2.5. LC-MS/MS confirming Sec incorporation for WT TrxR1, acTrxR1 <sup>K141</sup> , and acTrxR1 <sup>K307</sup> variants.....	70
Figure S2.6. LC-MS/MS confirming genetically encoded acK incorporation into acTrxR1 <sup>K141</sup> and acTrxR1 <sup>K307</sup> .....	71
Figure 3.1. TrxR1 activity is regulated by oxidation and acetylation.....	73
Figure 3.2. Genetic code expansion to incorporate acK and Sec in TrxR1 .....	75
Figure 3.3. Activity of un-modified TrxR1 and acTrxR1 variants with increasing peroxide levels .....	81

Figure 3.4. Initial velocity of un-modified and specifically acetylated TrxR1 variants with increasing oxidative damage.....	82
Figure 3.5. Aspirin acetylates TrxR1 .....	85
Figure 3.6. TrxR1 activity following aspirin incubation .....	86
Figure 3.7. Mapping acetylation sites in TrxR1 to the quaternary structure .....	88
Figure S3.1. Purified TrxR1 and site-specifically acetylated TrxR1 variants .....	98
Figure S3.2. Oxidation of TrxR1 and site-specifically acetylated TrxR1 variants.....	99
Figure S3.3. Quantification of TrxR1 western blot .....	100
Figure S3.4. MS/MS spectra of representative TrxR1 peptides showing lysine acetylation following aspirin incubation .....	101
Figure 4.1. Production of recombinant selenocysteine containing TrxR1 in <i>E. coli</i> and delivery to mammalian cells .....	104
Figure 4.2. Purity and biochemical activity of TrxR1 and TAT-TrxR1 variants .....	112
Figure 4.3. Measurement of endogenous TrxR1 activity in live cells .....	113
Figure 4.4. Immunoblotting confirms delivery of TAT-TrxR1 to cells .....	115
Figure 4.5. TAT-dependent delivery of active TrxR1 to mammalian cells.....	116

## List of Tables

Table 2.1. TrxR1 and acTrxR1 protein yields and activity.....	43
Table S2.1. ICP-MS selenium (Se) content determination for TrxR1 preparations.....	66
Table S2.2. Percentage of total TrxR1 existing in high activity dimers, or low activity tetramers or monomers .....	66
Table S3.1. MS/MS identified peptides showing lysine acetylation sites in TrxR1 .....	97



## List of Abbreviations

AA	amino acid
aaRS	aminoacyl-tRNA synthetase
AcCoA	acetyl-Coenzyme A
acK	N <sub>ε</sub> -acetyl-Lysine
acK	N <sub>ε</sub> -acetyl-Lysine
acKRS	N <sub>ε</sub> -acetyl-lysyl-tRNA synthetase
acTrxR1	acetylated thioredoxin reductase 1
Akt1	protein kinase B
ANOVA	pairwise single factor analysis of variance
aSelB	archaeal SelB
ASK1	apoptosis signal-regulating kinase
Asp	aspartate
ATG	aurothioglucose
ATP	adenosine triphosphate
CPP	cell penetrating peptide
Cys	cysteine
DHFR	dihydrofolate reductase
DMEM	Dulbecco's modified eagle medium
DNA	deoxyribonucleic acid
DTNB	5,5'-dithiobis-(2-nitrobenzoic acid)
DTT	dithiothreitol
EDTA	ethylenediaminetetraacetic acid
EFSec	elongation factor Sec
EFSep	mutant elongation factor for phosphoserine insertion
EF-Tu	elongation factor thermal unstable

EGTA	ethylene glycol-bis( $\beta$ -aminoethyl ether)-N,N,N',N'-tetraacetic acid
FAD	flavin adenine dinucleotide
FBP	FK506 binding protein
FPLC	fast protein liquid chromatography
FRB	FKBP-rapamycin binding domain of mammalian target of RAP
GAPDH	glyceraldehyde 3-phosphate
GCE	genetic code expansion
GFP	green fluorescent protein
H <sub>2</sub> O <sub>2</sub>	hydrogen peroxide
HDAC3	histone deacetylase 3
Hek293	Human embryonic kidney 293
HeLa	Henrietta Lacks
His	histidine
HIV	human immunodeficiency virus
ICP-MS	inductively coupled plasma mass spectrometry
IPTG	isopropyl $\beta$ -D-1-thiogalactopyranoside
LB	lysogeny broth
LCK	lymphocyte-specific protein kinase
LC-MS/MS	liquid chromatography and tandem mass spectrometry
Lys	lysine
LysRS	lysyl-tRNA synthetase
MALDI MS	matrix-assisted laser desorption/ionization mass spectrometry
MCF-7	Michigan cancer foundation-7
MEK	mitogen-activated protein kinase kinase
mRNA	messenger ribonucleic acid

MS	mass spectrometry
MsrB1	methionine sulfoxide Reductase B1
NADPH	nicotinamide adenine dinucleotide phosphate
ncAA	non-canonical amino acids
Ni-NTA	nickel nitrilotriacetic acid
NLS	nuclear Localization sequence
o-aaRS	orthogonal aminoacyl-tRNA synthetase
ORF	open reading frame
OTS	orthogonal translation system
PBS	phosphate buffered saline
PCR	polymerase chain reaction
PMSF	phenylmethylsulfonyl fluoride
Prx	peroxiredoxin
pSe	selenophosphate
pSer	O-phosphoserine
PSTK	O-phosphoseryl-tRNA <sup>Sec</sup> kinase
pThr	O-phosphothreonine
PTM	post-translational modification
pTyr	O-phosphotyrosine
PVDF	polyvinylidene difluoride
Pyl	pyrrolysine
PYL	PYR1-like domain
PylRS	pyrrolysyl-tRNA synthetase
Pyr	pyrabactin resistance
redox	reduction-oxidation
RF1	release factor 1

RFP	red fluorescent protein
RITA	reactivating p53 and Inducing Tumour Apoptosis
RNA	ribonucleic acid
ROS	reactive oxygen species
SBP2	selenocysteine insertion sequence binding protein 2
SDS	sodium dodecyl sulfate
SDS-PAGE	sodium dodecyl sulfate polyacrylamide gel electrophoresis
Se	selenium
Sec	selenocysteine
SecIS	selenocysteine insertion sequence
SecTRAPs	selenium compromised thioredoxin reductase-derived apoptotic proteins
Sec-tRNA <sup>Sec</sup>	selenocysteinyl-tRNA <sup>Sec</sup>
SelA	selenocysteine synthetase
SepRS	phosphoseryl-tRNA synthetase
SepSecS	O-phosphoseryl-tRNA:selenocysteinyl-tRNA synthetase
Ser	serine
SerRS	seryl-tRNA synthetase
sfGFP	superfolder green fluorescent protein
STAT1	signal transducer and activator of transcription
TAT	transactivator of Transcription
TAT-TrxR1	transactivator of transcription-linked thioredoxin reductase 1
THP-1	Human acute monocytic leukemia cells
TNB	thiobis-(2-nitrobenzoic acid)
tRNA	Transfer RNA
Trp	tryptophan

TrpRS	tryptophanyl-tRNA synthetase
Trx	thioredoxin
Trx1 <sup>Ox</sup>	oxidized thioredoxin 1
Trx1 <sup>Red</sup>	reduced thioredoxin 1
TrxR	thioredoxin reductase
TrxRFP1	thioredoxin 1 fused to red fluorescent protein
Tyr	tyrosine
TyrRS	tyrosyl-tRNA synthetase
U	selenocysteine
UTR	untranslated region
WT	wild type
$\alpha$ -acK	anti-acetyl-lysine antibody

# Chapter 1

## 1. Natural and Synthetic Genetic Code Expansion

### 1.1. Discovery and Evolution of the Genetic Code

#### 1.1.1. Discovery of the Genetic Code.

Following the discovery of the structure of deoxyribonucleic acid (DNA), Francis Crick proposed the central dogma of molecular biology that describes that the genetic information in cells can flow from DNA and RNA to proteins but not vice versa [1]. Crick's sequence hypothesis envisioned that the sequence of nucleic acids corresponds to the amino acid (AA) sequence of proteins and is used as a template for amino acid insertion during protein synthesis [1]. Indeed, in all cells, the DNA of a protein coding gene is converted into ribonucleic acid (RNA) known as messenger RNA (mRNA) through a process called transcription, and used by the ribosome as a template to direct AA insertion during protein synthesis [2]. The ribosome is a large ribonucleoprotein particle made up of one large and one small subunit that facilitates protein synthesis by creating peptide bonds between each AA to produce a polypeptide chain using the mRNA sequence as a template to direct AA insertion [3], according to the genetic code (Fig 1.1), which was deciphered by the Nirenberg [4] and Khorana [5] labs in 1965.

The genetic code consists of 64 nucleotide triplets, called codons, 61 of which correspond to one of the 20 naturally occurring AAs and 3 of which (UAG, UGA, and UAA) are termination signals, marking the end of the protein sequence [6] (Fig 1.1). Adapter molecules called transfer RNAs (tRNAs) bring AAs to the ribosome and determine the AA sequence of the polypeptide chain by binding to a specific codon or set of codons in the mRNA with a complementary tRNA anticodon [7] (Fig 1.1C). Aminoacyl-tRNA synthetases (aaRSs) catalyze the ligation of AAs to tRNAs through an adenosine triphosphate (ATP) dependent reaction, producing aminoacyl-tRNA substrates for the ribosome [8] (Fig 1.1A, B). Accurate translation of the genetic code requires that tRNAs

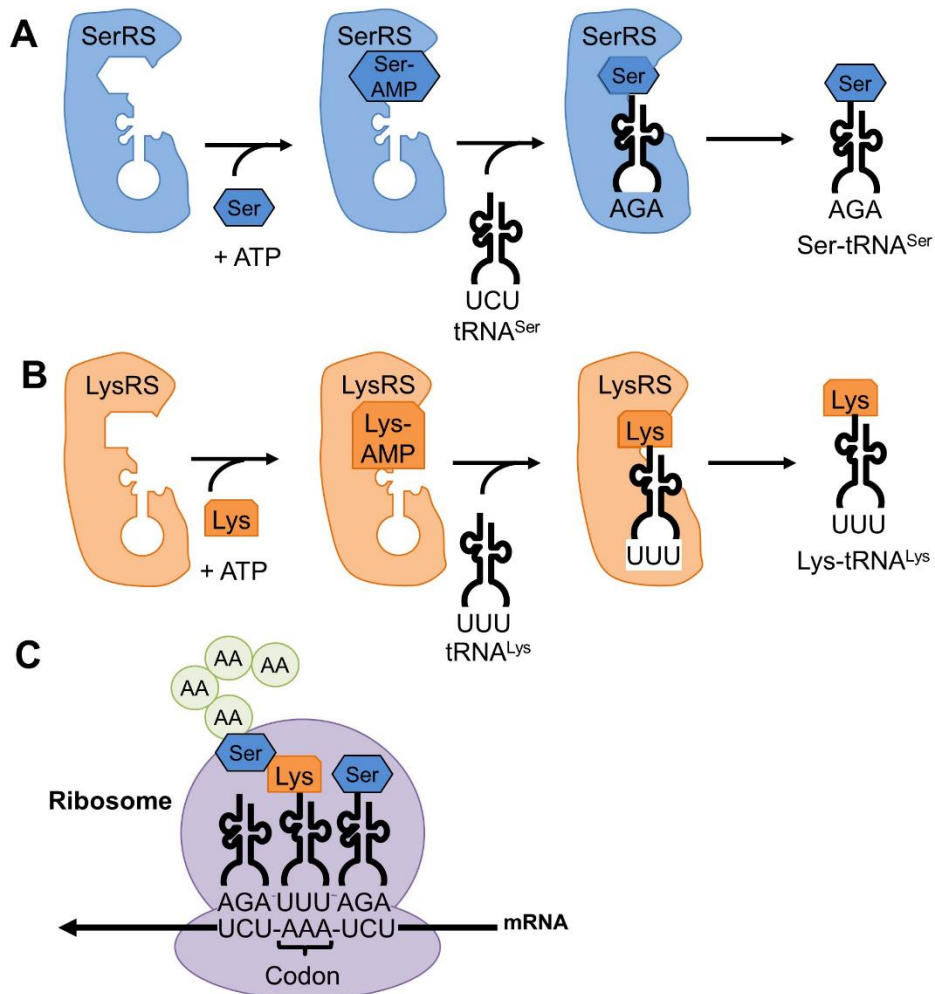


**Figure 1.1. Schematic of protein production by mRNA translation at the ribosome.**

The mRNA is translated to proteins at the ribosome, which catalyzes the formation of peptide bonds between AAs. AAs are brought to the ribosome by charged tRNAs and the AA sequence is determined by the tRNA anticodon binding to complementary codons on the mRNA. tRNAs are charged with AAs by aaRSs, which are specific for a certain AA and the tRNAs responsible for decoding codons corresponding to that AA, ensuring faithful translation of the genetic code. This is depicted with the AAs serine (Ser) (A) and lysine (Lys) (B). Ser is loaded onto tRNA<sup>Ser</sup> by seryl-tRNA synthetase (SerRS) (A), while Lys is loaded onto tRNA<sup>Lys</sup> by lysyl-tRNA synthetase (LysRS) (B). SerRS specifically recognizes Ser and tRNA<sup>Ser</sup> and does not recognize other AAs or tRNAs (for example, SerRS does not recognize Lys or tRNA<sup>Lys</sup>) and vice versa for LysRS – LysRS specifically recognizes Lys and tRNA<sup>Lys</sup>, but not other AAs or tRNAs. (C) Once charged, tRNAs enter the ribosome and bind the mRNA codon, and their AA is incorporated into the growing polypeptide chain by the ribosome. The uncharged tRNA is then released from the ribosome, is charged again by its corresponding aaRS, and the cycle repeats.

are aminoacylated by a specific aaRS with the correct AA corresponding to the codon complementary to the tRNA anticodon [8] (Fig 1.1). Identity elements in tRNAs are nucleotides that recognized by the cognate aaRSs and ensure the correct AA is added to tRNAs that decode codons associated with that specific AA, ensuring faithful translation of the genetic code [9].

### **1.1.2. Exceptions to the Standard Genetic Code: Selenocysteine.**

The genetic code was originally thought to be universal in all species. Overtime, diverse exceptions to the universal genetic code emerged [10]. While there are examples of codons taking on different meanings (codon reassignment), it was thought that only 20 different kinds of AAs were incorporated into proteins in cells. In the late 1980s, some UGA termination codons were found to site-specifically direct the co-translational incorporation of the 21<sup>st</sup> AA, selenocysteine (Sec), into proteins in some species representing all three domains of life [11-13].

Two distinct naturally occurring mechanisms in bacteria relative to archaea and eukaryotes to site-specifically change the meaning of UGA from translational termination to Sec insertion have been discovered [13-15]. In all Sec-decoding organisms, Sec is synthesized from serine (Ser) on its tRNA ( $\text{tRNA}^{\text{Sec}}$ );  $\text{tRNA}^{\text{Sec}}$  is first aminoacylated by an endogenous seryl-tRNA synthetase (SerRS) to give Ser- $\text{tRNA}^{\text{Sec}}$  [16, 17] (Fig 1.2).

In bacteria, selenocysteine synthase (SelA) converts Ser- $\text{tRNA}^{\text{Sec}}$  to Selenocysteinyl- $\text{tRNA}^{\text{Sec}}$  (Sec- $\text{tRNA}^{\text{Sec}}$ ) [18], while in eukaryotes and archaea the Ser- $\text{tRNA}^{\text{Sec}}$  is first phosphorylated by *O*-phosphoseryl- $\text{tRNA}^{\text{Sec}}$  kinase (PSTK) [19, 20], followed by conversion of phosphoseryl- $\text{tRNA}^{\text{Sec}}$  to Sec- $\text{tRNA}^{\text{Sec}}$  by *O*-Phosphoseryl-tRNA:selenocysteinyl-tRNA synthase (SepSecS) [21-23] (Fig 1.2). An RNA hairpin structure, the Selenocysteine Insertion Sequence (SecIS) occurs downstream of the Sec-encoding UGA codon (directly downstream of UGA in the open reading frame (ORF) in bacteria, and in the 3' untranslated region (UTR) in eukaryotes and archaea) [24] (Fig 1.2).



Specialized elongation factors (SelB in bacteria [25], elongation factor Sec (EFSec) in eukaryotes [26], or archaeal SelB (aSelB) in archaea [27]) bind Sec-tRNA<sup>Sec</sup> and bring it to the ribosome. In bacteria, SelB directly binds both Sec-tRNA<sup>Sec</sup> and SecIS to position Sec-tRNA<sup>Sec</sup> at UGA [25] (Fig 1.2). In eukaryotes, an additional protein, SecIS binding protein 2 (SBP2), binds SecIS [28] and then binds EFSec bound to Sec-tRNA<sup>Sec</sup> to localize

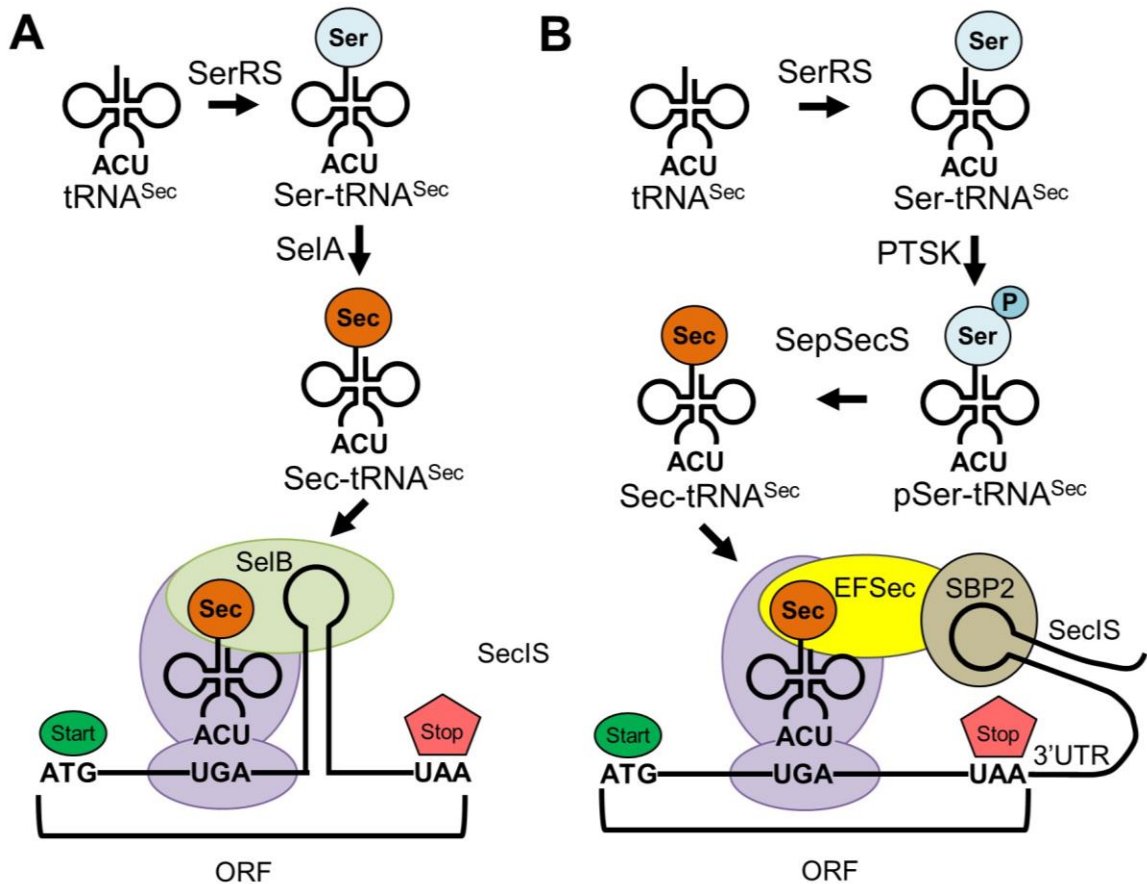


**Figure 1.2. Schemata of naturally occurring Sec insertion systems.** tRNA<sup>Sec</sup> is aminoacylated with Ser by SerRS. In bacteria, Sela converts Ser to Sec on tRNA<sup>Sec</sup> (A), while in eukaryotes, Ser on tRNA<sup>Sec</sup> is phosphorylated by PTSK, followed by conversion to Sec by SepSecS (B). Sec-tRNA is localized at the UGA codon by specialized elongation factors that bind an RNA hairpin loop, SecIS, that occurs following the UGA codon. SecIS is present directly downstream of UGA in the ORF in bacteria (A), while in eukaryotes, SecIS is present in the 3'UTR (B). In bacteria, SelB binds Sec-tRNA<sup>Sec</sup> and localizes it at the UGA codon by binding SecIS (A). In eukaryotes, SBP2 binds SecIS, then binds a specialized elongation factor, EFSec, which binds Sec-tRNA<sup>Sec</sup> to localize Sec-tRNA<sup>Sec</sup> at the UGA codon.

Sec-tRNA<sup>Sec</sup> to the UGA codon [26] (Fig 1.2). In archaea, Sec insertion is similar to eukaryotes; aSelB binds tRNA<sup>Sec</sup> [27] and positions it at the UGA codon by interacting with a currently unidentified SecIS binding protein [29].

### 1.1.3. Exceptions to the Standard Genetic Code: Pyrrolysine.

More recently, in the early 2000s, the UAG termination codon was found to be decoded as an unusual lysine derivative, Pyrrolysine (Pyl), in the methanogenic archaeon *Methanosarcina barkeri* [30] (Fig 1.3). Pyl was found in the active site of 3 archaeal methyltransferases [31] in several species of the *Methanosarcinaceae* family and the Pyl residue is crucial for utilizing methylamines as a carbon source [32]. Pyl is incorporated into proteins by reassignment of the UAG codon. This natural expansion of the genetic code requires the pyrrolysyl-tRNA synthetase (PylRS) and cognate tRNA<sup>Pyl</sup> that includes a 5'-CUA-3' anticodon to decode 5'-UAG-3' codon, where tRNA<sup>Pyl</sup> is aminoacylated with free Pyl through an ATP dependent reaction [33, 34] (Fig 1.3). Pyl-decoding organisms also biosynthesize Pyl from lysine with the activity of three genes, PylB, PylC, and PylD [35]. Since its discovery in *M. barkeri* [30], several other species were found to decode UAG as Pyl [36], including in other members of the archaeal *Methanosarcinaceae* family such as *Methanosarcina mazei* [37], *Methanogenium frigidum* [38], *Methanococcoides burtonii* [38], *Methanosarcina acetivorans* [39], *Methanomassiliicoccus luminyensis* [40], *Candidatus methanomethylophilus alvus* [40], and *Candidatus methanomassiliicoccus intestinalis* [40] and in several methanogenic bacterial species such as *Desulfitobacterium hafniense* [34], *Acetohalobium arabaticum* [41] and *D. dehalogenans* [41]. So far, over 150 species show evidence of Pyl-decoding, including diverse archaea and bacteria [42].

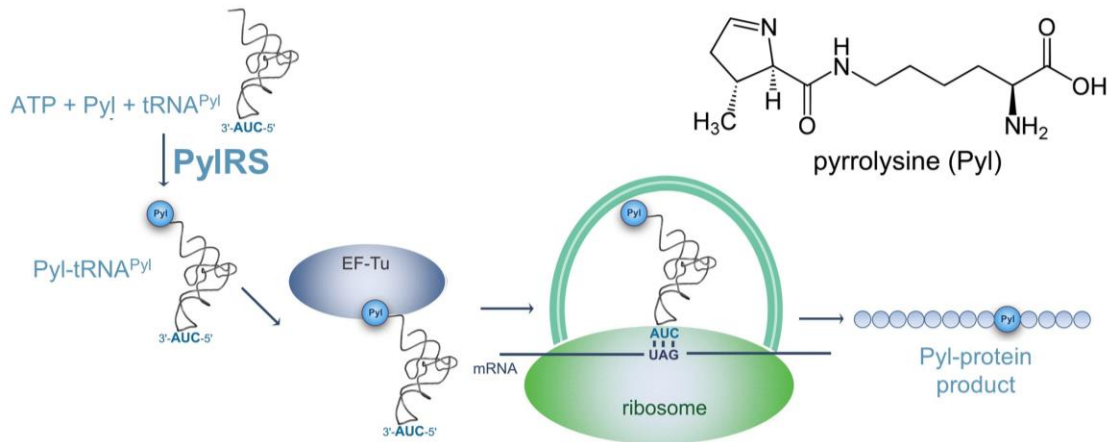


**Figure 1.3. Expanding the genetic code using pyrrolysyl-tRNA synthetase.** (A) Genetic code expansion schematic showing how the PylRS and tRNA<sup>Pyl</sup> pair reassign UAG stop codons to Pyl. Pyl is biosynthesized by the action of the *pylBCD* genes (not shown), and in an ATP-dependent reaction free Pyl is ligated to tRNA<sup>Pyl</sup> by the catalytic action of PylRS. The resulting Pyl-tRNA<sup>Pyl</sup> product is a substrate for elongation factor Tu (EF-Tu). The resulting complex enables decoding of UAG codons as Pyl on the ribosome to produce Pyl-containing proteins.

## 1.2. Genetic Code Expansion to Produce Recombinant Proteins with non-Canonical Amino Acids

Discovery of exceptions to genetic code in nature, such as recoding of selected UGA codons to Sec, or reassignment of UAG to Pyl, provided both the inspiration, and the molecular machinery required, for a new field of biotechnology called genetic code expansion (GCE). GCE is a technique used to produce proteins with the site-specific co-translational incorporation of an additional or non-canonical amino acid (ncAA) beyond the 20 standard AAs normally used in protein synthesis. Today, a wide variety of ncAAs with diverse functions can be installed by GCE, permitting many applications. GCE enables the inclusion of unique functional groups into proteins and involves a range of applications including site-directed post-translational modifications (PTMs) with *N*<sub>ε</sub>-acetyl-lysine (acK) [43], *O*-phosphoserine (pSer) [44], *O*-phosphothreonine (pThr) [45, 46] and *O*-phosphotyrosine (pTyr) [47], cross-linking ncAAs [48] allowing studies of protein-

protein interactions [49], fluorescent ncAAs [50] that enable imaging and localization studies [51], and more.

Several different GCE systems are available to produce proteins in a variety of host organisms, ranging from bacteria to human cells [52]. GCE often relies on the expression of exogenous aaRS/tRNA pairs that are already, or are engineered to be, orthogonal to the aaRSs and tRNAs in the host cell to accurately insert a desired ncAA at a reassigned codon [53]. Ideally, orthogonal aaRS (o-aaRS)/tRNA pairs do not cross react with endogenous aaRS/tRNA pairs [53]. An orthogonal tRNA will not be recognized and aminoacylated by endogenous aaRSs, and an o-aaRS must not recognize and aminoacylate endogenous tRNAs. A common strategy to identify o-aaRS/tRNA pairs is to import an aaRS/tRNA pair from a phylogenetically distant organism compared to the host expression system [53], where differences in identity elements as a result of phylogenetic distance can help prevent the o-aaRS/tRNA pair from cross-reacting with endogenous aaRS/tRNA pairs [54]. Often, further engineering is needed to improve orthogonality to further reduce, or completely prevent, cross-reactions with endogenous aaRSs and tRNAs [55].

### **1.2.1. Archaeal PylRS/tRNA<sup>Pyl</sup> Pairs for Genetic Code Expansion.**

The Pyl system discovered in the early 2000s [34] has become one of the main tools of the GCE field [53]. Most PylRS/tRNA<sup>Pyl</sup> pairs used for GCE are developed from the naturally occurring *M. barkeri* or *M. mazei* PylRS/tRNA<sup>Pyl</sup> pairs [56]. Expression of the PylRS/tRNA<sup>Pyl</sup> pair from *M. barkeri* allowed all instances of UAG to be decoded using Pyl-analogs in *Escherichia coli* [57]. Multiple PylRS/tRNA<sup>Pyl</sup> pairs from several species can decode UAG with Pyl-analogs in *E. coli*, including PylRSs from *M. mazei* [58] and *M. barkeri* [57] and *M. alvus* [59]. These naturally occurring PylRS/tRNA pairs are capable of inserting multiple Pyl-analogues in response to UAG codons in *E. coli* [60]. Several mutant

variants were quickly developed following the discovery of PylRS [37, 60-62], to vastly increase the number of ncAAs that can be inserted to over 200 [63], making the Pyl system the most versatile orthogonal translation system (OTS) known [64]. Expression of the *M. mazei* PylRS/tRNA<sup>Pyl</sup> pair and its variants in mammalian cells allows reassignment of UAG to ncAAs [65]. The PylRS/tRNA<sup>Pyl</sup> pair also functions as an orthogonal pair in mammalian cells to decode UAG codons [66].

### **1.2.2. *Methanocaldococcus jannaschii* TyrRS/tRNA<sup>Tyr</sup> Pair for Genetic Code Expansion.**

Another commonly used o-aaRS/tRNA pair in *E. coli* was developed from the tyrosyl-tRNA synthetase (TyrRS)/tRNA<sup>Tyr</sup> pair from *Methanocaldococcus jannaschii* [48, 55]. This is the most popular o-aaRS/tRNA pair after PylRS variants, and over two thirds of all ncAAs incorporated are done by wildtype or engineered PylRS/tRNA<sup>Pyl</sup> or *M. jannaschii* TyrRS/tRNA<sup>Tyr</sup> pairs [63]. Mutation of the *M. jannaschii* tRNA<sup>Tyr</sup> anticodon allowed decoding of UAG as tyrosine (Tyr) in *E. coli* [67], and further directed evolution experiments created up to 38 different *M. jannaschii* TyrRS variants each specific for a different ncAA [68]. This pair functions for ncAA incorporation in bacteria like *E. coli*, *Salmonella* [69], *Mycobacterium tuberculosis* [70], and *Streptomyces venezuelae* [71], but is not functional as an orthogonal pair in eukaryotic cells due to overlapping identity elements with the eukaryotic TyrRS/tRNA<sup>Tyr</sup> pair [63].

### **1.2.3. Other Orthogonal aaRS/tRNA Pairs Adapted for ncAA Insertion.**

Other aaRS/tRNA pairs, based on leucyl-, lysyl-, glutaminyl -, seryl-, histidyl-, prolyl-, and phenylalanyl-tRNA synthetases have been used to incorporate ncAAs into proteins in various different host species [72]. Several aaRS/tRNA pairs from

*Saccharomyces cerevisiae* are orthogonal in *E. coli* and have been adapted ncAA insertion in *E. coli* [68], such as the *S. cerevisiae* tRNA/aaRS pairs for aspartyl- [73], glutaminy- [74], phenylalanyl- [74], and tryptophanyl- [75] tRNA synthetase/tRNA pairs adapted for ncAA incorporation in *E. coli*. Several *E. coli* aaRS/tRNA pairs have also been adapted for ncAA insertion in *S. cerevisiae* or mammalian cells [72].

## **1.3. Genetic Code Expansion Applications**

### **1.3.1. Translational Control of Gene Expression.**

GCE has been used to regulate translation by controlling stop codon suppression within a target gene [76-78]. Normally, a UAG stop codon is inserted into the gene of interest at a permissive site for ncAA incorporation into the target protein. An o-aaRS/tRNA pair designed to recognize and insert ncAAs in response to UAG stop codons is co-expressed [79]. When no ncAA is present, the in-frame UAG codon stops translation of the target gene, preventing full-length protein production. An ncAA is added to induce translation of the target gene, allowing the o-aaRS/tRNA pair to decode the in-frame UAG codon, resulting in full translation of the target gene [76-78]. This technique has been used to for several applications, including biocontainment [80, 81], generating live attenuated virus vaccines [79, 82, 83], and to control expression of therapeutic proteins in mammalian cells [84].

A limitation to this technology is that o-aaRSs are often promiscuous and can mischarge the suppressor tRNA with endogenous AAs [85], leading to leaky expression of the target gene in the absence of ncAAs [81, 85]. This limitation has been alleviated using split o-aaRSs, where an o-aaRS is split into two genes, and each o-aaRS fragment is fused to chemically inducible dimerization domains which dimerize in the presence of small molecules [86]. Rapamycin or abscisic acid were used to induce dimerization between o-aaRS fragments fused to FK506 binding protein (FKBP) and FKBP-Rapamycin binding

domain of mammalian target of Rap (FRB), or to pyrabactin resistance (Pyr) and PYR1-like domains (PYL), respectively [86]. The o-aaRS remains inactive until the small molecule which induces dimerization is added, preventing aminoacylation of the suppressor tRNA with endogenous AAs in the absence of ncAA, allowing stringent control of gene expression [86].

### 1.3.2. Determining Protein-Protein interactions.

GCE can be used to elucidate protein-protein interactions (PPIs) by installing photocrosslinking ncAAs site-specifically into proteins [49, 87]. Photocrosslinker ncAAs contain side-chains that become highly reactive in response to UV light, and form covalent bonds with nearby molecules [49, 87]. Four commonly used photocrosslinker groups used are aryl azide, alkyl diazirine, trifluoromethylphenyl diazirine, and benzophenone [88], and ncAA containing these crosslinking groups include several phenylalanine derivatives [87] (P-benzoyl-L-phenylalanine [89], p-azido-L-phenylalanine [48], 4'-[3-(trifluoromethyl)-3H-diazirin-3-yl]-l-phenylalanine [90]) and lysine derivatives [87] ((3-(3-methyl-3H-diazirine-3-yl)-propaminocarbonyl-N<sup>ε</sup>-l-lysine [91], 3'-azibutyl-N-carbamoyl-lysine [92], and N<sup>ε</sup>-[[(4-(3-(trifluoromethyl)-3H-diazirin-3-yl)-benzyl)oxy]carbonyl]-l-lysine [93]). GCE-mediated insertion of these photocrosslinker ncAAs have allowed for the study of PPIs in both eukaryotic cells and in microbes. These approaches have been used to elucidate mammalian receptor-ligand [94, 95] and kinase-adaptor interactions [96, 97], as well as interactions between bacterial membrane proteins [98-100] and *E. coli* chaperone substrate interactions [91, 101, 102].

Split o-aaRS can also be used to detect PPIs with a green fluorescent protein (GFP) reporter that includes an in-frame stop codon [86]. Each fragment of the split o-aaRS is fused to suspected interacting peptides, and if an interaction occurs, the o-aaRS becomes active, charges the suppressor tRNA and by causing full-length GFP translation, allows the PPI to be quantitatively monitored by GFP fluorescence [86]. This technique has been used

to monitor the interaction between proteins that mediate infection by severe acute respiratory syndrome coronavirus 2 and anti-apoptotic proteins involved in the development of cancer [86].

### **1.3.3. Controlling Protein Function with Caged ncAAs.**

Protein function can be optically controlled by site-specifically replacing a natural AA with a photo-caged version of the same AA [103-105]. The caging group blocks protein function relying on that AA until it is exposed to light, which de-cages the AA and restores protein function [103-105]. Photo-caged versions of Tyr [106, 107], cysteine (Cys) [108-110], Ser [111], and lysine (Lys) [58, 66, 112] can be incorporated into proteins via GCE. Photo-caged Lys has been used to optically control the function of T7 RNA polymerase [113], isocitrate dehydrogenase [114], Cas9 nuclease [115], mitogen-activated protein kinase kinase (MEK) [116, 117] and lymphocyte-specific protein kinase (LCK) [118] kinases. Optical control of nuclear import has been achieved by inserting a photocaged lysine in the nuclear localization sequence (NLS) of p53 [66] and SatB1 [119], and in an NLS fused to GFP [66]. Caged Cys has been used to control the activity of potassium channels in the neurons of the brain of mouse embryos [120], *Renilla* luciferase [121], and Tobacco etch virus protease [109]. Caged Tyr was used to control the activity of T7 RNA polymerase [122], a zinc finger nuclease [123], and Cre recombinase [124], and to control the phosphorylation of signal transducer and activator of transcription (STAT1) [107, 111]. Finally, caged Ser was used to control the phosphorylation of STAT1 and the transcription factor Pho4 [111].

### **1.3.4. Other Applications of Genetic Code Expansion.**

There are several other applications of GCE [103, 125, 126], including the study of oxidative damage by genetically encoding nitrated Tyr [127, 128], visualizing protein



localization in live cells using ncAAs that can be conjugated to fluorescent dyes [129], and for the tagging and purification of newly synthesized proteins in mammalian cells by bio-orthogonal ncAA tagging [130]. The incorporation of ncAAs with unique absorption spectra can serve as infrared probes [131, 132] for the study of ligand binding [131] and conformational changes [132, 133], and as probes for nuclear magnetic resonance studies [134-137]. As detailed below, another major application of GCE is the study of PTMs [138].

## **1.4. Genetic Code Expansion to Program Post-Translational Modifications**

Following protein synthesis on the ribosomes, PTMs are chemical groups that are covalently added to the certain side chains of amino acids to regulate protein function [139]. Phosphorylation and acetylation are two of the most common PTMs observed [140]. Protein phosphorylation is an important regulatory mechanism in nearly all cellular processes, and is most well-known for its role in regulating signal transduction through cascades of protein kinases [141]. Proteins can be phosphorylated at Ser, Thr, and Tyr residues, and also at histidine (His) or aspartate (Asp) residues [142]. Protein phosphorylation is a reversible PTM that is regulated by kinases which phosphorylate proteins and phosphatases, which remove protein phosphorylation, and often regulates signalling pathways through regulating protein interactions with proteins containing phospho-binding domains [143].

Lysine acetylation is another reversible PTM that is mediated by addition of acetyl groups to lysine residues by acetyltransferases from acetyl coenzyme A (acCoA), and removal of acetyl groups by deacetylases [144, 145]. Lysine acetylation neutralizes the positive charge of lysine, which can disrupt electrostatic interactions between the lysine residue and other macromolecules such as proteins and nucleic acids [146]. Acetylation

controls protein function by regulating protein stability, enzymatic activity, protein localization, and by controlling protein-protein and protein-DNA interactions [147].

Programmed PTM incorporated into proteins using GCE allows for detailed studies of how acetylation, or phosphorylation, at a specific residue can affect proteins, expanding our knowledge on the functional acetylome and phosphoproteome. The enzymes responsible for acetylating or phosphorylating specific AA residues are often unknown, making homogenous production of proteins with site-specific PTMs difficult or impossible [103]. GCE bypasses this barrier by site-specifically genetically encoding PTMs by co-translational incorporation at UAG codons [103]. Multiple PTMs, including pSer [44], pTyr [47], pThr [45], and acK [43] can be co-translationally inserted into recombinant proteins site-specifically in *E. coli* utilizing GCE. The PylRS system has been adapted for insertion of exogenously provided acK at UAG stop codons [43, 148]. The first OTS to incorporate a phosphorylated amino acid into proteins [44] was derived from an archaeal pathway for cysteinyl-tRNA<sup>Cys</sup> biosynthesis [149, 150]. That pathway involves a phosphoseryl-tRNA intermediate [149, 150] that was engineered to produce phosphoproteins in *E. coli* [44]. The system requires a phosphoseryl-tRNA synthetase (SepRS) and tRNA<sup>Sep</sup> pair [44] in addition to a mutated elongation factor thermo unstable (EF-Tu) called EF<sup>Sep</sup> [151, 152].

#### **1.4.1. N<sub>ε</sub>-acetyl-Lysine Insertion via Genetic Code Expansion.**

Reassignment of the UAG codon to acK in *E. coli* was achieved by the development of N<sub>ε</sub>-acetyl-lysyl-tRNA synthetases (acKRSs) tRNA<sup>acK</sup> pairs by mutation of either *M. barkeri* PylRS [148] or *M. mazei* PylRS [43]. Transient transfection of mammalian cells with the *M. barkeri* derived acKRS tRNA<sup>acK</sup> pair [148] allowed acK insertion into proteins in mammalian cells [65]. However, heterogenous expression from transient transfections was a challenge. Genomic incorporation of acKRS tRNA<sup>acK</sup> (derived from the *M. mazei* PylRS/tRNA<sup>Pyl</sup> pair) created stable mammalian cell lines with homogenous expression to

allow acK insertion at specific sites in histones [153]. Reassignment of UAG to acK was achieved in a multicellular organism by creating transgenic mice expressing a genomically integrated *M. mazei* derived ackRS/tRNA<sup>acK</sup> pair [154].

The effect of Lys acetylation on several proteins has been determined using GCE to insert acK in response to UAG codons [138]. Using GCE to insert acK in response to UAG codons in *E. coli*, it was found that acetylation of human peroxiredoxin 1 increases its oligomerization and chaperone activity [155], acetylation of *E. coli* Malate dehydrogenase increases its activity [156], acetylation impairs the activity of *E. coli* TyrRS [157], *E. coli* isocitrate dehydrogenase [158], and *E. coli* Aconitase A [159], acetylation at K283 increases *E. coli* Citrate synthetase activity by increasing acCoA binding while acetylation at K295 decreases activity by decreasing AcCoA binding [160], acetylation increases *E. coli* Aconitase B activity [159], and acetylation of human ubiquitin alters ubiquitin patterns with different substrates, depending on the lysine residue acetylated [161].

#### **1.4.2. Phosphorylated Amino Acid Insertion via Genetic Code Expansion.**

Site-directed insertion of pSer was achieved by adapting the *M. jannaschii* tRNA<sup>Cys</sup> and *M. maripaludis* SepRS to produce an aaRS/tRNA pair orthogonal to *E. coli* that decodes UAG as pSer in the presence of EF<sup>Sep</sup>, a mutant form of EF-tu [44]. Two mutations of the *M. jannaschii* tRNA<sup>Cys</sup> changes the anticodon to decode UAG stop codons, and an additional mutation in the D-loop allowed the tRNA to be more efficiently aminoacylated by *M. maripaludis* SepRS, producing the *M. jannaschii* tRNA<sup>Sep</sup> *M. maripaludis* SepRS pair, which can provide tRNA<sup>Sep</sup> charged with pSer in cells [44]. However, this alone was not enough to allow decoding of UAG as pSer. EF-tu poorly binds tRNAs carrying negatively charged AAs [162], and molecular dynamics simulations

suggested pSer-tRNA<sup>Sep</sup> is not bound by EF-tu [163], preventing pSer incorporation, even with an orthogonal aaRS-tRNA pair providing the cell with tRNAs charged with pSer [44]. To overcome this, 6 mutations were introduced into EF-tu to produce EF<sub>Sep</sub>, which can bind pSer-tRNA<sup>Sep</sup> efficiently, allowing pSer incorporation at UAG codons by the *M. jannaschii* tRNA<sup>Sep</sup>, *M. maripaludis* SepRS pair in *E. coli* [44]. Insertion of pSer via GCE allowed site-specific phosphorylation to produce active human kinases, including mitogen-activated ERK activating kinase 1 kinase [44], protein kinase B (Akt1) [164], and ubiquitin [165].

pTyr insertion at UAG was achieved by directed evolution of the TyrRS system from *M. jannaschii* and simultaneously engineering the *E. coli* elongation factor EF-tu [166]. Further engineering of the SepRS tRNA<sup>Sep</sup> pair developed for pSer insertion produced the pThrRS-tRNA<sup>pThr</sup> pair which allows pThr insertion at UAG codons in *E. coli* [45]. Expression of the *Salmonella enterica* kinase PduX in *E. coli* allowed biosynthesis of pThr from Thr to supply pThr for insertion at UAG codons by the pThrRS/tRNA<sup>pThr</sup> pair in *E. coli* [45]. GCE mediated pThr insertion was optimized further to increase the efficiency of pThr insertion [46].

## 1.5. Limitations of Genetic Code Expansion

### 1.5.1. Mutual Orthogonality of aaRS/tRNA Pairs.

A vast number of ncAAs can be inserted site-specifically into proteins using OTSs [63, 68, 167]. Hundreds of different ncAAs [63] can be incorporated into proteins by GCE, but over two-thirds of these are incorporated by variants of the TyrRS or the PylRS systems [63]. Each o-aaRS/tRNA pair can only insert one ncAA, so although the PylRS/tRNA<sup>Pyl</sup> pair can co-translationally insert many Pyl analogues [60], on its own, the system can only be used to insert one of these reliably into a protein. A decade ago, a major limitation of GCE that engineering efforts are working to overcome is the incorporation of multiple

ncAAs simultaneously [63]. More recently, up to 5 mutually orthogonal PylRS/tRNA<sup>Pyl</sup> pairs have been developed [168]. One example of a mutually orthogonal PylRS pair involves the discovery of tRNA<sup>Pyl</sup> with A73 rather than the typically G73 discriminator base identity element. The unusual tRNA<sup>Pyl</sup> is found in Halophilic microbes, and the two different PylRS/tRNA<sup>Pyl</sup> pairs, one with G73 and one with A73, were used to incorporate two different ncAAs (3-iodo-Phe at a UAG codon and Boc-lysine at a UAA codon) into the small archaeal ubiquitin-like modifier protein [169].

### 1.5.2. Codon Availability.

The availability of codons that can be reassigned to ncAAs remains a limiting factor for GCE, making production of proteins simultaneously containing two or more ncAAs difficult or inefficient. GCE has mostly focused on using the one of the three stop codons (UAG, UAA, and UGA) [170]. By mutating the tRNA<sup>Pyl</sup> anticodon, the PylRS/tRNA<sup>Pyl</sup> system can reassign UAG, UAA, or UGA stop codons [171]. Indeed, production of a single protein containing two ncAAs incorporated via GCE simultaneously in *E. coli* was achieved using the Pyl system to reassign UAA stop codons and using the *M. jannaschii* TyrRS system to reassign UAG stop codons [172]. The approach used three stop codons in the ORF with two of the three stop codons being used to insert ncAAs, and the third (UGA) to direct translational termination.

So far, up to three different ncAAs have been simultaneously inserted site-specifically into a single polypeptide chain in *E. coli* by either reassigning all 3 stop codons [173], or by reassigning 2 stop codons and using UAU as a start codon (instead of AUG) to insert a ncAA at the N-terminal of proteins using an engineered initiator tRNA [174]. To reassign all 3 stop codons, a PylRS/tRNA<sup>Pyl</sup><sub>UAA</sub> pair decoded UAA to BocK, *E. coli* tryptophanyl-tRNA synthetase (TrpRS)/tRNA<sup>Tryptophan(Trp)</sup><sub>UCA</sub> decoded UGA to 5-hydroxytryptophan, and *M. jannaschii* TyrRS/tRNA<sup>Tyr</sup><sub>CUA</sub> decoded UAG to p-azido-phenylalanine in the engineered *E. coli* strain ATMW1 [173], which has had the

endogenous *E. coli* TrpRS/tRNA<sup>Trp</sup><sub>UCA</sub> substituted with its yeast counterpart to allow insertion of ncAA with the *E. coli* TrpRS/tRNA<sup>Trp</sup><sub>UCA</sub> pair [175]. Translational termination can be achieved by multiple consecutive stop codons even in the presence of an orthogonal pair capable of decoding the stop codon [176]. Three consecutive UAA stop codons were used to direct translational termination, and a self-cleaving tag was used to remove partial ncAA insertion by the PylRS/tRNA<sup>Pyl</sup><sub>UUA</sub> at the C-terminal translational termination site [173]. Drawbacks to this system includes the lack of a dedicated stop codon resulting in the need for a self-cleaving tag to ensure C-terminus homogeneity [173], the need for an engineered *E. coli* strain [173] which may be difficult to duplicate in other host systems, and is difficult to combine with other engineered *E. coli* strains, such as the C321.ΔA *E. coli* strain [177] developed to increase ncAA insertion efficiency at UAG codons by deletion of the release factor 1 (RF1) gene to reduce competition at UAG with orthogonal tRNAs, and mutation of all native UAG stop codons to UAA [177]. Another drawback is the low yield of ncAA containing protein, e.g., proteins containing 3 ncAAs were produced with only 2% of the yield of wildtype protein [173], which could be a result of competition of the orthogonal tRNAs with endogenous release factors, or toxic effects perhaps from elongated endogenous proteins produced due to endogenous stop codon readthrough, as seen with pSer insertion at UAG codons [178].

Another approach reassigned a UAG codon and two quadruplet codons (AGGA and AGTA) with the help of an orthogonal and engineered ribosome with improved efficiency in the decoding UAG and quadruplet codons [179]. However, frame-shifting at the site of the 4-base codon is well documented [180, 181], and it is unclear if, and why, this orthogonal and engineered ribosome would be immune to this effect.

### **1.5.3. Sense Codon Reassignment Limitations.**

Due to the degeneracy of the genetic code, it is widely believed that many sense codons (>20) should be available for recoding/reassignment to ncAAs [170]. In 2013,

Krishnakumar *et al.* tested this by attempting to use the Pyl system to reassign the CGG arginine (Arg) codon in *Mycoplasma capricolum* [170]. The CGG codon in *M. capricolum* has been called an unused or “open” sense codon [182], because the *M. capricolum* genome only contains 6 CGG arginine (Arg) codons and lacks a tRNA dedicated to decoding CGG [170]. Unfortunately, expression of PylRS and tRNA<sup>Pyl</sup> with an CCG anticodon (tRNA<sup>Pyl</sup><sub>CCG</sub>) in *M. capricolum* resulted in loading of tRNA<sup>Pyl</sup><sub>CCG</sub> with Arg by endogenous ArgRS and decoding of CGG as Arg [170]. tRNA<sup>Pyl</sup> variants with CCG anticodons are aminoacylated in *E. coli* while tRNA<sup>Pyl</sup> variants with CUA and GAG anticodons were not [170], suggesting that cross-reactivity with endogenous translation machinery may prove to be an additional barrier when attempting to decode sense codons.

A major identify element of ArgRS in *E. coli* and *S. cerevisiae* is the tRNA C35 anticodon base [120, 183, 184]. Every tRNA that is charged with a given canonical AA (iso-acceptor tRNAs) can be charged by a single aaRS [185], and unfortunately, 16 of the 20 endogenous aminoacylation systems used in *E. coli* use the tRNA anti-codon as an identity element [9]. This makes it difficult to reassign most sense codons to ncAAs of interest because altering the anticodon of orthogonal tRNAs eliminates their orthogonality and makes them targets for endogenous aaRSs. A comprehensive study of sense codon reassignment in *E. coli* found that orthogonal *M. jannaschii* TyrRS [186] and *M. bakeri* PylRS [187] pairs could effectively outcompete many sense codons, providing up to 65% missense suppression of the Arg AGG codon.

## 1.6. Genetic Code Expansion with Selenocysteine

The *E. coli* Sec insertion system provides molecular machinery to bypass barriers to installing ncAAs at sense codons. Instead of reassigning all codons to Sec globally, this system can site-specifically recode a single UGA stop codon to Sec (Fig 1.2A) in nature. Examples of Cys codons and other sense codons that are recoded to Sec have also been

identified [188]. This system recodes a single instance of a codon to Sec in a site-specific manner (Fig 1.2A). A hairpin loop structure, SecIS, forms on the mRNA downstream of the recoding site [189]. SecIS is bound by an elongation factor SelB, which localizes the Sec-tRNA at the UGA codon [189].

The dependence of this system on the presence of SecIS downstream of the recoding site to direct Sec insertion by binding SelB presents challenges to using this system for Sec insertion [190]. For some proteins with Sec occurring at the C-terminal, bacterial SecIS can be inserted into the 3'-UTR to allow recombinant production without changes to the ORF [16, 189]. A mammalian selenoprotein was recombinantly produced by fusing an engineered bacterial SecIS element with the rat thioredoxin reductase (TrxR) gene without causing changes to the protein sequence [191]. Recombinant production of human TrxR as well was achieved without changing the amino acid sequence with a similar method [189, 192] (Fig 2.1).

For production in a bacterial host, other Sec-containing proteins with internal Sec residues require a SecIS present in the protein ORF, and have been produced by engineering artificial SecISs that minimize changes to the ORF to reduce or eliminate unintended effects on the protein [16]. A Sec-containing glutathione S-transferase was produced recombinantly in *E. coli* by inserting a shortened bacterial SecIS from the *E. coli* *fdhF* gene downstream of the Sec codon, which resulted in 6 point mutations that had no effect on enzyme activity or substrate binding [193]. In another case, a Sec-containing human Methionine Sulfoxide Reductase B1 (MsrB1) was produced by mutating the ORF downstream of the UGA Sec codon to generate a SecIS functional in *E. coli* [194]. This engineered SecIS mutated 4 residues in MsrB1, but these mutations were shown to have little to no effect on enzyme activity [194]. More recently site-specific Sec incorporation was engineered into yeast for the first time, and the functional and Sec-containing human MsrB1 protein was produced [195]. An interesting aspect of the *E. coli* Sec insertion system is the ability to change the meaning of sense codons. By simply changing the



tRNA<sup>Sec</sup> anticodon, Sec can be inserted at 58 of the 64 possible codons with some efficiency, and can completely convert all 3 stop codons, and 15 different sense codons, to encode Sec [189]. By combining the Sec system with other OTSs like the PylRS system, 2 or more ncAAs could be inserted into a single polypeptide chain co-translationally.

## **1.7. The Mammalian Thioredoxin System Function and Role in Disease**

### **1.7.1. Thioredoxin Reductase, a Critical Selenoprotein in Redox Biology.**

Mammalian TrxR is a key redox regulator in mammalian cells and is a selenoprotein that is a powerful oxidoreductase containing selenium (Se) in the form of Sec [196]. TrxR, along with its major substrate, thioredoxin (Trx), make up one of the major disulfide reduction systems in the cell [197]. Sec is an analog of cysteine with Se taking the place of sulfur [198]. Se makes Sec a much more powerful nucleophile than Cys, making Sec-containing reductases better electron donors for redox reactions due to their lower redox potential [199]. Cys to Sec substitutions in Cys-containing reductases reduce redox potential and increase enzyme activity [199], while Sec to Cys substitutions in TrxR eliminates its activity with some substrates and drastically reduces its activity with other substrates [200, 201]. Due to its high nucleophilicity, Sec is also targeted in many medically relevant TrxR inhibitors, providing a unique mechanism to specifically target the activity of this selenoprotein [202-205]. These TrxR inhibitors include the platinum-containing compound, cisplatin, which is a widely used chemotherapeutic drug, and the gold-containing compound, auranofin, which is used to treat rheumatoid arthritis [206], and has been identified as a potential anti-cancer drug [207].

TrxR is the main driver of the thioredoxin (Trx) system, which is involved in oxidative stress responses in eukaryotes, bacteria, and archaea [208]. In addition to ROS

defense, the Trx system has diverse roles in many different species, garnering interest in Trx research from a diverse range of fields. Much research on the Trx systems have been done by both the agricultural and medical community [209]. The plant Trx system plays a role in plant growth, controlling rates of photosynthesis, and detecting levels of sunlight, garnering interest from the agricultural community [209]. In mammalian cells, the Trx system is involved in disease progression, including in diabetes, Alzheimer's disease, and the formation of various types of cancer [210], garnering interest from the medical community.

### **1.7.2. The Mammalian Thioredoxin System.**

In addition to glutathione system, the Trx system is one of the two main redox regulatory systems in mammalian cells [211] (Fig 1.4). The Trx system consists of several electron-transferring enzymes that work together to transfer electrons from nicotinamide adenine dinucleotide phosphate (NADPH) to a wide range of substrates to maintain the redox balance of the cell, protect against oxidative damage and reactive oxygen species (ROS), such as hydrogen peroxide ( $H_2O_2$ ), and to control the function of various proteins through redox regulation [211] (Fig 1.4).

In the Trx system, TrxR transfers electrons from NADPH to thioredoxin (Trx) [212-214]. After being reduced by TrxR, Trx reduces cellular proteins, such as peroxiredoxin (Prx), before being recycled again by TrxR [211] (Fig 1.4). Similarly, after receiving an electron from Trx, Prx can then reduce ROS such as  $H_2O_2$  before being recycled again by Trx [215] (Fig 1.4). Prx can reduce several different ROS [216] including  $H_2O_2$  [217], peroxynitrate [218], alkyl hydroperoxide [219], and peroxynitrate [220]. Some ROS can also be directly reduced by TrxR (lipid hydroperoxides [221] and  $H_2O_2$  [200]) and Trx (hydroxyl radicals [222]), providing multiple layers of oxidative defense (Fig 1.4). TrxR can also reduce several other proteins besides Trx [214], and Trx can reduce several proteins besides Prx [223] (Fig 1.4).

In addition to oxidative defense, the Trx system regulates many other cellular processes including gene expression, embryonic development, cell proliferation, and apoptosis [224]. The Trx system is involved in so many diverse processes because of redox regulation of a wide range of protein substrates such as ribonuclease reductase, peroxiredoxin, glucocorticoid receptors, transcription factors, and protein tyrosine phosphatases [225]. In mammalian cells, there are three genes encoding three main TrxR isoforms, TrxR1, TrxR2, and TrxR3 [226]. TrxR1 localizes to the cytosol, TrxR2 localizes to the mitochondria, and TrxR3 is present primarily in the testes [226].

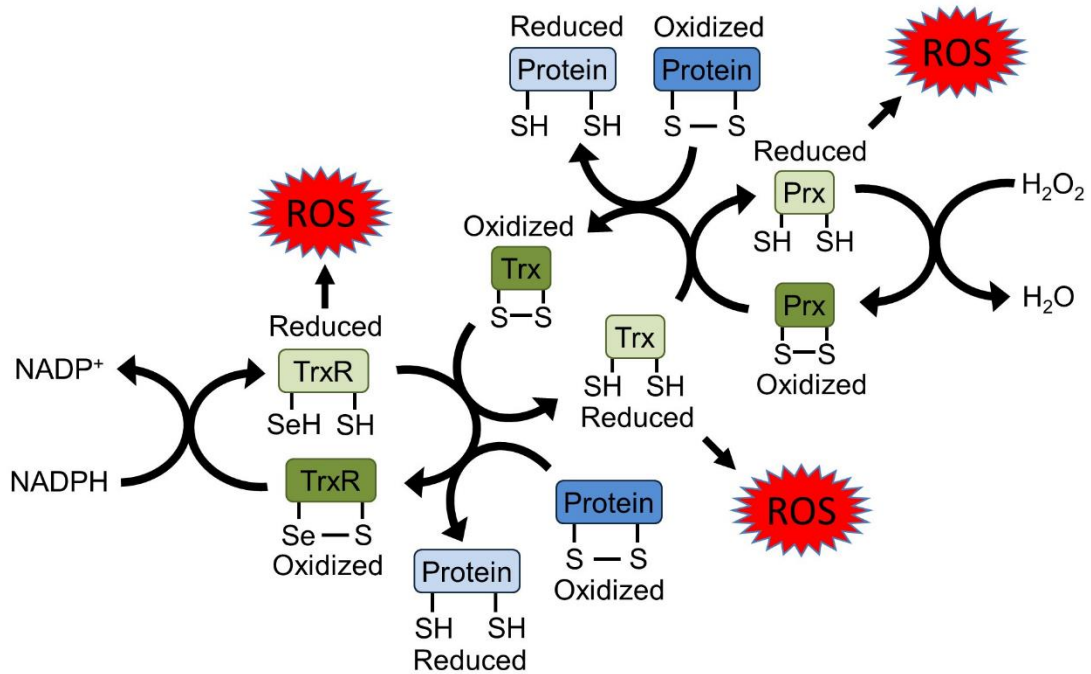


**Figure 1.4. Electron flow through the thioredoxin system.** Electron flow through the thioredoxin (Trx) system is mediated by TrxR using electrons from NADPH. TrxR reduces Trx before the oxidized TrxR is reduced again using electrons from NADPH. Trx then reduces Prx, or other target proteins, before oxidized Trx is reduced again by TrxR. Prx then reduces ROS such as H<sub>2</sub>O<sub>2</sub>, before oxidized Prx is reduced again by Trx. TrxR and Trx can also directly reduce ROS, providing the cell with a powerful ROS defence system. TrxR and Trx also reduce a wide variety of other proteins, with diverse functions, resulting in the Trx system being involved in nearly every aspect of cellular function. TrxR contains a highly nucleophilic Se atom in its active site in the form of Sec, making it a powerful reductase, capable of driving electrons through this system.

### **1.7.3. The Thioredoxin System and Disease.**

Because the flow of electrons into the Trx system depends on TrxR activity, and because of the diverse roles of the Trx system, TrxR is involved in the development and progression of many diseases [223, 227-229]. Aberrations to the Trx system has been observed in many diseases, such as Alzheimer's disease [230], rheumatoid arthritis [231], asthma [232], various forms of cardiovascular disease [233], and in many more diseases [223, 227-229], including in several types of cancer (non-small cell lung carcinoma [234], renal cell carcinoma [235], thyroid cancer [236], breast cancer [236], cervical carcinoma [237], colorectal cancer [238], and many more [239]). Overactive TrxR activity is linked to chemotherapeutic resistance of some cancer cells by helping to defend against ROS generated by radiation-based chemotherapies [240]. The activity of TrxR is also used as a diagnostic maker for the early detection of lung [241] and breast cancers [242]. Anti-cancer drugs, such as ethaselen, that target TrxR activity, have been developed to combat drug-resistant lung cancers [243].

### **1.7.4. TrxR and Post-Translational Modifications.**

In a mouse model of age-related macular degeneration and glaucoma, overexpression of amyloid  $\beta$  was correlated with increased TrxR activity without changes to total TrxR protein levels [244]. Differential total TrxR activity and alterations to TrxR1 acetylation was also associated with a cardiomyopathy phenotype in transgenic mice [245]. These studies suggest that PTMs, such as acetylation, regulate TrxR1 activity. At the time my thesis work began, TrxR1 was known to be acetylated at three specific lysine residues that had been experimentally identified in multiple studies in humans and mice [246-248], but there were no data regarding the functional impact of these acetylation sites on TrxR activity.

## 1.8. Thesis Project, Goals, and Hypothesis

The Sec system has the potential to bypass barriers to installing unnatural amino acids at nonsense or sense codons, and if combined with other OTSs, may permit the production of proteins with 2 or more ncAAs installed in the same polypeptide. I produced recombinant and active human TrxR1 in *E. coli* containing two different ncAAs simultaneously by using the *E. coli* Sec insertion system to recode a single UGA stop codon to Sec, and a mutant PylRS/tRNA<sup>Pyl</sup> system to reassign the UAG stop codon to acK at three specific sites in TrxR1 [192]. My work produced a selenoprotein with programmed acetylation for the first time and demonstrated that the Sec insertion system is compatible with the versatile Pyl OTS.

*I hypothesized site-specific acetylation will modify TrxR1 activity in vitro and affect redox activity in live cells.* My biochemical characterizations uncovered a model whereby acetylation regulates TrxR1 activity by modulating oligomerization of TrxR1 monomers [192]. Further research demonstrated the acetylation prevents the irreversible inactivation of TrxR1 by oxidation-induced covalent linkages of TrxR1 subunits, demonstrating acetylation protects the Trx system from oxidative damage [249]. Finally, in the last chapter, I pioneered the use of a cell penetrating peptide (CPP) derived from the human immunodeficiency virus (HIV) transactivator of transcription (TAT) protein to allow delivery of active and Sec-containing TrxR1 produced in *E. coli* to the cytosol of human cells in culture [250], paving the way for studies of human proteins with programmed modification produced via GCE in engineered bacteria in the native and homologous context of the mammalian cell.

## 1.9. References

1. Crick, F.H., *On protein synthesis*. Symp Soc Exp Biol, 1958. **12**: p. 138-63.
2. Brenner, S., F. Jacob, and M. Meselson, *An unstable intermediate carrying information from genes to ribosomes for protein synthesis*. Nature, 1961. **190**: p. 576-581.
3. Ramakrishnan, V., *Ribosome structure and the mechanism of translation*. Cell, 2002. **108**(4): p. 557-72.
4. Nirenberg, M., et al., *RNA codewords and protein synthesis, VII. On the general nature of the RNA code*. Proc Natl Acad Sci U S A, 1965. **53**(5): p. 1161-8.
5. Soll, D., et al., *Studies on polynucleotides, XLIX. Stimulation of the binding of aminoacyl-sRNA's to ribosomes by ribotrinnucleotides and a survey of codon assignments for 20 amino acids*. Proc Natl Acad Sci U S A, 1965. **54**(5): p. 1378-85.
6. Crick, F.H., et al., *General nature of the genetic code for proteins*. Nature, 1961. **192**: p. 1227-32.
7. Ibba, M. and D. Soll, *Quality control mechanisms during translation*. Science, 1999. **286**(5446): p. 1893-7.
8. Ibba, M., A.W. Curnow, and D. Soll, *Aminoacyl-tRNA synthesis: divergent routes to a common goal*. Trends Biochem Sci, 1997. **22**(2): p. 39-42.
9. Giege, R., M. Sissler, and C. Florentz, *Universal rules and idiosyncratic features in tRNA identity*. Nucleic Acids Res, 1998. **26**(22): p. 5017-35.
10. Mukai, T., et al., *Rewriting the Genetic Code*. Annu Rev Microbiol, 2017. **71**: p. 557-577.
11. Bock, A., et al., *Selenoprotein synthesis: an expansion of the genetic code*. Trends Biochem Sci, 1991. **16**(12): p. 463-7.
12. Commans, S. and A. Bock, *Selenocysteine inserting tRNAs: an overview*. FEMS Microbiol Rev, 1999. **23**(3): p. 335-51.
13. Rother, M. and V. Quitzke, *Selenoprotein synthesis and regulation in Archaea*. Biochim Biophys Acta Gen Subj, 2018. **1862**(11): p. 2451-2462.
14. Peng, J.J., et al., *Mechanisms Affecting the Biosynthesis and Incorporation Rate of Selenocysteine*. Molecules, 2021. **26**(23).
15. Lobanov, A.V., D.L. Hatfield, and V.N. Gladyshev, *Eukaryotic selenoproteins and selenoproteomes*. Biochim Biophys Acta, 2009. **1790**(11): p. 1424-8.
16. Chung, C.Z. and N. Krahn, *The selenocysteine toolbox: A guide to studying the 21st amino acid*. Arch Biochem Biophys, 2022. **730**: p. 109421.
17. Schmidt, R.L. and M. Simonovic, *Synthesis and decoding of selenocysteine and human health*. Croat Med J, 2012. **53**(6): p. 535-50.
18. Forchhammer, K., et al., *Selenocysteine synthase from Escherichia coli. Nucleotide sequence of the gene (selA) and purification of the protein*. J Biol Chem, 1991. **266**(10): p. 6318-23.
19. Carlson, B.A., et al., *Identification and characterization of phosphoseryl-tRNA[Ser]Sec kinase*. Proc Natl Acad Sci U S A, 2004. **101**(35): p. 12848-53.
20. Sherrer, R.L., P. O'Donoghue, and D. Soll, *Characterization and evolutionary history of an archaeal kinase involved in selenocysteinyl-tRNA formation*. Nucleic Acids Res, 2008. **36**(4): p. 1247-59.

21. Lee, B.J., et al., *Identification of a selenocysteyl-tRNA(Ser) in mammalian cells that recognizes the nonsense codon, UGA*. J Biol Chem, 1989. **264**(17): p. 9724-7.
22. Yuan, J., et al., *RNA-dependent conversion of phosphoserine forms selenocysteine in eukaryotes and archaea*. Proc Natl Acad Sci U S A, 2006. **103**(50): p. 18923-7.
23. Xu, X.M., et al., *Biosynthesis of selenocysteine on its tRNA in eukaryotes*. PLoS Biol, 2007. **5**(1): p. e4.
24. Krol, A., *Evolutionarily different RNA motifs and RNA-protein complexes to achieve selenoprotein synthesis*. Biochimie, 2002. **84**(8): p. 765-74.
25. Ringquist, S., et al., *Recognition of the mRNA selenocysteine insertion sequence by the specialized translational elongation factor SELB*. Genes Dev, 1994. **8**(3): p. 376-85.
26. Zavacki, A.M., et al., *Coupled tRNA(Sec)-dependent assembly of the selenocysteine decoding apparatus*. Mol Cell, 2003. **11**(3): p. 773-81.
27. Rother, M., et al., *Identification and characterisation of the selenocysteine-specific translation factor SelB from the archaeon Methanococcus jannaschii*. J Mol Biol, 2000. **299**(2): p. 351-8.
28. Fletcher, J.E., et al., *The selenocysteine incorporation machinery: interactions between the SECIS RNA and the SECIS-binding protein SBP2*. RNA, 2001. **7**(10): p. 1442-53.
29. Meng, K., et al., *Unconventional genetic code systems in archaea*. Front Microbiol, 2022. **13**: p. 1007832.
30. Hao, B., et al., *A new UAG-encoded residue in the structure of a methanogen methyltransferase*. Science, 2002. **296**(5572): p. 1462-6.
31. Soares, J.A., et al., *The residue mass of L-pyrrolysine in three distinct methylamine methyltransferases*. J Biol Chem, 2005. **280**(44): p. 36962-9.
32. Mahapatra, A., et al., *Characterization of a Methanosarcina acetivorans mutant unable to translate UAG as pyrrolysine*. Mol Microbiol, 2006. **59**(1): p. 56-66.
33. Krzycki, J.A., *The direct genetic encoding of pyrrolysine*. Curr Opin Microbiol, 2005. **8**(6): p. 706-12.
34. Srinivasan, G., C.M. James, and J.A. Krzycki, *Pyrrolysine encoded by UAG in Archaea: charging of a UAG-decoding specialized tRNA*. Science, 2002. **296**(5572): p. 1459-62.
35. Gaston, M.A., et al., *The complete biosynthesis of the genetically encoded amino acid pyrrolysine from lysine*. Nature, 2011. **471**(7340): p. 647-50.
36. Gaston, M.A., R. Jiang, and J.A. Krzycki, *Functional context, biosynthesis, and genetic encoding of pyrrolysine*. Curr Opin Microbiol, 2011. **14**(3): p. 342-9.
37. Kavran, J.M., et al., *Structure of pyrrolysyl-tRNA synthetase, an archaeal enzyme for genetic code innovation*. Proc Natl Acad Sci U S A, 2007. **104**(27): p. 11268-73.
38. Saunders, N.F., et al., *Mechanisms of thermal adaptation revealed from the genomes of the Antarctic Archaea Methanogenium frigidum and Methanococcoides burtonii*. Genome Res, 2003. **13**(7): p. 1580-8.
39. Heinemann, I.U., et al., *The appearance of pyrrolysine in tRNA<sup>His</sup> guanylyltransferase by neutral evolution*. Proc Natl Acad Sci U S A, 2009. **106**(50): p. 21103-8.

40. Borrel, G., et al., *Unique characteristics of the pyrrolysine system in the 7th order of methanogens: implications for the evolution of a genetic code expansion cassette*. Archaea, 2014. **2014**: p. 374146.
41. Prat, L., et al., *Carbon source-dependent expansion of the genetic code in bacteria*. Proc Natl Acad Sci U S A, 2012. **109**(51): p. 21070-5.
42. Guo, L.T., et al., *Ancestral archaea expanded the genetic code with pyrrolysine*. J Biol Chem, 2022. **298**(11): p. 102521.
43. Umehara, T., et al., *N-acetyl lysyl-tRNA synthetases evolved by a CcdB-based selection possess N-acetyl lysine specificity in vitro and in vivo*. FEBS Lett, 2012. **586**(6): p. 729-33.
44. Park, H.S., et al., *Expanding the genetic code of Escherichia coli with phosphoserine*. Science, 2011. **333**(6046): p. 1151-4.
45. Zhang, M.S., et al., *Biosynthesis and genetic encoding of phosphothreonine through parallel selection and deep sequencing*. Nat Methods, 2017. **14**(7): p. 729-736.
46. Moen, J.M., et al., *Enhanced access to the human phosphoproteome with genetically encoded phosphothreonine*. Nat Commun, 2022. **13**(1): p. 7226.
47. Hoppmann, C., et al., *Site-specific incorporation of phosphotyrosine using an expanded genetic code*. Nat Chem Biol, 2017. **13**(8): p. 842-844.
48. Chin, J.W., et al., *Addition of p-azido-L-phenylalanine to the genetic code of Escherichia coli*. J Am Chem Soc, 2002. **124**(31): p. 9026-7.
49. Nguyen, T.A., M. Cigler, and K. Lang, *Expanding the Genetic Code to Study Protein-Protein Interactions*. Angew Chem Int Ed Engl, 2018. **57**(44): p. 14350-14361.
50. Lee, S., J. Kim, and M. Koh, *Recent Advances in Fluorescence Imaging by Genetically Encoded Non-canonical Amino Acids*. J Mol Biol, 2022. **434**(8): p. 167248.
51. Jones, C.M., et al., *Genetic encoding of a highly photostable, long lifetime fluorescent amino acid for imaging in mammalian cells*. Chem Sci, 2021. **12**(36): p. 11955-11964.
52. Li, X. and C.C. Liu, *Biological applications of expanded genetic codes*. ChemBiochem, 2014. **15**(16): p. 2335-41.
53. Krahn, N., et al., *Engineering aminoacyl-tRNA synthetases for use in synthetic biology*. Enzymes, 2020. **48**: p. 351-395.
54. Melnikov, S.V. and D. Soll, *Aminoacyl-tRNA Synthetases and tRNAs for an Expanded Genetic Code: What Makes them Orthogonal?* Int J Mol Sci, 2019. **20**(8).
55. Wang, L. and P.G. Schultz, *A general approach for the generation of orthogonal tRNAs*. Chem Biol, 2001. **8**(9): p. 883-90.
56. Cho, C.C., et al., *The Pyrrolysyl-tRNA Synthetase Activity can be Improved by a P188 Mutation that Stabilizes the Full-Length Enzyme*. J Mol Biol, 2022. **434**(8): p. 167453.
57. Ambrogelly, A., et al., *Pyrrolysine is not hardwired for cotranslational insertion at UAG codons*. Proc Natl Acad Sci U S A, 2007. **104**(9): p. 3141-6.
58. Chen, P.R., et al., *A facile system for encoding unnatural amino acids in mammalian cells*. Angew Chem Int Ed Engl, 2009. **48**(22): p. 4052-5.



59. Willis, J.C.W. and J.W. Chin, *Mutually orthogonal pyrrolysyl-tRNA synthetase/tRNA pairs*. Nat Chem, 2018. **10**(8): p. 831-837.
60. Carla R. Polycarpo, S.H., Amélie Bérubé, John L. Wood, Dieter Söll, Alexandre Ambrogelly *Pyrrolysine analogues as substrates for pyrrolysyl-tRNA synthetase*. FEBS Letters, 2006. **580**(28-29): p. 6695-6700.
61. Wang, Y.S., et al., *A rationally designed pyrrolysyl-tRNA synthetase mutant with a broad substrate spectrum*. J Am Chem Soc, 2012. **134**(6): p. 2950-3.
62. Yanagisawa, T., et al., *Expanded genetic code technologies for incorporating modified lysine at multiple sites*. Chembiochem, 2014. **15**(15): p. 2181-7.
63. Vargas-Rodriguez, O., et al., *Upgrading aminoacyl-tRNA synthetases for genetic code expansion*. Curr Opin Chem Biol, 2018. **46**: p. 115-122.
64. Wright, D.E. and P. O'Donoghue, *The Molecular Architecture of Unnatural Amino Acid Translation Systems*. Structure, 2019. **27**(8): p. 1192-1194.
65. Mukai, T., et al., *Adding l-lysine derivatives to the genetic code of mammalian cells with engineered pyrrolysyl-tRNA synthetases*. Biochem Biophys Res Commun, 2008. **371**(4): p. 818-22.
66. Gautier, A., et al., *Genetically encoded photocontrol of protein localization in mammalian cells*. J Am Chem Soc, 2010. **132**(12): p. 4086-8.
67. Wang, L., et al., *A new functional suppressor tRNA/aminoacyl- tRNA synthetase pair for the in vivo incorporation of unnatural amino acids into proteins*. J Am Chem Soc, 2000. **122**(20): p. 5010-5011.
68. Liu, C.C. and P.G. Schultz, *Adding new chemistries to the genetic code*. Annu Rev Biochem, 2010. **79**: p. 413-44.
69. Gan, Q., et al., *Expanding the genetic code of Salmonella with non-canonical amino acids*. Sci Rep, 2016. **6**: p. 39920.
70. Wang, F., et al., *Genetic incorporation of unnatural amino acids into proteins in Mycobacterium tuberculosis*. PLoS One, 2010. **5**(2): p. e9354.
71. He, J., et al., *Development of an Unnatural Amino Acid Incorporation System in the Actinobacterial Natural Product Producer Streptomyces venezuelae ATCC 15439*. ACS Synth Biol, 2016. **5**(2): p. 125-32.
72. Andrews, J., Q. Gan, and C. Fan, *"Not-so-popular" orthogonal pairs in genetic code expansion*. Protein Sci, 2023. **32**(2): p. e4559.
73. Pastrnak, M., T.J. Magliery, and P.G. Schultz, *A New Orthogonal Suppressor tRNA/Aminoacyl-tRNA Synthetase Pair for Evolving an Organism with an Expanded Genetic Code*. Helv Chim Acta, 2000. **83**(9): p. 2277-2286.
74. Furter, R., *Expansion of the genetic code: site-directed p-fluoro-phenylalanine incorporation in Escherichia coli*. Protein Sci, 1998. **7**(2): p. 419-26.
75. Chatterjee, A., et al., *A tryptophanyl-tRNA synthetase/tRNA pair for unnatural amino acid mutagenesis in E. coli*. Angew Chem Int Ed Engl, 2013. **52**(19): p. 5106-9.
76. Nodling, A.R., et al., *Using genetically incorporated unnatural amino acids to control protein functions in mammalian cells*. Essays Biochem, 2019. **63**(2): p. 237-266.
77. Kato, Y., *Translational Control using an Expanded Genetic Code*. Int J Mol Sci, 2019. **20**(4).

78. Kato, Y., *Tight Translational Control Using Site-Specific Unnatural Amino Acid Incorporation with Positive Feedback Gene Circuits*. ACS Synth Biol, 2018. **7**(8): p. 1956-1963.
79. Wang, N., et al., *Construction of a live-attenuated HIV-1 vaccine through genetic code expansion*. Angew Chem Int Ed Engl, 2014. **53**(19): p. 4867-71.
80. Rovner, A.J., et al., *Recoded organisms engineered to depend on synthetic amino acids*. Nature, 2015. **518**(7537): p. 89-93.
81. Mandell, D.J., et al., *Biocontainment of genetically modified organisms by synthetic protein design*. Nature, 2015. **518**(7537): p. 55-60.
82. Si, L., et al., *Generation of influenza A viruses as live but replication-incompetent virus vaccines*. Science, 2016. **354**(6316): p. 1170-1173.
83. Yuan, Z., et al., *Controlling Multicycle Replication of Live-Attenuated HIV-1 Using an Unnatural Genetic Switch*. ACS Synth Biol, 2017. **6**(4): p. 721-731.
84. Chen, C., et al., *Genetic-code-expanded cell-based therapy for treating diabetes in mice*. Nat Chem Biol, 2022. **18**(1): p. 47-55.
85. Kwok, H.S., et al., *Engineered Aminoacyl-tRNA Synthetases with Improved Selectivity toward Noncanonical Amino Acids*. ACS Chem Biol, 2019. **14**(4): p. 603-612.
86. Jiang, H.K., et al., *Split aminoacyl-tRNA synthetases for proximity-induced stop codon suppression*. Proc Natl Acad Sci U S A, 2023. **120**(8): p. e2219758120.
87. Yang, Y., H. Song, and P.R. Chen, *Genetically encoded photocrosslinkers for identifying and mapping protein-protein interactions in living cells*. IUBMB Life, 2016. **68**(11): p. 879-886.
88. Tanaka, Y., M.R. Bond, and J.J. Kohler, *Photocrosslinkers illuminate interactions in living cells*. Mol Biosyst, 2008. **4**(6): p. 473-80.
89. Chin, J.W., et al., *Addition of a photocrosslinking amino acid to the genetic code of Escherichiacoli*. Proc Natl Acad Sci U S A, 2002. **99**(17): p. 11020-4.
90. Tippmann, E.M., et al., *A genetically encoded diazirine photocrosslinker in Escherichia coli*. Chembiochem, 2007. **8**(18): p. 2210-4.
91. Zhang, M., et al., *A genetically incorporated crosslinker reveals chaperone cooperation in acid resistance*. Nat Chem Biol, 2011. **7**(10): p. 671-7.
92. Ai, H.W., et al., *Probing protein-protein interactions with a genetically encoded photo-crosslinking amino acid*. Chembiochem, 2011. **12**(12): p. 1854-7.
93. Yanagisawa, T., et al., *Wide-range protein photo-crosslinking achieved by a genetically encoded N(epsilon)-(benzyloxycarbonyl)lysine derivative with a diazirinyl moiety*. Mol Biosyst, 2012. **8**(4): p. 1131-5.
94. Coin, I., et al., *Photo-cross-linkers incorporated into G-protein-coupled receptors in mammalian cells: a ligand comparison*. Angew Chem Int Ed Engl, 2011. **50**(35): p. 8077-81.
95. Coin, I., et al., *Genetically encoded chemical probes in cells reveal the binding path of urocortin-I to CRF class B GPCR*. Cell, 2013. **155**(6): p. 1258-69.
96. Hino, N., et al., *Genetic incorporation of a photo-crosslinkable amino acid reveals novel protein complexes with GRB2 in mammalian cells*. J Mol Biol, 2011. **406**(2): p. 343-53.
97. Hino, N., et al., *Protein photo-cross-linking in mammalian cells by site-specific incorporation of a photoreactive amino acid*. Nat Methods, 2005. **2**(3): p. 201-6.

98. Okuda, S., E. Freinkman, and D. Kahne, *Cytoplasmic ATP hydrolysis powers transport of lipopolysaccharide across the periplasm in E. coli*. *Science*, 2012. **338**(6111): p. 1214-7.
99. Freinkman, E., S.S. Chng, and D. Kahne, *The complex that inserts lipopolysaccharide into the bacterial outer membrane forms a two-protein plug-and-barrel*. *Proc Natl Acad Sci U S A*, 2011. **108**(6): p. 2486-91.
100. Mori, H. and K. Ito, *Different modes of SecY-SecA interactions revealed by site-directed in vivo photo-cross-linking*. *Proc Natl Acad Sci U S A*, 2006. **103**(44): p. 16159-64.
101. Lakshminpathy, S.K., et al., *Identification of nascent chain interaction sites on trigger factor*. *J Biol Chem*, 2007. **282**(16): p. 12186-93.
102. Liu, C., et al., *Coupled chaperone action in folding and assembly of hexadecameric Rubisco*. *Nature*, 2010. **463**(7278): p. 197-202.
103. Davis, L. and J.W. Chin, *Designer proteins: applications of genetic code expansion in cell biology*. *Nat Rev Mol Cell Biol*, 2012. **13**(3): p. 168-82.
104. Baker, A.S. and A. Deiters, *Optical control of protein function through unnatural amino acid mutagenesis and other optogenetic approaches*. *ACS Chem Biol*, 2014. **9**(7): p. 1398-407.
105. Courtney, T. and A. Deiters, *Recent advances in the optical control of protein function through genetic code expansion*. *Curr Opin Chem Biol*, 2018. **46**: p. 99-107.
106. Deiters, A., et al., *A genetically encoded photocaged tyrosine*. *Angew Chem Int Ed Engl*, 2006. **45**(17): p. 2728-31.
107. Arbely, E., et al., *Photocontrol of tyrosine phosphorylation in mammalian cells via genetic encoding of photocaged tyrosine*. *J Am Chem Soc*, 2012. **134**(29): p. 11912-5.
108. Wu, N., et al., *A genetically encoded photocaged amino acid*. *J Am Chem Soc*, 2004. **126**(44): p. 14306-7.
109. Nguyen, D.P., et al., *Genetic encoding of photocaged cysteine allows photoactivation of TEV protease in live mammalian cells*. *J Am Chem Soc*, 2014. **136**(6): p. 2240-3.
110. Kang, J.Y., et al., *In vivo expression of a light-activatable potassium channel using unnatural amino acids*. *Neuron*, 2013. **80**(2): p. 358-70.
111. Lemke, E.A., et al., *Control of protein phosphorylation with a genetically encoded photocaged amino acid*. *Nat Chem Biol*, 2007. **3**(12): p. 769-72.
112. Hancock, S.M., et al., *Expanding the genetic code of yeast for incorporation of diverse unnatural amino acids via a pyrrolysyl-tRNA synthetase/tRNA pair*. *J Am Chem Soc*, 2010. **132**(42): p. 14819-24.
113. Hemphill, J., et al., *Genetically encoded light-activated transcription for spatiotemporal control of gene expression and gene silencing in mammalian cells*. *J Am Chem Soc*, 2013. **135**(36): p. 13433-9.
114. Walker, O.S., et al., *Photoactivation of Mutant Isocitrate Dehydrogenase 2 Reveals Rapid Cancer-Associated Metabolic and Epigenetic Changes*. *J Am Chem Soc*, 2016. **138**(3): p. 718-21.
115. Hemphill, J., et al., *Optical Control of CRISPR/Cas9 Gene Editing*. *J Am Chem Soc*, 2015. **137**(17): p. 5642-5.

116. Liu, J., et al., *Genetic Code Expansion in Zebrafish Embryos and Its Application to Optical Control of Cell Signaling*. J Am Chem Soc, 2017. **139**(27): p. 9100-9103.
117. Gautier, A., A. Deiters, and J.W. Chin, *Light-activated kinases enable temporal dissection of signaling networks in living cells*. J Am Chem Soc, 2011. **133**(7): p. 2124-7.
118. Liaunardy-Jopeace, A., et al., *Encoding optical control in LCK kinase to quantitatively investigate its activity in live cells*. Nat Struct Mol Biol, 2017. **24**(12): p. 1155-1163.
119. Engelke, H., et al., *Control of protein function through optochemical translocation*. ACS Synth Biol, 2014. **3**(10): p. 731-6.
120. Tamura, K., et al., *In vitro study of E.coli tRNA(Arg) and tRNA(Lys) identity elements*. Nucleic Acids Res, 1992. **20**(9): p. 2335-9.
121. Uprety, R., et al., *Genetic encoding of caged cysteine and caged homocysteine in bacterial and mammalian cells*. Chembiochem, 2014. **15**(12): p. 1793-9.
122. Chou, C., D.D. Young, and A. Deiters, *Photocaged t7 RNA polymerase for the light activation of transcription and gene function in pro- and eukaryotic cells*. Chembiochem, 2010. **11**(7): p. 972-7.
123. Chou, C. and A. Deiters, *Light-activated gene editing with a photocaged zinc-finger nuclease*. Angew Chem Int Ed Engl, 2011. **50**(30): p. 6839-42.
124. Edwards, W.F., D.D. Young, and A. Deiters, *Light-activated Cre recombinase as a tool for the spatial and temporal control of gene function in mammalian cells*. ACS Chem Biol, 2009. **4**(6): p. 441-5.
125. Neumann, H., *Rewiring translation - Genetic code expansion and its applications*. FEBS Lett, 2012. **586**(15): p. 2057-64.
126. Chung, C.Z., K. Amikura, and D. Soll, *Using Genetic Code Expansion for Protein Biochemical Studies*. Front Bioeng Biotechnol, 2020. **8**: p. 598577.
127. Neumann, H., et al., *Genetically encoding protein oxidative damage*. J Am Chem Soc, 2008. **130**(12): p. 4028-33.
128. Porter, J.J., et al., *Genetically Encoded Protein Tyrosine Nitration in Mammalian Cells*. ACS Chem Biol, 2019. **14**(6): p. 1328-1336.
129. Beliu, G., et al., *Bioorthogonal labeling with tetrazine-dyes for super-resolution microscopy*. Commun Biol, 2019. **2**: p. 261.
130. Mahdavi, A., et al., *Engineered Aminoacyl-tRNA Synthetase for Cell-Selective Analysis of Mammalian Protein Synthesis*. J Am Chem Soc, 2016. **138**(13): p. 4278-81.
131. Schultz, K.C., et al., *A genetically encoded infrared probe*. J Am Chem Soc, 2006. **128**(43): p. 13984-5.
132. Ye, S., et al., *FTIR analysis of GPCR activation using azido probes*. Nat Chem Biol, 2009. **5**(6): p. 397-9.
133. Ye, S., et al., *Tracking G-protein-coupled receptor activation using genetically encoded infrared probes*. Nature, 2010. **464**(7293): p. 1386-9.
134. Cellitti, S.E., et al., *In vivo incorporation of unnatural amino acids to probe structure, dynamics, and ligand binding in a large protein by nuclear magnetic resonance spectroscopy*. J Am Chem Soc, 2008. **130**(29): p. 9268-81.

135. Jones, D.H., et al., *Site-specific labeling of proteins with NMR-active unnatural amino acids*. J Biomol NMR, 2010. **46**(1): p. 89-100.
136. Jackson, J.C., J.T. Hammill, and R.A. Mehl, *Site-specific incorporation of a (19)F-amino acid into proteins as an NMR probe for characterizing protein structure and reactivity*. J Am Chem Soc, 2007. **129**(5): p. 1160-6.
137. Wilkins, B.J., et al., *Site-specific incorporation of fluorotyrosines into proteins in Escherichia coli by photochemical disguise*. Biochemistry, 2010. **49**(8): p. 1557-9.
138. Chen, H., et al., *Recent Development of Genetic Code Expansion for Posttranslational Modification Studies*. Molecules, 2018. **23**(7).
139. Walsh, C.T., S. Garneau-Tsodikova, and G.J. Gatto, Jr., *Protein posttranslational modifications: the chemistry of proteome diversifications*. Angew Chem Int Ed Engl, 2005. **44**(45): p. 7342-72.
140. Ramazi, S. and J. Zahiri, *Posttranslational modifications in proteins: resources, tools and prediction methods*. Database (Oxford), 2021. **2021**.
141. Graves, J.D. and E.G. Krebs, *Protein phosphorylation and signal transduction*. Pharmacol Ther, 1999. **82**(2-3): p. 111-21.
142. Deribe, Y.L., T. Pawson, and I. Dikic, *Post-translational modifications in signal integration*. Nat Struct Mol Biol, 2010. **17**(6): p. 666-72.
143. Jin, J. and T. Pawson, *Modular evolution of phosphorylation-based signalling systems*. Philos Trans R Soc Lond B Biol Sci, 2012. **367**(1602): p. 2540-55.
144. Yang, X.J., *The diverse superfamily of lysine acetyltransferases and their roles in leukemia and other diseases*. Nucleic Acids Res, 2004. **32**(3): p. 959-76.
145. Hyndman, K.A. and M.A. Knepper, *Dynamic regulation of lysine acetylation: the balance between acetyltransferase and deacetylase activities*. Am J Physiol Renal Physiol, 2017. **313**(4): p. F842-F846.
146. Shvedunova, M. and A. Akhtar, *Modulation of cellular processes by histone and non-histone protein acetylation*. Nat Rev Mol Cell Biol, 2022. **23**(5): p. 329-349.
147. Narita, T., B.T. Weinert, and C. Choudhary, *Functions and mechanisms of non-histone protein acetylation*. Nat Rev Mol Cell Biol, 2019. **20**(3): p. 156-174.
148. Neumann, H., S.Y. Peak-Chew, and J.W. Chin, *Genetically encoding N(epsilon)-acetyllysine in recombinant proteins*. Nat Chem Biol, 2008. **4**(4): p. 232-4.
149. Sauerwald, A., et al., *RNA-dependent cysteine biosynthesis in archaea*. Science, 2005. **307**(5717): p. 1969-72.
150. Hohn, M.J., et al., *Emergence of the universal genetic code imprinted in an RNA record*. Proc Natl Acad Sci U S A, 2006. **103**(48): p. 18095-100.
151. George, S., et al., *Ubiquitin phosphorylated at Ser57 hyper-activates parkin*. Biochim Biophys Acta Gen Subj, 2017. **1861**(11 Pt B): p. 3038-3046.
152. Balasuriya, N., et al., *Phosphorylation-dependent substrate selectivity of protein kinase B (AKT1)*. J Biol Chem, 2020. **295**(24): p. 8120-8134.
153. Elsasser, S.J., et al., *Genetic code expansion in stable cell lines enables encoded chromatin modification*. Nat Methods, 2016. **13**(2): p. 158-64.
154. Han, S., et al., *Expanding the genetic code of Mus musculus*. Nat Commun, 2017. **8**: p. 14568.
155. Pan, Y., et al., *Significant enhancement of hPrx1 chaperone activity through lysine acetylation*. Chembiochem, 2014. **15**(12): p. 1773-6.

156. Venkat, S., et al., *Studying the Lysine Acetylation of Malate Dehydrogenase*. J Mol Biol, 2017. **429**(9): p. 1396-1405.
157. Venkat, S., et al., *Biochemical Characterization of the Lysine Acetylation of Tyrosyl-tRNA Synthetase in Escherichia coli*. Chembiochem, 2017. **18**(19): p. 1928-1934.
158. Venkat, S., et al., *Characterizing Lysine Acetylation of Isocitrate Dehydrogenase in Escherichia coli*. J Mol Biol, 2018. **430**(13): p. 1901-1911.
159. Araujo, J., et al., *Studying Acetylation of Aconitase Isozymes by Genetic Code Expansion*. Front Chem, 2022. **10**: p. 862483.
160. Venkat, S., et al., *Characterizing lysine acetylation of Escherichia coli type II citrate synthase*. FEBS J, 2019. **286**(14): p. 2799-2808.
161. Lacoursiere, R.E., P. O'Donoghue, and G.S. Shaw, *Programmed ubiquitin acetylation using genetic code expansion reveals altered ubiquitination patterns*. FEBS Lett, 2020. **594**(7): p. 1226-1234.
162. Dale, T., L.E. Sanderson, and O.C. Uhlenbeck, *The affinity of elongation factor Tu for an aminoacyl-tRNA is modulated by the esterified amino acid*. Biochemistry, 2004. **43**(20): p. 6159-66.
163. Eargle, J., et al., *Dynamics of Recognition between tRNA and elongation factor Tu*. J Mol Biol, 2008. **377**(5): p. 1382-405.
164. Balasuriya, N., et al., *Genetic code expansion and live cell imaging reveal that Thr-308 phosphorylation is irreplaceable and sufficient for Akt1 activity*. J Biol Chem, 2018. **293**(27): p. 10744-10756.
165. George, S., et al., *Generation of phospho-ubiquitin variants by orthogonal translation reveals codon skipping*. FEBS Lett, 2016. **590**(10): p. 1530-42.
166. Fan, C., K. Ip, and D. Soll, *Expanding the genetic code of Escherichia coli with phosphotyrosine*. FEBS Lett, 2016. **590**(17): p. 3040-7.
167. Lajoie, M.J., D. Soll, and G.M. Church, *Overcoming Challenges in Engineering the Genetic Code*. J Mol Biol, 2016. **428**(5 Pt B): p. 1004-21.
168. Beattie, A.T., D.L. Dunkelmann, and J.W. Chin, *Quintuply orthogonal pyrrolysyl-tRNA synthetase/tRNA(Pyl) pairs*. Nat Chem, 2023. **15**(7): p. 948-959.
169. Zhang, H., et al., *The tRNA discriminator base defines the mutual orthogonality of two distinct pyrrolysyl-tRNA synthetase/tRNAPyl pairs in the same organism*. Nucleic Acids Res, 2022. **50**(8): p. 4601-4615.
170. Krishnakumar, R., et al., *Transfer RNA misidentification scrambles sense codon recoding*. Chembiochem, 2013. **14**(15): p. 1967-72.
171. Wan, W., J.M. Tharp, and W.R. Liu, *Pyrrolysyl-tRNA synthetase: an ordinary enzyme but an outstanding genetic code expansion tool*. Biochim Biophys Acta, 2014. **1844**(6): p. 1059-70.
172. Wan, W., et al., *A facile system for genetic incorporation of two different noncanonical amino acids into one protein in Escherichia coli*. Angew Chem Int Ed Engl, 2010. **49**(18): p. 3211-4.
173. Italia, J.S., et al., *Mutually Orthogonal Nonsense-Suppression Systems and Conjugation Chemistries for Precise Protein Labeling at up to Three Distinct Sites*. J Am Chem Soc, 2019. **141**(15): p. 6204-6212.

174. Tharp, J.M., et al., *Genetic Encoding of Three Distinct Noncanonical Amino Acids Using Reprogrammed Initiator and Nonsense Codons*. ACS Chem Biol, 2021. **16**(4): p. 766-774.
175. Italia, J.S., et al., *An orthogonalized platform for genetic code expansion in both bacteria and eukaryotes*. Nat Chem Biol, 2017. **13**(4): p. 446-450.
176. Zheng, Y., et al., *Performance of optimized noncanonical amino acid mutagenesis systems in the absence of release factor 1*. Mol Biosyst, 2016. **12**(6): p. 1746-9.
177. Lajoie, M.J., et al., *Genomically recoded organisms expand biological functions*. Science, 2013. **342**(6156): p. 357-60.
178. Heinemann, I.U., et al., *Enhanced phosphoserine insertion during Escherichia coli protein synthesis via partial UAG codon reassignment and release factor 1 deletion*. FEBS Lett, 2012. **586**(20): p. 3716-22.
179. Dunkelmann, D.L., et al., *Engineered triply orthogonal pyrrolysyl-tRNA synthetase/tRNA pairs enable the genetic encoding of three distinct non-canonical amino acids*. Nat Chem, 2020. **12**(6): p. 535-544.
180. Farabaugh, P.J., *Translational frameshifting: implications for the mechanism of translational frame maintenance*. Prog Nucleic Acid Res Mol Biol, 2000. **64**: p. 131-70.
181. O'Donoghue, P., et al., *Near-cognate suppression of amber, opal and quadruplet codons competes with aminoacyl-tRNA<sup>Pyl</sup> for genetic code expansion*. FEBS Lett, 2012. **586**(21): p. 3931-7.
182. Oba, T., et al., *CGG: an unassigned or nonsense codon in Mycoplasma capricolum*. Proc Natl Acad Sci U S A, 1991. **88**(3): p. 921-5.
183. McClain, W.H., et al., *Nucleotides that determine Escherichia coli tRNA(Arg) and tRNA(Lys) acceptor identities revealed by analyses of mutant opal and amber suppressor tRNAs*. Proc Natl Acad Sci U S A, 1990. **87**(23): p. 9260-4.
184. Sissler, M., R. Giege, and C. Florentz, *Arginine aminoacylation identity is context-dependent and ensured by alternate recognition sets in the anticodon loop of accepting tRNA transcripts*. EMBO J, 1996. **15**(18): p. 5069-76.
185. Woese, C.R., et al., *Aminoacyl-tRNA synthetases, the genetic code, and the evolutionary process*. Microbiol Mol Biol Rev, 2000. **64**(1): p. 202-36.
186. Schmitt, M.A., W. Biddle, and J.D. Fisk, *Mapping the Plasticity of the Escherichia coli Genetic Code with Orthogonal Pair-Directed Sense Codon Reassignment*. Biochemistry, 2018. **57**(19): p. 2762-2774.
187. Schwark, D.G., M.A. Schmitt, and J.D. Fisk, *Directed Evolution of the Methanosarcina barkeri Pyrrolysyl tRNA/aminoacyl tRNA Synthetase Pair for Rapid Evaluation of Sense Codon Reassignment Potential*. Int J Mol Sci, 2021. **22**(2).
188. Mukai, T., et al., *Facile Recoding of Selenocysteine in Nature*. Angew Chem Int Ed Engl, 2016. **55**(17): p. 5337-41.
189. Brocker, M.J., et al., *Recoding the genetic code with selenocysteine*. Angew Chem Int Ed Engl, 2014. **53**(1): p. 319-23.
190. Fu, X., D. Soll, and A. Sevostyanova, *Challenges of site-specific selenocysteine incorporation into proteins by Escherichia coli*. RNA Biol, 2018. **15**(4-5): p. 461-470.

191. Arner, E.S., et al., *High-level expression in Escherichia coli of selenocysteine-containing rat thioredoxin reductase utilizing gene fusions with engineered bacterial-type SECIS elements and co-expression with the selA, selB and selC genes*. J Mol Biol, 1999. **292**(5): p. 1003-16.
192. Wright, D.E., et al., *Acetylation Regulates Thioredoxin Reductase Oligomerization and Activity*. Antioxid Redox Signal, 2018. **29**(4): p. 377-388.
193. Jiang, Z., et al., *Expression of selenocysteine-containing glutathione S-transferase in Escherichia coli*. Biochem Biophys Res Commun, 2004. **321**(1): p. 94-101.
194. Kim, H.Y. and V.N. Gladyshev, *Methionine sulfoxide reduction in mammals: characterization of methionine-R-sulfoxide reductases*. Mol Biol Cell, 2004. **15**(3): p. 1055-64.
195. Hoffman, K.S., et al., *Recoding UAG to selenocysteine in Saccharomyces cerevisiae*. RNA, 2023.
196. Hatfield, D.L., et al., *Selenium and selenocysteine: roles in cancer, health, and development*. Trends Biochem Sci, 2014. **39**(3): p. 112-20.
197. Labunskyy, V.M., D.L. Hatfield, and V.N. Gladyshev, *Selenoproteins: molecular pathways and physiological roles*. Physiol Rev, 2014. **94**(3): p. 739-77.
198. Johansson, L., G. Gafvelin, and E.S. Arner, *Selenocysteine in proteins-properties and biotechnological use*. Biochim Biophys Acta, 2005. **1726**(1): p. 1-13.
199. Arner, E.S., *Selenoproteins-What unique properties can arise with selenocysteine in place of cysteine?* Exp Cell Res, 2010. **316**(8): p. 1296-303.
200. Zhong, L. and A. Holmgren, *Essential role of selenium in the catalytic activities of mammalian thioredoxin reductase revealed by characterization of recombinant enzymes with selenocysteine mutations*. J Biol Chem, 2000. **275**(24): p. 18121-8.
201. Lee, S.R., et al., *Mammalian thioredoxin reductase: oxidation of the C-terminal cysteine/selenocysteine active site forms a thioselenide, and replacement of selenium with sulfur markedly reduces catalytic activity*. Proc Natl Acad Sci U S A, 2000. **97**(6): p. 2521-6.
202. Scalcon, V., A. Bindoli, and M.P. Rigobello, *Significance of the mitochondrial thioredoxin reductase in cancer cells: An update on role, targets and inhibitors*. Free Radic Biol Med, 2018. **127**: p. 62-79.
203. Zhang, J., et al., *Small molecule inhibitors of mammalian thioredoxin reductase as potential anticancer agents: An update*. Med Res Rev, 2019. **39**(1): p. 5-39.
204. Yang, Y., et al., *Piperlongumine Inhibits Thioredoxin Reductase 1 by Targeting Selenocysteine Residues and Sensitizes Cancer Cells to Erastin*. Antioxidants (Basel), 2022. **11**(4).
205. Urig, S. and K. Becker, *On the potential of thioredoxin reductase inhibitors for cancer therapy*. Semin Cancer Biol, 2006. **16**(6): p. 452-65.
206. Gromer, S., S. Urig, and K. Becker, *The thioredoxin system--from science to clinic*. Med Res Rev, 2004. **24**(1): p. 40-89.
207. Onodera, T., I. Momose, and M. Kawada, *Potential Anticancer Activity of Auranofin*. Chem Pharm Bull (Tokyo), 2019. **67**(3): p. 186-191.
208. Hirt, R.P., et al., *The diversity and evolution of thioredoxin reductase: new perspectives*. Trends Parasitol, 2002. **18**(7): p. 302-8.
209. Geigenberger, P., et al., *The Unprecedented Versatility of the Plant Thioredoxin System*. Trends Plant Sci, 2017. **22**(3): p. 249-262.



210. Schieber, M. and N.S. Chandel, *ROS function in redox signaling and oxidative stress*. *Curr Biol*, 2014. **24**(10): p. R453-62.
211. Lu, J. and A. Holmgren, *The thioredoxin antioxidant system*. *Free Radic Biol Med*, 2014. **66**: p. 75-87.
212. Tamura, T. and T.C. Stadtman, *A new selenoprotein from human lung adenocarcinoma cells: purification, properties, and thioredoxin reductase activity*. *Proc Natl Acad Sci U S A*, 1996. **93**(3): p. 1006-11.
213. Luthman, M. and A. Holmgren, *Rat liver thioredoxin and thioredoxin reductase: purification and characterization*. *Biochemistry*, 1982. **21**(26): p. 6628-33.
214. Arner, E.S., L. Zhong, and A. Holmgren, *Preparation and assay of mammalian thioredoxin and thioredoxin reductase*. *Methods Enzymol*, 1999. **300**: p. 226-39.
215. Chae, H.Z., et al., *Characterization of three isoforms of mammalian peroxiredoxin that reduce peroxides in the presence of thioredoxin*. *Diabetes Res Clin Pract*, 1999. **45**(2-3): p. 101-12.
216. Wood, Z.A., et al., *Structure, mechanism and regulation of peroxiredoxins*. *Trends Biochem Sci*, 2003. **28**(1): p. 32-40.
217. Kang, S.W., et al., *Mammalian peroxiredoxin isoforms can reduce hydrogen peroxide generated in response to growth factors and tumor necrosis factor- $\alpha$* . *J Biol Chem*, 1998. **273**(11): p. 6297-302.
218. Dubuisson, M., et al., *Human peroxiredoxin 5 is a peroxynitrite reductase*. *FEBS Lett*, 2004. **571**(1-3): p. 161-5.
219. Chae, H.Z., et al., *Cloning and sequencing of thiol-specific antioxidant from mammalian brain: alkyl hydroperoxide reductase and thiol-specific antioxidant define a large family of antioxidant enzymes*. *Proc Natl Acad Sci U S A*, 1994. **91**(15): p. 7017-21.
220. Peshenko, I.V. and H. Shichi, *Oxidation of active center cysteine of bovine 1-Cys peroxiredoxin to the cysteine sulfenic acid form by peroxide and peroxynitrite*. *Free Radic Biol Med*, 2001. **31**(3): p. 292-303.
221. Bjornstedt, M., et al., *Human thioredoxin reductase directly reduces lipid hydroperoxides by NADPH and selenocystine strongly stimulates the reaction via catalytically generated selenols*. *J Biol Chem*, 1995. **270**(20): p. 11761-4.
222. Das, K.C. and C.K. Das, *Thioredoxin, a singlet oxygen quencher and hydroxyl radical scavenger: redox independent functions*. *Biochem Biophys Res Commun*, 2000. **277**(2): p. 443-7.
223. Holmgren, A. and J. Lu, *Thioredoxin and thioredoxin reductase: current research with special reference to human disease*. *Biochem Biophys Res Commun*, 2010. **396**(1): p. 120-4.
224. Lu, J. and A. Holmgren, *Thioredoxin system in cell death progression*. *Antioxid Redox Signal*, 2012. **17**(12): p. 1738-47.
225. Zhang, Y., et al., *Role of Selenoproteins in Redox Regulation of Signaling and the Antioxidant System: A Review*. *Antioxidants (Basel)*, 2020. **9**(5).
226. Arner, E.S., *Focus on mammalian thioredoxin reductases--important selenoproteins with versatile functions*. *Biochim Biophys Acta*, 2009. **1790**(6): p. 495-526.
227. Mahmood, D.F., et al., *The thioredoxin system as a therapeutic target in human health and disease*. *Antioxid Redox Signal*, 2013. **19**(11): p. 1266-303.

228. Liu, Y., et al., *Role of Thioredoxin-1 and its inducers in human health and diseases*. Eur J Pharmacol, 2022. **919**: p. 174756.
229. Lillig, C.H. and A. Holmgren, *Thioredoxin and related molecules--from biology to health and disease*. Antioxid Redox Signal, 2007. **9**(1): p. 25-47.
230. Lovell, M.A., et al., *Decreased thioredoxin and increased thioredoxin reductase levels in Alzheimer's disease brain*. Free Radic Biol Med, 2000. **28**(3): p. 418-27.
231. Maurice, M.M., et al., *Expression of the thioredoxin-thioredoxin reductase system in the inflamed joints of patients with rheumatoid arthritis*. Arthritis Rheum, 1999. **42**(11): p. 2430-9.
232. Yamada, Y., et al., *Elevated serum levels of thioredoxin in patients with acute exacerbation of asthma*. Immunol Lett, 2003. **86**(2): p. 199-205.
233. Whayne, T.F., Jr., N. Parinandi, and N. Maulik, *Thioredoxins in cardiovascular disease*. Can J Physiol Pharmacol, 2015. **93**(11): p. 903-11.
234. Soini, Y., et al., *Widespread expression of thioredoxin and thioredoxin reductase in non-small cell lung carcinoma*. Clin Cancer Res, 2001. **7**(6): p. 1750-7.
235. Lichtenfels, R., et al., *Identification of metabolic enzymes in renal cell carcinoma utilizing PROTEOMEX analyses*. Biochim Biophys Acta, 2003. **1646**(1-2): p. 21-31.
236. Lincoln, D.T., et al., *Thioredoxin and thioredoxin reductase expression in thyroid cancer depends on tumour aggressiveness*. Anticancer Res, 2010. **30**(3): p. 767-75.
237. Hedley, D., et al., *Up-regulation of the redox mediators thioredoxin and apurinic/aprimidinic excision (APE)/Ref-1 in hypoxic microregions of invasive cervical carcinomas, mapped using multispectral, wide-field fluorescence image analysis*. Am J Pathol, 2004. **164**(2): p. 557-65.
238. Raffel, J., et al., *Increased expression of thioredoxin-1 in human colorectal cancer is associated with decreased patient survival*. J Lab Clin Med, 2003. **142**(1): p. 46-51.
239. Jia, J.J., et al., *The role of thioredoxin system in cancer: strategy for cancer therapy*. Cancer Chemother Pharmacol, 2019. **84**(3): p. 453-470.
240. Roh, J.L., et al., *Targeting of the Glutathione, Thioredoxin, and Nrf2 Antioxidant Systems in Head and Neck Cancer*. Antioxid Redox Signal, 2017. **27**(2): p. 106-114.
241. Selenius, M., et al., *Selenium and the selenoprotein thioredoxin reductase in the prevention, treatment and diagnostics of cancer*. Antioxid Redox Signal, 2010. **12**(7): p. 867-80.
242. Dong, C., et al., *Role of thioredoxin reductase 1 in dysplastic transformation of human breast epithelial cells triggered by chronic oxidative stress*. Sci Rep, 2016. **6**: p. 36860.
243. Wang, L., et al., *Ethaselen: a potent mammalian thioredoxin reductase 1 inhibitor and novel organoselenium anticancer agent*. Free Radic Biol Med, 2012. **52**(5): p. 898-908.
244. Lamoke, F., et al., *Loss of thioredoxin function in retinas of mice overexpressing amyloid beta*. Free Radic Biol Med, 2012. **53**(3): p. 577-88.

245. Banerjee Mustafi, S., et al., *Aggregate-prone R120GCRYAB triggers multifaceted modifications of the thioredoxin system*. *Antioxid Redox Signal*, 2014. **20**(18): p. 2891-906.
246. Choudhary, C., et al., *Lysine acetylation targets protein complexes and co-regulates major cellular functions*. *Science*, 2009. **325**(5942): p. 834-40.
247. Hornbeck, P.V., et al., *PhosphoSitePlus, 2014: mutations, PTMs and recalibrations*. *Nucleic Acids Res*, 2015. **43**(Database issue): p. D512-20.
248. Weinert, B.T., et al., *Lysine succinylation is a frequently occurring modification in prokaryotes and eukaryotes and extensively overlaps with acetylation*. *Cell Rep*, 2013. **4**(4): p. 842-51.
249. Wright, D.E., N. Panaseiko, and P. O'Donoghue, *Acetylated Thioredoxin Reductase 1 Resists Oxidative Inactivation*. *Front Chem*, 2021. **9**: p. 747236.
250. Wright, D.E., et al., *Delivery of the selenoprotein thioredoxin reductase 1 to mammalian cells*. *Front Mol Biosci*, 2022. **9**: p. 1031756.

## Chapter 2

### 2. Acetylation Regulates Thioredoxin Reductase

#### Oligomerization and Activity

##### 2.1. Introduction

Human cells naturally defend against reactive oxygen species (ROS) using a network of redox enzymes including the selenoprotein thioredoxin reductase 1 (TrxR1) [1]. Selenoproteins contain the 21<sup>st</sup> genetically encoded amino acid, selenocysteine (Sec). In cells, the Sec550 residue in TrxR1 is required for most of its activity [2] in reducing oxidized compounds, e.g., ubiquinone [3], and oxidatively damaged cellular proteins via a redox coupled reaction with thioredoxin (Trx). TrxR1 catalyzes the transfer of electrons from NADPH to Trx1. The reduced Trx1 in turn resolves oxidized species and reduces cellular proteins. The resulting oxidized Trx1 is then recycled by the TrxR1 enzyme. In addition to ROS defense, the Trx system is involved in regulating gene expression, embryonic development, cell proliferation, and apoptosis [4].

Overactive TrxR1 is associated with chemotherapeutic resistance, and TrxR1 activity is co-opted by cancer cells to defend against ROS generated by therapeutic compounds [5]. TrxR1 activity levels are diagnostic for early detection of lung [6] and breast cancers [7], and TrxR1 has emerged as a target to combat drug resistant lung cancers, e.g., etaselen [8]. In mouse models of age-related macular degeneration and glaucoma, overexpression of amyloid  $\beta$  was associated with increased TrxR1 activity despite unperturbed TrxR1 protein abundance, implicating posttranslational modifications in regulating TrxR1 activity [9]. Differential total TrxR activity and changes in TrxR1 acetylation status were also associated with a cardiomyopathy phenotype in transgenic mice [10] and in retinal tissue from diabetic rat models and human post-mortem patient

samples [11]. TrxR1 is acetylated on at least 3 specific sites on the protein surface that have been experimentally identified in humans and mice [12-14].

Due to the emerging association of TrxR1 acetylation, cellular redox status and disease, we investigated how acetylation signaling modulates TrxR1 activity. Because the acetyl transferase(s) that acetylate TrxR1 in the cell are unknown, it was not possible to produce site-specifically acetylated TrxR1 variants using an upstream enzyme or from expression in human cell culture. We overcame this barrier by using two genetic code expansion systems (Fig 2.1) that enabled co-translational incorporation of both Sec and  $N_\epsilon$ -acetyl-lysine (acK) residues at specific sites, resulting in site-specifically acetylated and differentially active human TrxR1 selenoprotein variants.

## 2.2. Results

To biochemically characterize the impact of site-specific acetylation on the reduction activity of TrxR1, we produced TrxR1 variants in *Escherichia coli* with 22 different genetically encoded amino acids, including the non-canonical amino acids (ncAAs) acK and Sec (Fig 2.1). The data show, for the first time, that we produced protein with 22 different amino acids with equal efficiency and fidelity to protein production with the 20 standard amino acids (Table 2.1).

### 2.2.1. *E. coli* Host Strain Alters Expression of TrxR1 with 22 Amino Acids.

We combined two genetic code expansion systems in *E. coli* to produce site-specifically acetylated TrxR1 variants (Fig 2.1). We reassigned UAG codons from stop to acK using a mutant UAG-decoding pyrrolysyl-tRNA synthetase known as  $N_\epsilon$ -acetyl-lysyl-tRNA synthetase (acKRS) and tRNA<sup>Py1</sup> pair [15], and we simultaneously recoded a specified UGA codon from stop to Sec with the native *E. coli* Sec insertion system (Fig 2.1). We

produced and purified wild type (WT) TrxR1 with Sec at position 550, and 3 site-specifically acetylated TrxR1 (acTrxR1) variants (acTrxR1<sup>K141</sup>, acTrxR1<sup>K200</sup>, and acTrxR1<sup>K307</sup>) (Fig S2.1). Production of these protein variants required the two-plasmid system depicted in Fig 2.1 and described in Methods.

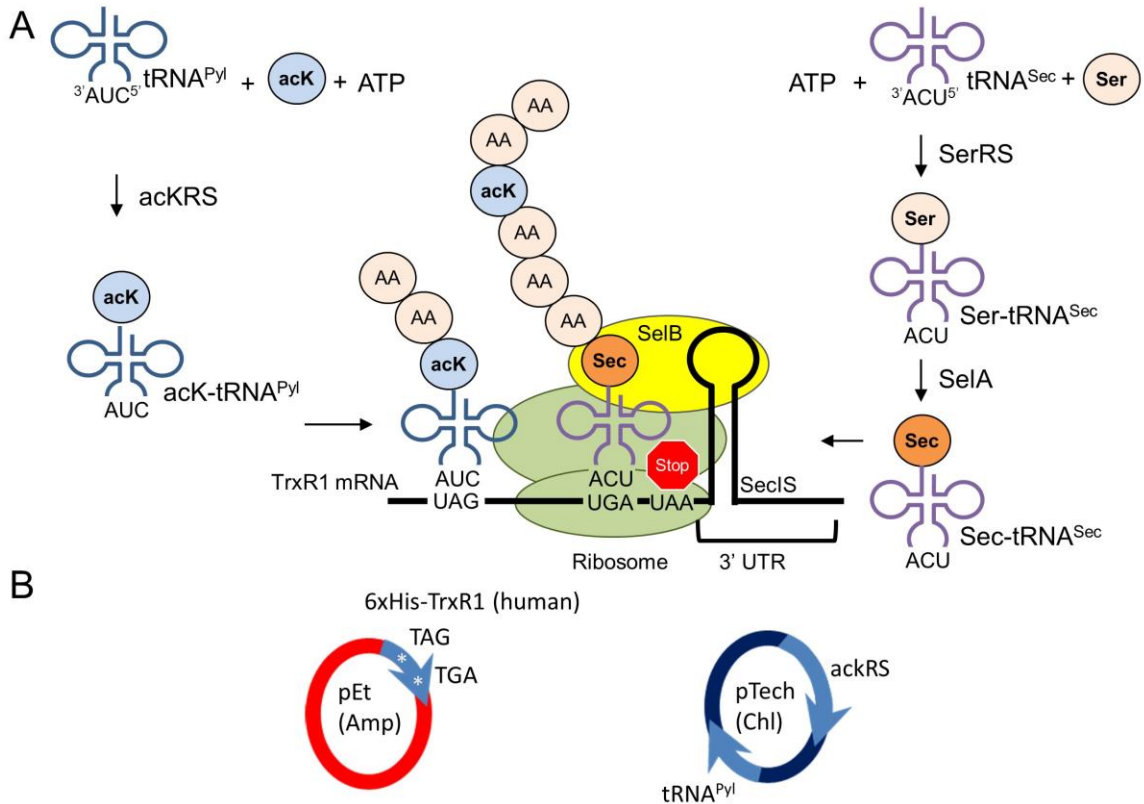


**Figure 2.1. Schematic for genetically encoding 22 amino acids.** (A) Genetically encoding acK and Sec:  $\text{ackRS}$  ligates acK to  $\text{tRNA}^{\text{Pyl}}$ , which reassigns all UAG stop codons to acK. This allows insertion of acK at a specific UAG codon in TrxR1. For Sec insertion,  $\text{tRNA}^{\text{Sec}}$  is aminoacylated with serine (Ser) by seryl-tRNA synthetase (SerRS), followed by conversion of Ser-tRNA to Sec-tRNA by selenocysteine synthase (SelA). The elongation factor SelB binds  $\text{Sec-tRNA}^{\text{Sec}}$  as well as the Sec Insertion Sequence (SecIS), which we designed into the 3' UTR of the TrxR1 mRNA. The SecIS localizes  $\text{Sec-tRNA}^{\text{Sec}}$  at the UGA codon, allowing for Sec insertion at a single UGA stop codon. (B) The two-plasmid system used for production of acetylated TrxR1: the pTech vector expresses  $\text{ackRS}$  and  $\text{tRNA}^{\text{Pyl}}$ , required for reassignment of UAG codons to acK. The pET vector expresses TrxR1 with a TAG at the desired acetylation sites (141, 200, or 307), as well as SecIS in the 3' UTR (see methods). In this system, UAG genetically encodes acK, while SecIS following down-stream of the UGA codon is required for Sec insertion. The Sec synthesis and insertion system is endogenous to *E. coli*, encoded in the *E. coli* genome (SelA, SelB, SelC, SelD, SerRS).

We tested the expression of TrxR1 and acTrxR1 variants in *E. coli* BL21 DE3 and in an *E. coli* strain (C321.ΔA.exp) that lacks release factor 1 (RF1) and all genome encoded UAG codons (*E. coli* ΔRF1) [16]. RF1 terminates translation at UAG. *E. coli* ΔRF1 should allow for more efficient reassignment of UAG to acK, since there is less competition between acK-tRNA<sup>PyI</sup> and RF1 for binding UAG. With the acK incorporation system (Fig 2.1A), we demonstrated efficient UAG read-through per cell using a green fluorescent protein (GFP) reporter in *E. coli* ΔRF1 (Fig S2.2). Unfortunately, and concordant with our previous work [17], the *E. coli* ΔRF1 strain produces significantly less recombinant TrxR1 (Table 2.1) due to phenotypic defects resulting in slow growth and markedly reduced cell densities [16, 17]. Potential benefits from RF1 deletion are subsumed by the more efficient protein producing strain BL21, which produces more overall UAG translation per 1 *E. coli* culture.

Fascinatingly, BL21 protein production efficiency was indistinguishable (2-2.6 mg/l culture) for variants of TrxR1 containing 20 (Sec550Tyr), 21 (wildtype, WT), or 22 (acTrxR1<sup>K200</sup>) genetically encoded amino acids (Table 2.1). In BL21, we observed yields for protein containing 22 genetically encoded amino acids of up to 2.6 mg/l culture, whereas the *E. coli* ΔRF1 showed a maximal protein production of 0.6 mg/l culture. BL21 produced 1.2 to 5-fold more TrxR1 or acTrxR1 compared to *E. coli* ΔRF1 (Table 2.1).

### **2.2.2. Physical Characterization of TrxR1 Variants.**

We confirmed insertion of Sec and acK into the same protein variants by multiple independent mass spectroscopic methods. Independent mass spectrometry (MS) techniques confirmed quantitative incorporation of Sec and/or acK in each TrxR1 variant (Fig 2.2, Fig S2.3, S2.4, S2.5, S2.6). Matrix-assisted laser desorption/ionization mass spectrometry (MALDI MS) analysis of the acTrxR1 variants confirmed site-specific acetylation at each of the anticipated sites (Fig S2.3) and verified Sec incorporation in WT TrxR1 (Fig S2.4). Additionally, we found no evidence of de-acetylation in the MALDI MS

**Table 2.1. TrxR1 and acTrxR1 protein yields and activity.**

TrxR1 variant	$\Delta$ RF1 protein yield (mg/L)	BL21 protein yield (mg/L)	DTNB assay		9,10-phenanthrequinone assay		Insulin linked Trx1 assay	
			Initial velocity (pmol TNB/s)	Relative activity (x-fold)	Initial velocity (pmol NADPH consumed/s)	Relative activity (x-fold)	Initial velocity (pmol NADPH consumed/s)	Relative activity (x-fold)
WT TrxR1	0.4	2.4	0.24 $\pm$ 0.01	1.0	1.23 $\pm$ 0.03	1.0	0.22 $\pm$ 0.02	1.0
acTrxR1 <sup>K141</sup>	0.4	0.7	0.42 $\pm$ 0.03	1.8	1.53 $\pm$ 0.05	1.2	0.41 $\pm$ 0.01	1.8
acTrxR1 <sup>K200</sup>	0.5	2.6	0.49 $\pm$ 0.01	2.1	1.78 $\pm$ 0.14	1.4	0.42 $\pm$ 0.01	1.9
acTrxR1 <sup>K307</sup>	0.6	0.7	0.64 $\pm$ 0.07	2.7	1.61 $\pm$ 0.08	1.3	0.43 $\pm$ 0.01	2.0
TrxR1 <sup>Sec550Tyr</sup> (inactive)	n.d.	2.1	n.d.	-	-	-	n.d.	-

Protein yield was measured using the Bradford assay and noted above in mg of TrxR1 produced per liter of *E. coli* culture from the indicated strain. TrxR1 growth and purification conditions are indicated in Methods section. Initial velocity for the TrxR1 variants on each substrate was calculated from the data shown in Fig 2 (Fig 2A for the DTNB assay, Fig 2B for the 9,10-phenanthrequinone assay, and Fig 2C for the insulin linked Trx1 assay). The relative activity of the TrxR1 variants for each substrate was calculated by setting the velocity (TNB/sec or NADPH consumed/sec) of WT TrxR1 to 1 (Fig 2D).

n.d. – not determined

data (Fig S2.3). To verify Sec incorporation, and to determine the number of active molecules in each sample, we quantified the amount of selenium (Se) in the TrxR1 variants. Because Sec is required for TrxR1 activity, the amount of Se covalently bound to the protein indicates the amount of active TrxR1. Inductively coupled plasma mass spectrometry (ICP-MS) verified quantitative insertion of Sec in the TrxR1 variants (Table S2.1). LC-MS/MS revealed acK incorporation (Fig 2.2, Fig S2.6) and Sec incorporation (Fig 2.2, Fig S2.5) at the desired locations for acTrxR1<sup>K141</sup> (Fig S2.5B, S2.6A), acTrxR1<sup>K200</sup> (Fig 2.2), and acTrxR1<sup>K307</sup> (Fig S2.5C, S2.6B) as well as Sec incorporation



for WT TrxR1 (Fig S2.5A). In each MS experiment, we were unable to detect deacetylation or mistranslation at the UAG or UGA encoded loci.

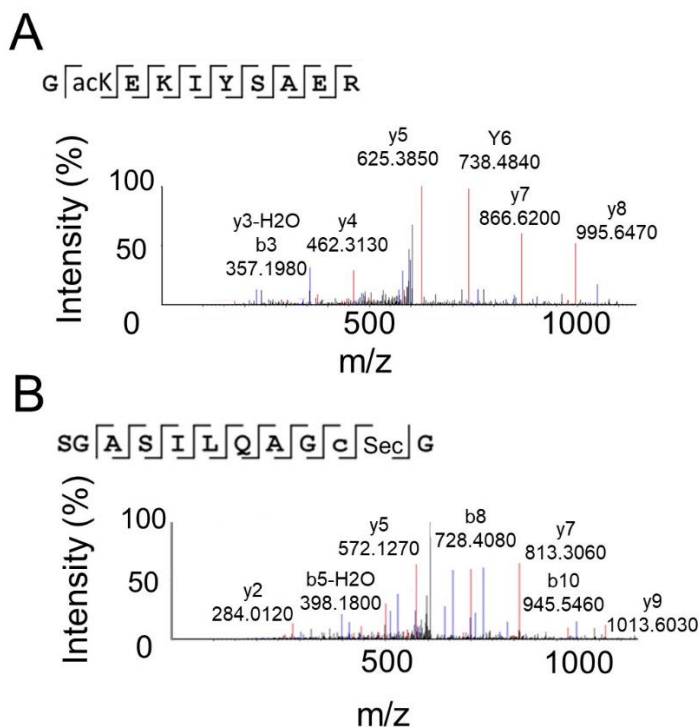


**Figure 2.2. Physical identification of acK and Sec in acTrxR1<sup>K200</sup>.** MS data for other TrxR1 variants is shown in Figs S2.3-S2.6. Liquid chromatography mass spectrometry/mass spectrometry (LC-MS/MS) of polypeptides from trypsin digested acTrxR1<sup>K200</sup>, demonstrating (A) acK and (B) Sec incorporation at the desired locations.

### 2.2.3. Reversible Activation of TrxR1.

The enzymatic activity of TrxR1 was assessed on three substrates: 5,5'-Dithiobis-(2-nitrobenzoic acid) (DTNB), 9,10-phenanthroquinone, and thioredoxin 1 (Trx1) in an insulin coupled assay [18]. DTNB is a long established artificial substrate for TrxR1 [18], while 9,10-phenanthroquinone and the Trx1 insulin linked assays are dependent on the presence of Sec in TrxR1 [19]. DTNB and the quinone assays measure TrxR1 reduction activity directly, while the insulin linked assay also includes Trx1 and recapitulates a model TrxR1 redox pathway *in vitro*.

In comparison to WT TrxR1, each acTrxR1 variant had statistically significantly higher activity on all substrates tested (Fig 2.3, Table 2.1). acTrxR1<sup>K307</sup> was most active on DTNB assays, while acTrxR1<sup>K200</sup> showed the highest activity on the quinone substrate (Fig 2.3D, Table 2.1), suggesting acetylation may affect TrxR1 substrate preference. Although TrxR1 lacking the Sec residue is still active with DTNB at a low level, 9,10-phenanthrenequinone reduction by TrxR1 is Sec-dependent [20]. We observed that a disabled

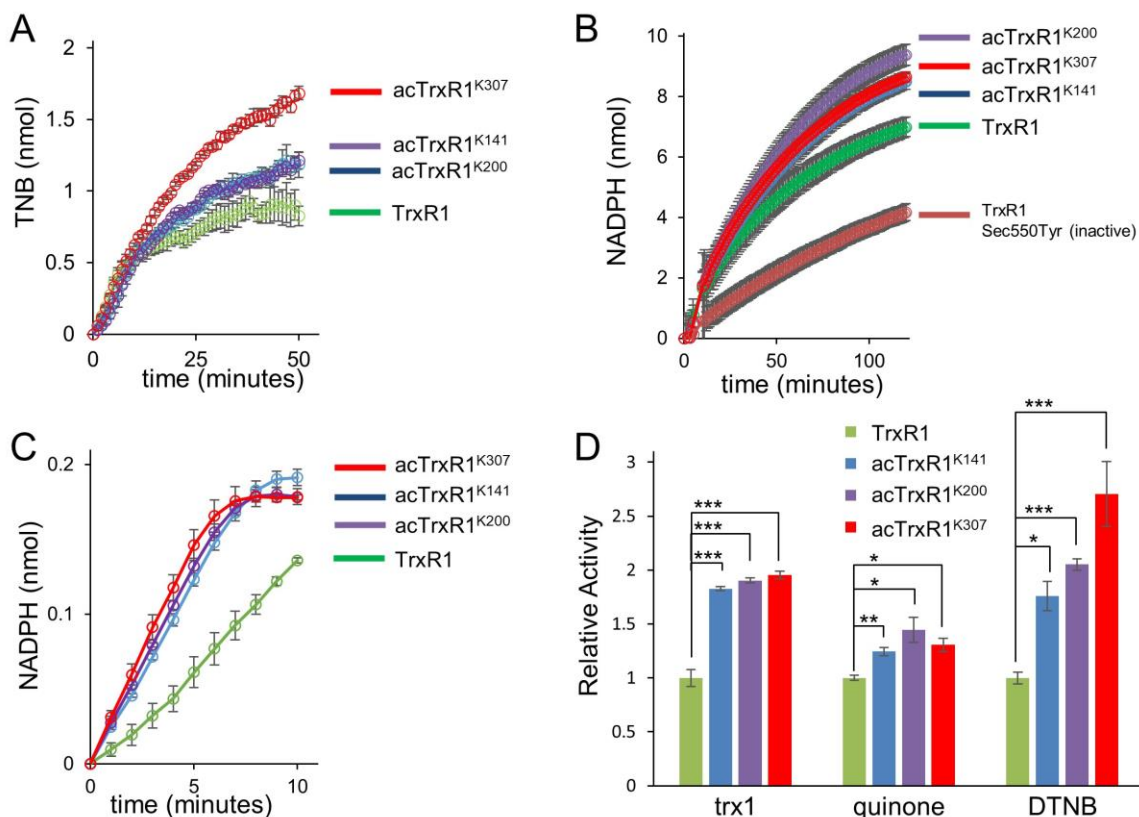


**Figure 2.3. Activity of TrxR1 and acTrxR1 variants.** *In vitro* activity assay of WT and acTrxR1 variants using a colorimetric (A) DTNB reduction assay measuring TNB production (412 nm) with 50 nM of each TrxR1 variant, (B) a 9,10-Phenanthrenequinone reduction assay with 100 nM of each TrxR1 variant monitoring NADPH depletion (340 nm), or (C) a Trx1-insulin linked assay using 200 nM of TrxR1 and 6  $\mu$ M Trx1 monitoring NADPH depletion (340 nm). In the Trx1-insulin linked assay, TrxR1 reduces Trx1, which then reduces insulin before being reduced again by TrxR1. (D) The relative activity of the TrxR1 variants for each substrate, where the velocity (TNB/sec or NADPH consumed/sec) of WT TrxR1 is set to 1. These velocities were calculated from the data shown (A-C). (\* indicates a  $p < 0.05$ , \*\*  $p$ -value  $< 0.01$ , \*\*\*  $p$ -value  $< 0.005$ .) Error bars represent one standard deviation based on triplicate measurements. A no enzyme control has been subtracted from all enzyme assays shown.

TrxR1 variant (Sec550Tyr) shows basal activity in the quinone assay (Fig 2.3B). In agreement with the MS data, the activity data demonstrate WT and acTrxR1s all contain Sec (Fig 2.3B). Co-translational incorporation of acK had no apparent effect on the proper folding of the enzyme (Fig 2.4).

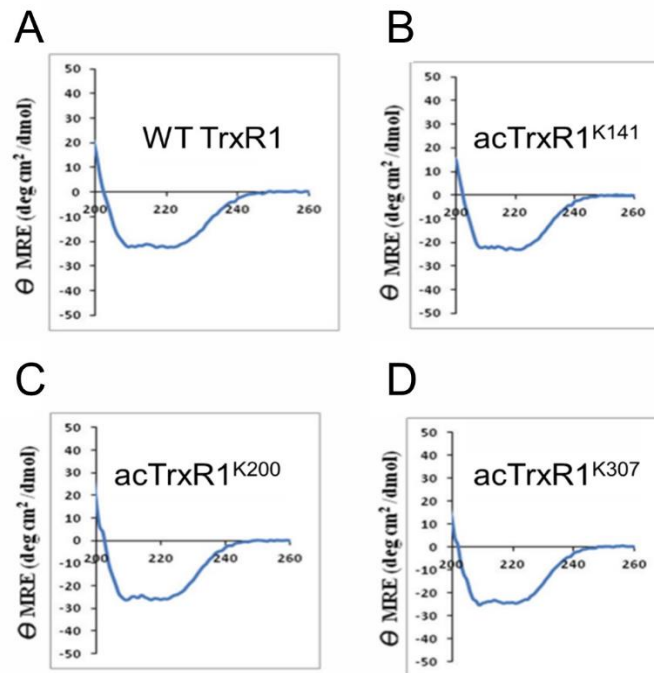


**Figure 2.4. Circular dichroism (CD) spectra of TrxR1 variants.** CD spectra demonstrates properly folded WT TrxR1 and acTrxR1 variants, indicating no changes in protein folding caused by co-translational incorporation of acK. Data are collected in units of mean residue ellipticity (in deg cm<sup>2</sup>/dmol).

We performed a series of TrxR1 activity assays with or without pre-incubation with histone deacetylase 3 (HDAC3). HDAC3 decreased the activity of the acTrxR1<sup>K141</sup> and acTrxR1<sup>K307</sup> variants to WT TrxR1 levels, but HDAC3 did not alter WT TrxR1 activity (Fig 2.5). HDAC3 caused a slight decrease in the activity of acTrxR1<sup>K200</sup>, but this decrease was at the borderline of statistical significance (Fig 2.5). Although not evident in the MS data, these data suggest acTrxR1<sup>K200</sup> may be either partially de-acetylated or perhaps less accessible to HDAC3. The data show conclusively that acetylation is a reversible

mechanism to enhance TrxR1 activity at sites K141 and K307. A single acetylation at K307 leads to 2.7-fold increased TrxR1 activity (Fig 2.3, Table 2.1).

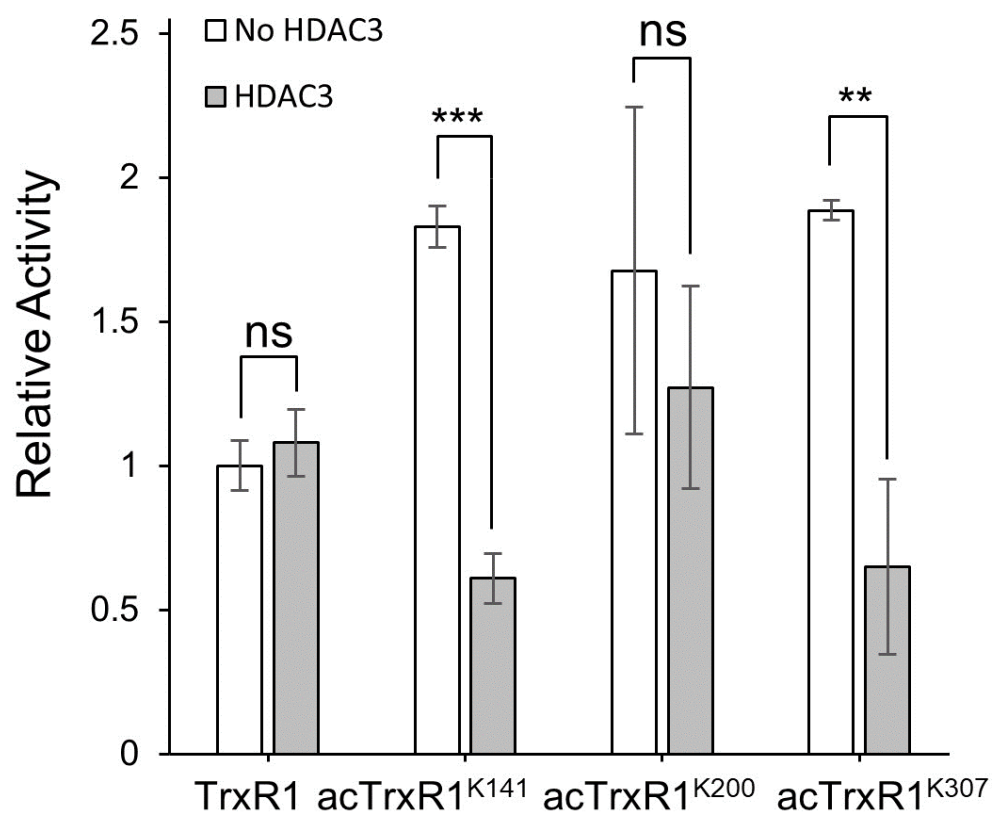


**Figure 2.5. Effect of histone deacetylase on TrxR1 variants.** The *in vitro* activity of TrxR1 variants, using 3.75 nM TrxR1 incubated with or without HDAC3, was measured by monitoring TNB production (412 nm). The relative activity for each variant incubated with (filled bars) or without (open bars) HDAC3, where the initial velocity of unacetylated TrxR1 incubated without HDAC3 is set to 1. Error bars represent one standard deviation (\* indicates a  $p < 0.05$ , \*\*  $p$ -value  $< 0.01$ , \*\*\*  $p$ -value  $< 0.005$ , ns - not significant). All error bars represent one standard deviation of triplicate measurements.

#### 2.2.4. Acetylation Alters TrxR1 Quaternary Structure.

In solution, catalytically active dimeric TrxR1 exists in equilibrium with inactive tetramers and higher order multimers [20]. A structure of the TrxR1 tetramer [20] revealed that all 3 lysine acetylation sites are localized at the dimer-dimer interface (Fig 2.6, PBD 4KPR [20] and 3EAN [21]). In fact, acetylation will interfere with charge balanced hydrogen bond networks of glutamate or aspartate and lysine residues lining the tetramer interface (Fig

2.6B, C). Acetylation at K141 disrupts a symmetrical hydrogen bond network at the core of the dimer-dimer interface between K141 and E143 (Fig 2.6B). Additionally, acetylation at K200 or K307 likely perturbs a distinct and extensive hydrogen bond and salt bridge network between glutamate and lysine residues at the edges of the tetramer (Fig 2.6C). In fact, a recent report identified acetylation at K147, which is also located in the TrxR1 dimer-dimer interface, in human lung treated with the HDAC inhibitor suberoylanilide hydroxamic acid (52).

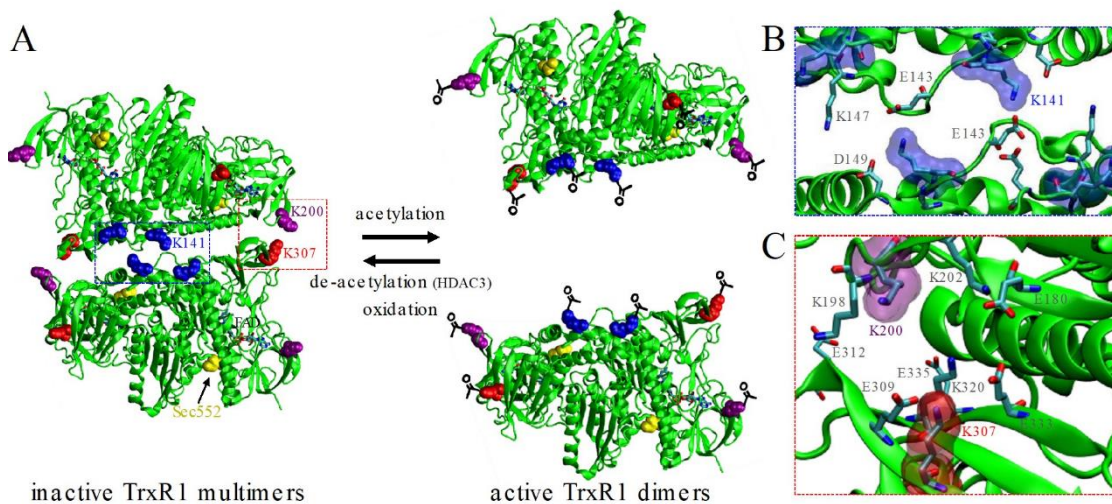


**Figure 2.6. Mechanistic basis for acetylation-dependent enhanced TrxR1 activity.** (A) Acetylation of K141 (blue), K200 (purple) or K307 (red) on the surface of TrxR1 dimers interferes with salt bridges and hydrogen bonds (B-C) in the TrxR1 tetramer interface. Close up view of the interactions at the tetramer interface with (B) K141, (C), K200 and K307 (PBD: 4KPR (39) and 3EAN (5)).

Catalytically active TrxR1 dimers were separated from low activity monomers and tetramers for each TrxR1 variant by native size exclusion chromatography (Fig 2.7). DTNB activity assays demonstrated the TrxR1 variants were successfully separated. In agreement with a previous study on the role of Trp114 oxidation in driving TrxR1 tetramer formation [20], the highest activity fractions contained dimers, while fractions containing monomers or tetramers showed markedly reduced activity (Fig 2.7B). The oxidation of Trp114 also leads to a covalent linkage between two TrxR1 monomers [20], forming a non-productive and covalently linked dimer. As evident in the Western blot (Fig 2.7), we observed fewer

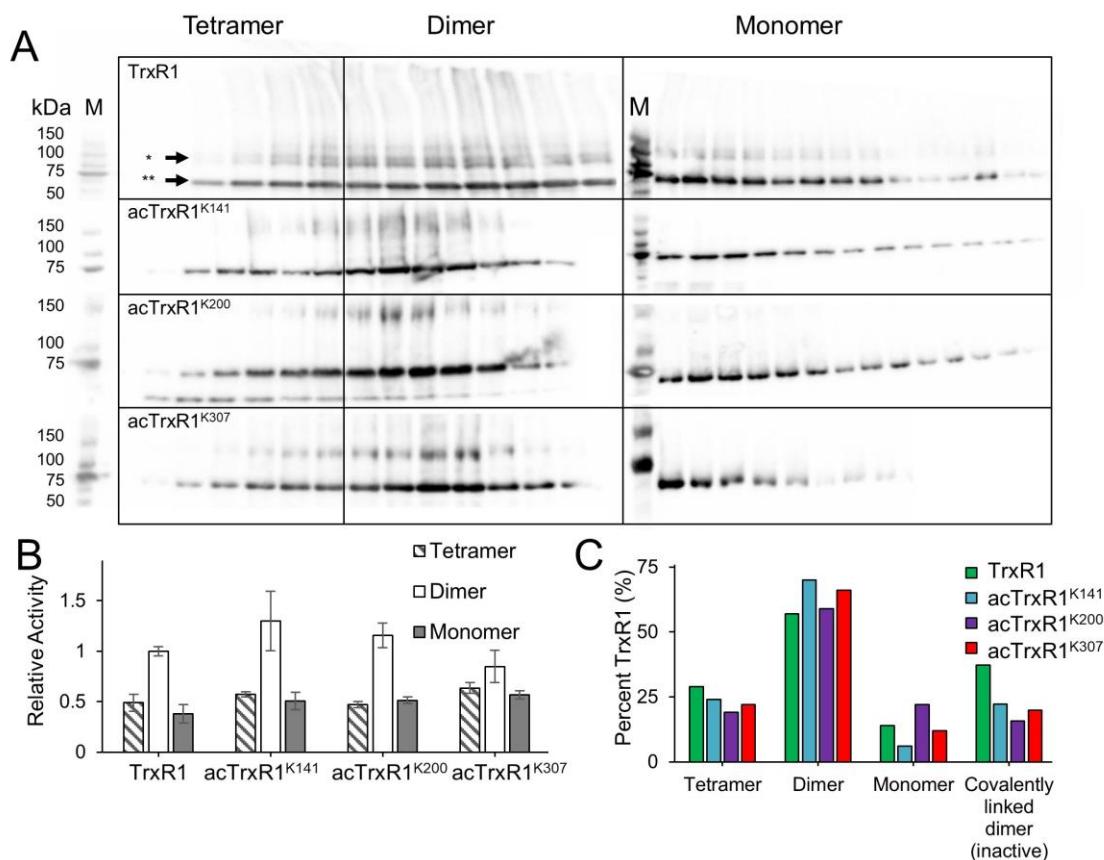


**Figure 2.7. Characterization of WT TrxR1 and acTrxR1 oligomerization.**

(A) Different oligomeric states of the TrxR1 variants were separated in native conditions on a size exclusion column. His<sub>6</sub>-TrxR1 present in the fractions was visualized by Western blotting (anti-His). Arrows indicate TrxR1 subunits (\*) or covalently linked and non-productive TrxR1 dimers (\*\*) formed during tetramerization. M indicates a molecular weight marker. (B) DTNB activity assays (100 nM TrxR1) demonstrated that high activity dimers were successfully separated from low activity tetramers and monomers. Relative activity is based on initial velocity (TNB/sec), where the unacetylated dimer is set to 1. Error bars represent one standard deviation based on triplicate experiments. (C) The percent of TrxR1 existing as dimers, tetramers, monomers, or covalently linked inactive dimers was plotted for each TrxR1 variant. Percentages are calculated based on densitometry of the Western blot (A).

covalently linked inactive TrxR1 subunits in the acetylated TrxR1 variants compared to WT TrxR1 (Fig 2.7A, C). Western blot analysis of the fractions confirms that a larger fraction of the acTrxR1s eluted as catalytically active dimers compared to WT TrxR1 (Fig 2.7C, Table S2.2). The data further suggest that the acTrxR1 and WT TrxR1 dimer fraction

have similar activity (Fig 2.7B), and the increased activity observed in the bulk measurements (Fig 2.3) are attributable to the increased population of active dimers in acTrxR1, decreased tetramer formation in acTrxR1 (Fig 2.7C, Table S2.2), and decreased amounts of non-productive covalently linked dimer in acTrxR1 compared to WT TrxR1 (Fig 2.7C). The data suggest a novel mechanism (Fig 2.6), whereby acetylation reduces tetramer/multimer formation and promotes the formation of active TrxR1 dimers.

## **2.3. Discussion**

### **2.3.1. Acetylation Controls TrxR1 Structure and Activity.**

Lysine acetylation is found in all domains of life [23-25] with 36,000 acetylation sites identified in human, rat, and mouse cells [13, 14]. The human acetylome is enriched in proteins that form macromolecular complexes [13]. Acetylation of p53 blocks its oligomerization leading to nuclear export [26]. Histone acetylation prevents oligomerization, inhibiting chromatin condensation and increasing transcriptional activity [27]. Although not previously known for thioredoxin reductase, our data indicate that a similar mechanism may allow cells to control the pool of active molecules by suppressing TrxR1 oligomerization (Fig 2.6). Acetylation of TrxR1 may also counteract oxidative inactivation of the enzyme. Oxidative modification at Trp114 [20], centrally located in the dimer-dimer interface, was shown to reduce TrxR1 activity by promoting TrxR1 oligomerization, which represents a counter-acting mechanism relative to acetylation [20] (Fig 2.6). Indeed, the data suggest that TrxR1 acetylation may enable reactivation of oxidatively damaged TrxR1 multimers (Fig 2.7). Additionally, acetylation of the TrxR1 substrate, Trx1, increases the activity of Trx1 through a currently unknown mechanism [28]. Acetylation of another protein target of the Trx system, peroxiredoxin (Prx), prevents superoxidation of the Prx protein, increases its reduction activity, and prevents the formation of high molecular weight complexes with Prx and other proteins [29].

### **2.3.2. Relevance to Human Disease.**

The ability to regulate TrxR1 activity via acetylation will have relevance to major human diseases, including neurodegeneration, cancer, diabetes, and aging [30], which are characterized or complicated by elevated ROS. Decreased TrxR1 activity without changes in TrxR1 levels has been implicated in age-related macular degeneration and glaucoma resulting from overexpression of amyloid  $\beta$  peptides [9], indicating post-translational modifications control TrxR1 activity. Differential acetylation of TrxR1 was also documented in human cells [13] and in a mouse model of cardiomyopathy [10]. Initial findings have implicated TrxR1 regulation by de-acetylation in diabetes. In hyperglycemic rats, physical association with HDAC6 and decreased acetylation of TrxR1 correlated with reduced TrxR1 activity [11] in agreement with our data.

In several forms of cancer, TrxR1 expression and activity are used as diagnostic markers for early detection [6, 7]. As our data indicate, acetylation increases TrxR1 activity, and future work will include investigating TrxR1 acetylation as a potential diagnostic marker. Cells can overcome ROS generating cancer therapies and turn off apoptotic pathways by over-expressing TrxR1 [31]. Additionally, inhibiting the Trx system has been shown to increase the effectiveness of radiation therapy in treating some forms of breast cancer [32]. Oxidative stress is known to reduce TrxR1 activity by inducing tetramer formation [20]. Previous data suggest the cell responds to oxidative stress by acetylating TrxR1, perhaps enabling resistance to therapies that generate ROS [10]. We hypothesize that, in the cell, acetylation of TrxR1 reduces the oxidative stress induced tetramerization of TrxR1 [20] generated by radiation and chemotherapies [33]. Together these studies suggest that identifying and inhibiting TrxR acetylases may serve as another route to increase the effectiveness of cancer therapies.



### **2.3.3. Impacts of enhanced TrxR activity on cellular signaling.**

The Trx system is directly involved in cellular signaling linked to cell proliferation and viability [4]. A classic example includes the role of reduced Trx1 in inhibiting apoptosis. Reduced Trx1 inhibits apoptosis signal-regulating kinase (ASK1) by directly binding to the kinase [31]. Inhibition of TrxR with 1-chloro-2,4-dinitrobenzene in human embryonic kidney 293 (HEK293) cells activated ASK1 leading to apoptosis [31]. This provides a direct link between TrxR activity and its negative regulation of apoptosis. Additionally, Trx1 activity is involved in activating transcription factors involved in cell proliferation [4], such as nuclear factor- $\kappa$ B [34], and activator protein 1 [35]. We have definitively shown that acetylation increases the intrinsic activity of TrxR1 (Fig 2.3A, B) which leads to an increased rate of Trx1 reduction, thus increasing the activity of the Trx system in reduction of cellular targets, such as insulin (Fig 2.3C). Together these observations suggest acetylation signaling on TrxR1 may be involved in inhibiting apoptosis and regulating cell viability by increasing the overall activity of the Trx system.

### **2.3.4. Codon Recoding and Codon Reassignment Mechanisms are Mutually Orthogonal.**

Efficient protein production with more than 20 amino acids is a major challenge in the area of genetic code expansion. Protein production at 1.5 mg/l culture with 2 different ncAAs in the cell was recently demonstrated by reassigning a UAG codon and a quadruplet codon (AGUA) in the same gene [36]. This experiment relied on co-expression of a mutant orthogonal ribosome alongside the endogenous ribosome. Translation products without one or both of the 2 ncAAs were also observed [36], and it is unclear why this mutant ribosome would be immune to frame-shifting at the site of the 4-base codon, which is well-documented [37, 38].

In an independent experiment, a GFP reporter containing 2 different ncAAs was produced at 1-10 mg/l culture by reassigning both UAG and UAA stop codons [39]. The corresponding ‘wild type’ GFP variant was produced at 56 mg/L culture [40]. These data suggest that GFP with 22 different amino acids was produced at 6-50 fold lower levels compared to a GFP containing only the 20 natural amino acids. In contrast, here we established protein synthesis with 22 different amino acids in a recombinant human protein for the first time at > 2 mg/l culture. Our data indicate we achieved equal efficiency to standard protein production with 20 amino acids.

A key bottleneck in genetic code expansion is a limited availability of ‘reassignable’ codons [41]. Traditional genetic code expansion systems alter the meaning of the UAG codon at each instance of that codon in the entire transcriptome [42, 43]. The Sec insertion machinery recodes the UGA codon only at genetic loci that are specified by a downstream Sec insertion sequence element (SecIS) [44] (Fig 2.1). This means that UGA normally stops protein synthesis, but at specific sites determined by the position of SecIS, the Sec machinery is recruited to change the meaning of UGA from stop to Sec. Sec is not hardwired to UGA [45, 46], and we have previously shown that by simply mutating the tRNA<sup>Sec</sup> anti-codon, each stop codon and 15 sense codons can be recoded with high fidelity to Sec [45]. A recent study showed that recoding UAG to Sec using a Sec-tRNA<sup>Sec</sup> with the corresponding UAG-decoding anticodon results in increased UAG translation with Sec in a RF1 deficient *E. coli* strain [47]. We have shown here (Table 2.1), and previously [17] that despite enhanced UAG read-through per cell in the same RF1 deficient *E. coli* strain (Fig S2.2), we are able to produce ncAA-containing proteins more efficiently in BL21 as evidenced by 5-100 fold higher protein yields per liter *E. coli* culture. This is likely due to the decreased fitness of the RF1 deficient *E. coli* strain, resulting in slower growth [16], and less overall protein production. Together these data suggest that with an efficient genetic code expansion system, RF1 competition (and translational stopping at UAG) is

off-set by higher cell densities and overall more efficient protein production in BL21 compared to RF1 deficient *E. coli*.

Because the Sec system shows surprising efficiency at stop codon [47] and sense codon recoding [45], we are currently engineering this system to incorporate other ncAAs [48]. The data here are vital to this engineering effort as they demonstrate that the Sec codon recoding machinery is compatible with, and orthogonal to, traditional genetic code expansion systems based on UAG codon reassignment. In addition, because our system for protein synthesis with 22 amino acids uses normal 3-base codons and the native ribosome, it is highly efficient and will be portable to other host expression systems, including mammalian cells [49, 50] with minimal intervention.

### **2.3.5. Innovation.**

Proteins are normally synthesized in cells with 20 amino acids, but most are post-translationally modified at many sites with unknown consequences to protein function. We used two mutually orthogonal translation systems to incorporate 22 genetically encoded amino acids into a single protein with efficiency and fidelity identical to normal protein synthesis. In doing so, we produced a purified human enzyme in a native and more fully active form, and importantly, we uncovered acetylation as a novel mechanism of enhancing TrxR1 activity that has broad implications for cellular signaling and disease pathways related to deregulation of the cellular redox status.

## **2.4. Methods and Materials**

### **2.4.1. Bacterial Strains and Plasmids.**

Site-specific insertion of acK into proteins relies on translational read-through of the stop codon UAG (Fig 2.1). In an attempt to enhance UAG translation with acK, we expressed TrxR1 variants in an *Escherichia coli* release factor 1 (RF1) deletion strain and in *E. coli*

BL21 (DE3) (C2527H; New England Biolabs, Ipswich, MA, USA). We employed an *E. coli*  $\Delta$ RF1 strain (C321. $\Delta$ A.exp, from G. Church [16] via Addgene strain #49018) that also has all genomic TAG codons mutated to TAA [16]. pET-pylT-GFP, containing superfolder GFP (sfGFP) with an in frame UAG codon at position 2, and pylT as described previously [51], was used for accessing acK incorporation in *E. coli*  $\Delta$ RF1 (Fig S2.2).

Site-specific insertion of Sec relies on the translational read-through and site-specific recoding of the stop codon UGA (Fig 2.1). *E. coli*'s native Sec insertion machinery was used to site-specifically insert Sec as previously [45]. *E. coli* naturally produces Sec-tRNA<sup>Sec</sup><sub>UCA</sub> that binds to a specialized elongation factor (SelB), which in turn recognizes a RNA-hairpin loop (Sec insertion sequence, SecIS) downstream of the recoded UGA codon (Fig 2.1). Human TrxR1 was recombinantly expressed in *E. coli* by placing an *E. coli* SecIS sequence (derived from the *E. coli fdhF* gene) in the 3' untranslated region (UTR) of the TrxR1 expression construct, as previously [45].

In order to develop a system capable of co-translational incorporation of both Sec and acK in the same polypeptide, human TrxR1 (isoform 4), including the 3' *fdhF* SecIS and an in-frame UGA codon (Sec550), was PCR amplified from pRSF-TrxR1-SerS [45] with primers (TRXF-NdeI 5'-CATATGTCCTGCGAAGACGGTCGTGCGC-3', TRXR-SacI 5'-GAGCTCTCGGCCGCATAGGCTAACGATTG-3'). The PCR product was digested NdeI/SacI (NEB) and ligated to pET-pylT [51] digested with NdeI/SacI to give pET-pylT-TrxR1 (WT). Quickchange PCR, as described previously [52], was conducted on pET-pylT-TrxR1 (WT) to introduce UAG codons in the TrxR1 expression construct at positions 141, 200, or 307 (residues numbers are based on isoform 4 numbering). pKTS-ackRS1 [53] containing an engineered *N*<sub>ε</sub>-acetyl-lysyl-tRNA synthetase (acKRS) [15, 51], or pTech-acKRS containing acKRS and tRNA<sup>PylT-opt</sup> [54] was also required for site specific acK incorporation. pRSF-TrxR1-SerS [45] containing UAC at codon 550 was used for producing inactive TrxR1 Sec550Tyr.

### 2.4.2. TrxR1 Production and Purification.

The human TrxR1 variants were overexpressed from the plasmids pET-pyIT-TrxR1 in *E. coli*  $\Delta$ RF1 [16] or *E. coli* BL21 DE3 that had been co-transformed with pKTS-acKRS1 [53] or pTech-acKRS [54]. Starting from a single colony after transformation on selective agar plates, cells were grown at 37°C overnight in a 25 mL preculture containing LB selective medium (ampicillin 100  $\mu$ g/ml, kanamycin 25  $\mu$ g/ml for pKTS-acKRS1, or ampicillin 100  $\mu$ g/ml, chlorophenical 34  $\mu$ g/ml for pTech-acKRS). Cells were grown at 37°C in 1 L LB selective medium (ampicillin 100  $\mu$ g/ml, kanamycin 25  $\mu$ g/ml for pKTS-acKRS1; or ampicillin 100  $\mu$ g/ml, chlorophenical 34  $\mu$ g/ml for pTech-acKRS) supplemented with 10  $\mu$ M sodium selenite (sigma, **214485**) and 2.5 mM *N*<sub>ε</sub>-acetyl-lysine (sigma, **A2010**) following inoculation with a 25 ml pre-culture. An additional 1.5 mM *N*<sub>ε</sub>-acetyl-lysine was added at OD<sub>600</sub> = 1.0, for a total of 4 mM *N*<sub>ε</sub>-acetyl-lysine. Because optimal selenoprotein expression requires late induction [45], at OD<sub>600</sub> = 1.2 the temperature was shifted to 20°C and protein expression was then induced at OD<sub>600</sub> = 1.5 with 100  $\mu$ M or 1 mM Isopropyl  $\beta$ -D-1-thiogalactopyranoside (IPTG, sigma **I6758**) and continued for 18 h shaking at 20°C.

After the cells were harvested by centrifugation, the cell pellet was re-suspended in 30 mL phosphate buffer (100 mM potassium phosphate, pH 7.2, 10% glycerol). The cells were supplemented with lysozyme (0.05 mg/mL, Biobasic, LDB0308) and subsequently disrupted by sonication (Q125, QSonica). The centrifuged lysate (6250 $\times$ g, 1 hour, 4°C) was purified by affinity chromatography using 1 mL nickel nitrilotriacetic acid (Ni-NTA) resin (Qiagen, 30230) in a gravity flow column equilibrated with 25 mL phosphate buffer. After washing with 50 mL phosphate buffer supplemented with 45 mM imidazole the proteins were eluted with 5 x 1 mL phosphate buffer (230 mM imidazole). Protein concentration was assessed by Bradford protein assay (Bio-Rad, #5000006) at 595 nm according to manufacturer's instructions.

Following affinity chromatography, the TrxR1 variants were further purified by size-exclusion chromatography. TrxR1 variants were purified in a AKTA Pure L1 Fast Protein Liquid Chromatography (FPLC) system (GE Healthcare, 29018225) using a Superdex<sup>TM</sup> 200 Increase 10/300 GL column (GE Healthcare, 28990944) pre-equilibrated in 20 mM sodium phosphate, 150 mM sodium chloride, pH 7.5, with a flowrate of 0.3 mL/min. Elutions were collected in 0.5 mL fractions.

#### **2.4.3. *In vitro* TrxR1 Activity Assay: DTNB.**

Enzymatic activity of purified TrxR1 variants was assessed colorimetrically by monitoring  $\beta$ -Nicotinamide adenine dinucleotide 2'-phosphate (NADPH, sigma, **N7505**) dependent reduction of Ellman's reagent (DTNB, 5,5'-Dithiobis-(2-nitrobenzoic acid); Sigma, **D8130**). A plate reader (Syngery H1 Hybrid Multi-Mode Reader, Biotek, 11-120-534) auto-dispenser was used to add DTNB (in phosphate buffer) to each well to start the reactions, which included final concentrations of 5 mM DTNB, 300  $\mu$ M NADPH, and 50 nM (Fig 2.3A) or 100 nM (Fig 2.7B) TrxR1 in a final volume of 100  $\mu$ l per well. Reduction of DTNB produces thiobis-(2-nitrobenzoic acid) (TNB), which has an absorption of 421 nm. This reaction was monitored at 412 nm every minute for 50 minutes. Reactions were performed in triplicate. For all activity assays, error bars display 1 standard deviation based on at least triplicate experiments. A control lacking the TrxR1 enzyme was conducted in triplicate, and has been subtracted from all enzyme assays.

#### **2.4.4. *In vitro* TrxR1 Activity Assay: 9,10-phenanthrene Quinone.**

Enzymatic activity of purified TrxR1 variants were assessed colorimetrically by following oxidation of NADPH resulting from TrxR1 mediated and Sec-dependent reduction of 9,10-phenanthrene quinone (Aldrich, **275034**). NADPH consumption was monitored by incubating 100 nM TrxR1 with 300  $\mu$ M NADPH and 50  $\mu$ M 9,10-phenanthrene quinone

in phosphate buffer (100 mM potassium phosphate, pH 7.0, 1 mM Ethylenediaminetetraacetic acid (EDTA, Sigma, [E9884](#))). TrxR1 and NADPH in phosphate buffer with EDTA was added to the wells of a 96 well plate. A 96 well plate reader auto-dispenser was used to add 9,10-phenanthrene quinone in phosphate buffer to each well to start the reaction with a final volume of 100  $\mu$ l. The assay mixture was monitored at 340 nm every minute for 2 hours, in a 96 well plate reader. A no enzyme control was conducted in triplicate, and subtracted from the TrxR1 reactions. Reactions were performed in triplicate.

#### **2.4.5. Histone Deacetylase 3 (HDAC3) Assays.**

Partially purified (Ni-NTA resin purified) WT and acTrxR1 variants (0.75  $\mu$ M) were incubated with 4  $\mu$ M Histone Deacetylase 3 (HDAC3, **SRP2072 Sigma**) for 2 hours at 37°C. Following this incubation, the enzymatic activity of TrxR1 variants incubated with, or without HDAC3, was assessed colorimetrically by the *in vitro* DTNB activity assay described above with a final TrxR1 concentration of 3.75 nM. Reactions were performed in triplicate, and error bars represent one standard deviation.

#### **2.4.6. Insulin Linked TrxR1 Activity Assays.**

The enzymatic activity of TrxR1 on recombinant human Trx1 (Sigma, T8690) was assessed by following the oxidation of NADPH (340 nm) resulting from TrxR1 mediated reduction of Trx1. In this insulin linked assay, Trx1 then reduces human recombinant insulin (Sigma, 91077C) before being reduced by TrxR1 again. 200 nM TrxR1 was incubated with 50  $\mu$ M NADPH, 1 mM EDTA, 80  $\mu$ M Insulin, and 6  $\mu$ M Trx1 in phosphate buffer in a volume of 200  $\mu$ l in wells of a 96 well plate. The reaction was started by the addition of Trx1 and insulin. The reactions were monitored at 340 nm every minute for 10 minutes using a plate reader. Reactions were performed in triplicate. Error bars represent

one standard deviation. A no TrxR1 control (performed in triplicate) has been subtracted from all reactions.

#### **2.4.7. Statistical Analysis.**

All errors bars represent one standard deviation. All p-values were derived from an Anova one way statistical analysis of data produced in triplicate. Initial velocity calculations in Table 2.1 are calculated from the linear phase of the activity curves (Fig 2.3).

#### **2.4.8. Mass Spectrometry.**

Mass spectrometric analyses of purified TrxR1 variants were performed at the MALDI mass spectrometry facility (The University of Western Ontario) for tandem Matrix-Assisted Laser Desorption/Ionization Mass Spectrometry (MALDI-MS/MS) and the UWO Biological Mass Spectrometry Laboratory (The University of Western Ontario) or the W. M. Keck Biotechnology Resource Laboratory (Yale University) for tandem Liquid Chromatography Mass Spectrometry (LC-MS/MS). TrxR1 variants were run on a 15% sodium dodecyl sulfate (SDS) gel, coomassie stained, and prepared for MALDI-MS/MS or LC-MS/MS by digestion with trypsin protease. A MassPREP automated digester station (PerkinElmer) was used to digest the TrxR1 variants with 5 ng/μl trypsin (Promega). Coomassie stained gel pieces were de-stained with 50 mM ammonium bicarbonate and 50% acetonitrile. TrxR1 variants were then reduced with 10 mM dithiothreitol (DTT) and alkylated with 55 mM acrylamide and digested with trypsin. LC-MS/MS was performed using a Q-ToF Micro mass spectrometer (Waters) equipped with a Z-spray source and run in positive ion mode (+0.1% formic acid) or using Thermo Scientific LTQ-Orbitrap XL mass spectrometer. MALDI-MS/MS was performed using an AB Sciex 5800 TOF/TOF system, MALDI TOF TOF (Framingham, MA, USA) equipped with a 349 nm Nd:YLF OptiBeam On-Axis laser using a laser pulse rate of 400 Hz and reflectron positive mode.



The MALDI matrix used was  $\alpha$ -cyano-4-hydroxycinnamic acid, prepared as 5 mg/ml in 6 mM ammonium phosphate monobasic, 50% acetonitrile, 0.1 % trifluoroacetic acid, and was mixed with the samples at a 1:1 ratio (v/v). Inductively coupled plasma (ICP) mass spectroscopy was performed to quantify the amount of selenium per amount of protein for TrxR1 variants at Biotron Analytical Services (The University of Western Ontario).

#### **2.4.9. Western Blot analysis of TrxR1 Expression.**

Purified TrxR1 proteins were re-suspended in 1 × SDS loading buffer (250 mM Tris/HCl pH 6.8, 40% glycerol (v/v), 10% SDS (w/v), 0.05% bromphenol blue (w/v), 5% 2-mercaptoethanol) and loaded in 10% SDS-polyacrylamide gel electrophoresis (SDS-PAGE). The blot was carried out with a TransBlot Turbo Transfer System (Biorad). Anti-His antibodies (from Mouse, Sigma, **H1029**) and Mouse IgG HRP linked (from Sheep, GE Healthcare, **GENA931**) were used. Chemiluminescent signal detection was performed on a ChemiDoc MP system (Biorad).

#### **2.4.10. Size Exclusion Chromatography.**

TrxR1 variants and proteins from a high molecular weight calibration kit (GE Healthcare, 28403842) were individually separated in a AKTA Pure L1 Fast Protein Liquid Chromatography (FPLC) system using a Superdex<sup>TM</sup> 200 Increase 10/300 GL column pre-equilibrated in 20 mM sodium phosphate, 150 mM sodium chloride, pH 7.5. Elutions were collected in 0.5 mL fractions. The high molecular weight calibration kit used the following proteins: Ovalbomin (43 kDa, 3 mg/mL), Conalbumin (75 kDa, 3 mg/mL), Aldolase (158 kDa, 3 mg/mL), Ferritin (440 kDa, 1 mg/mL), Thyroglobulin (669 kDa, 3 mg/mL), and Blue Dextran (2000 kDa, 1 mg/mL).

## **2.5. Acknowledgements**

This work is supported by grants to P.O. from the Natural Sciences and Engineering Research Council of Canada (RGPIN 04282-2014), Canada Research Chairs (950-229917), Canada Foundation for Innovation (229917), Ontario Research Fund (229917), Canadian Cancer Society Research Institute (704324), and Western University. We are thankful to Ilka Heinemann, Shawn Li, Lars Konermann, Noah Reynolds and Dieter Söll for discussions.

## 2.6. References

1. Schweizer, U. and N. Fradejas-Villar, *Why 21? The significance of selenoproteins for human health revealed by inborn errors of metabolism*. FASEB J, 2016. **30**(11): p. 3669-3681.
2. Tamura, T. and T.C. Stadtman, *A new selenoprotein from human lung adenocarcinoma cells: purification, properties, and thioredoxin reductase activity*. Proc Natl Acad Sci U S A, 1996. **93**(3): p. 1006-11.
3. Xia, L., et al., *The mammalian cytosolic selenoenzyme thioredoxin reductase reduces ubiquinone. A novel mechanism for defense against oxidative stress*. J Biol Chem, 2003. **278**(4): p. 2141-6.
4. Lu, J. and A. Holmgren, *Thioredoxin system in cell death progression*. Antioxid Redox Signal, 2012. **17**(12): p. 1738-47.
5. Roh, J.L., et al., *Targeting of the glutathione, thioredoxin, and Nrf2 antioxidant systems in head and neck cancer*. Antioxid Redox Signal, 2017. **27**(2): p. 106-114.
6. Selenius, M., et al., *Selenium and the selenoprotein thioredoxin reductase in the prevention, treatment and diagnostics of cancer*. Antioxid Redox Signal, 2010. **12**(7): p. 867-80.
7. Dong, C., et al., *Role of thioredoxin reductase 1 in dysplastic transformation of human breast epithelial cells triggered by chronic oxidative stress*. Sci Rep, 2016. **6**: p. 36860.
8. Wang, L., et al., *Ethaselen: a potent mammalian thioredoxin reductase 1 inhibitor and novel organoselenium anticancer agent*. Free Radic Biol Med, 2012. **52**(5): p. 898-908.
9. Lamoke, F., et al., *Loss of thioredoxin function in retinas of mice overexpressing amyloid beta*. Free Radic Biol Med, 2012. **53**(3): p. 577-88.
10. Banerjee Mustafi, S., et al., *Aggregate-prone R120GCRYAB triggers multifaceted modifications of the thioredoxin system*. Antioxid Redox Signal, 2014. **20**(18): p. 2891-906.
11. Lamoke, F., et al., *Epigenetic Regulation of Endogenous Antioxidants in the Diabetic Retina*. Investigative Ophthalmology & Visual Science, 2011. **52**(4448): p. -.
12. Weinert, B.T., et al., *Lysine succinylation is a frequently occurring modification in prokaryotes and eukaryotes and extensively overlaps with acetylation*. Cell Rep, 2013. **4**(4): p. 842-51.
13. Choudhary, C., et al., *Lysine acetylation targets protein complexes and co-regulates major cellular functions*. Science, 2009. **325**(5942): p. 834-40.
14. Hornbeck, P.V., et al., *PhosphoSitePlus, 2014: mutations, PTMs and recalibrations*. Nucleic Acids Res, 2015. **43**(Database issue): p. D512-20.
15. Neumann, H.P.-C., S. Y.; Chin, J. W., *Genetically encoding Nepsilon-acetyllysine in recombinant proteins*. Nature Chemical Biology, 2008. **4**(4): p. 232-234.
16. Lajoie, M.J., et al., *Genomically recoded organisms expand biological functions*. Science, 2013. **342**(6156): p. 357-60.
17. George, S., et al., *Generation of phospho-ubiquitin variants by orthogonal translation reveals codon skipping*. FEBS Lett, 2016. **590**(10): p. 1530-42.
18. Luthman, M. and A. Holmgren, *Rat liver thioredoxin and thioredoxin reductase: purification and characterization*. Biochemistry, 1982. **21**(26): p. 6628-33.

19. Cenas, N., et al., *Interactions of quinones with thioredoxin reductase: a challenge to the antioxidant role of the mammalian selenoprotein*. J Biol Chem, 2004. **279**(4): p. 2583-92.
20. Xu, J., et al., *The conserved Trp114 residue of thioredoxin reductase I has a redox sensor-like function triggering oligomerization and crosslinking upon oxidative stress related to cell death*. Cell Death Dis, 2015. **6**: p. e1616.
21. Cheng, Q., et al., *Crystal structure and catalysis of the selenoprotein thioredoxin reductase I*. J Biol Chem, 2009. **284**(6): p. 3998-4008.
22. Wu, Q., et al., *Suberoylanilide hydroxamic acid treatment reveals crosstalks among proteome, ubiquitylome and acetylome in non-small cell lung cancer A549 cell line*. Sci Rep, 2015. **5**: p. 9520.
23. Wolfe, A.J., *Bacterial protein acetylation: new discoveries unanswered questions*. Curr Genet, 2016. **62**(2): p. 335-41.
24. Soppa, J., *Protein acetylation in archaea, bacteria, and eukaryotes*. Archaea, 2010. **2010**: p. doi:10.1155/2010/820681.
25. Eichler, J. and J. Maupin-Furlow, *Post-translation modification in Archaea: lessons from Haloferax volcanii and other haloarchaea*. FEMS Microbiol Rev, 2013. **37**(4): p. 583-606.
26. Kawaguchi, Y., et al., *Charge modification at multiple C-terminal lysine residues regulates p53 oligomerization and its nucleus-cytoplasm trafficking*. J Biol Chem, 2006. **281**(3): p. 1394-400.
27. Tse, C., et al., *Disruption of higher-order folding by core histone acetylation dramatically enhances transcription of nucleosomal arrays by RNA polymerase III*. Mol Cell Biol, 1998. **18**(8): p. 4629-38.
28. Ungerstedt, J.S., et al., *Role of thioredoxin in the response of normal and transformed cells to histone deacetylase inhibitors*. Proc Natl Acad Sci U S A, 2005. **102**(3): p. 673-8.
29. Parmigiani, R.B., et al., *HDAC6 is a specific deacetylase of peroxiredoxins and is involved in redox regulation*. Proc Natl Acad Sci U S A, 2008. **105**(28): p. 9633-8.
30. Schieber, M. and N.S. Chandel, *ROS function in redox signaling and oxidative stress*. Curr Biol, 2014. **24**(10): p. R453-62.
31. Saitoh, M., et al., *Mammalian thioredoxin is a direct inhibitor of apoptosis signal-regulating kinase (ASK) 1*. EMBO J, 1998. **17**(9): p. 2596-606.
32. Rodman, S.N., et al., *Enhancement of Radiation Response in Breast Cancer Stem Cells by Inhibition of Thioredoxin- and Glutathione-Dependent Metabolism*. Radiat Res, 2016. **186**(4): p. 385-395.
33. Gorrini, C., I.S. Harris, and T.W. Mak, *Modulation of oxidative stress as an anticancer strategy*. Nat Rev Drug Discov, 2013. **12**(12): p. 931-47.
34. Hirota, K., et al., *Distinct roles of thioredoxin in the cytoplasm and in the nucleus. A two-step mechanism of redox regulation of transcription factor NF-kappaB*. J Biol Chem, 1999. **274**(39): p. 27891-7.
35. Hirota, K., et al., *AP-1 transcriptional activity is regulated by a direct association between thioredoxin and Ref-1*. Proc Natl Acad Sci U S A, 1997. **94**(8): p. 3633-8.
36. Wang, K., et al., *Optimized orthogonal translation of unnatural amino acids enables spontaneous protein double-labelling and FRET*. Nat Chem, 2014. **6**(5): p. 393-403.

37. Farabaugh, P.J., *Translational frameshifting: implications for the mechanism of translational frame maintenance*. Prog Nucleic Acid Res Mol Biol, 2000. **64**: p. 131-70.
38. O'Donoghue, P., et al., *Near-cognate suppression of amber, opal and quadruplet codons competes with aminoacyl-tRNA<sup>Pyl</sup> for genetic code expansion*. FEBS Lett, 2012. **586**(21): p. 3931-7.
39. Wan, W., et al., *A facile system for genetic incorporation of two different noncanonical amino acids into one protein in Escherichia coli*. Angew Chem Int Ed Engl, 2010. **49**(18): p. 3211-4.
40. Huang, Y., et al., *A convenient method for genetic incorporation of multiple noncanonical amino acids into one protein in Escherichia coli*. Mol Biosyst, 2010. **6**(4): p. 683-6.
41. O'Donoghue, P., et al., *Upgrading protein synthesis for synthetic biology*. Nat Chem Biol, 2013. **9**(10): p. 594-8.
42. Heinemann, I.U., et al., *Enhanced phosphoserine insertion during Escherichia coli protein synthesis via partial UAG codon reassignment and release factor 1 deletion*. FEBS Lett, 2012. **586**(20): p. 3716-22.
43. Aerni, H.R., et al., *Revealing the amino acid composition of proteins within an expanded genetic code*. Nucleic Acids Res, 2015. **43**(2): p. e8.
44. Heider, J., C. Baron, and A. Bock, *Coding from a distance: dissection of the mRNA determinants required for the incorporation of selenocysteine into protein*. EMBO J, 1992. **11**(10): p. 3759-66.
45. Bröcker, M.J., et al., *Recoding the genetic code with selenocysteine*. Angew Chem Int Ed Engl, 2014. **53**(1): p. 319-23.
46. Mukai, T., et al., *Facile Recoding of Selenocysteine in Nature*. Angew Chem Int Ed Engl, 2016. **55**(17): p. 5337-41.
47. Cheng, Q. and E.S. Arner, *Selenocysteine insertion at a predefined UAG codon in a release factor 1 (RF1) depleted Escherichia coli host strain bypasses species barriers in recombinant selenoprotein translation*. J Biol Chem, 2017.
48. Stafforst, T., *The selenocysteine incorporation machinery allows the dual use of sense codons: a new strategy for expanding the genetic code?* Chembiochem, 2014. **15**(3): p. 356-8.
49. Turanov, A.A., et al., *UGA codon position-dependent incorporation of selenocysteine into mammalian selenoproteins*. Nucleic Acids Res, 2013. **41**(14): p. 6952-9.
50. Elsasser, S.J., et al., *Genetic code expansion in stable cell lines enables encoded chromatin modification*. Nat Methods, 2016. **13**(2): p. 158-64.
51. Guo, L.T., et al., *Polyspecific pyrrolysyl-tRNA synthetases from directed evolution*. Proc Natl Acad Sci U S A, 2014. **111**(47): p. 16724-9.
52. Edelheit, O., A. Hanukoglu, and I. Hanukoglu, *Simple and efficient site-directed mutagenesis using two single-primer reactions in parallel to generate mutants for protein structure-function studies*. BMC Biotechnol, 2009. **9**: p. 61.
53. Umehara, T., et al., *N-acetyl lysyl-tRNA synthetases evolved by a CcdB-based selection possess N-acetyl lysine specificity in vitro and in vivo*. FEBS Lett, 2012. **586**(6): p. 729-33.

54. Fan, C., et al., *Rationally evolving tRNAPyl for efficient incorporation of noncanonical amino acids*. *Nucleic Acids Res*, 2015. **43**(22): p. e156.

## 2.7. Chapter 2 Appendix – Supplementary Tables & Figures

### 2.7.1. Supplementary Tables.

**Table S2.1. ICP-MS selenium (Se) content determination for TrxR1 preparations.**

<b>TrxR1 variant</b>	<b>Protein (<math>\mu</math>M)</b>	<b>Selenium (<math>\mu</math>M)</b>	<b>Sec Occupancy (%)*</b>
TrxR1 WT	25.8	21.5 $\pm$ 2.4	83 $\pm$ 9
acTrxR1 <sup>K141</sup>	24.2	25.0	103
acTrxR1 <sup>K200</sup>	25.2	25.5 $\pm$ 2.3	101 $\pm$ 9
acTrxR1 <sup>K307</sup>	22.6	21.8 $\pm$ 2.2	96 $\pm$ 10

\*The Sec-occupancy is calculated as a ration of the amount of Se detected by ICP-MS to the amount of protein in each sample. The data are based on triplicate measurements.

**Table S2.2. Percentage of total TrxR1 existing in high activity dimers, or low activity tetramers or monomers.**

<b>TrxR1 variants</b>	<b>TrxR1 Tetramer (% Total TrxR1)</b>	<b>TrxR1 Dimer (% Total TrxR1)</b>	<b>TrxR1 Monomer (% Total TrxR1)</b>
WT	29	57	14
acTrxR1 <sup>K141</sup>	24	70	6
acTrxR1 <sup>K200</sup>	22	59	22
acTrxR1 <sup>K307</sup>	19	66	12

A western blot was conducted on 0.5 mL elutions of TrxR1 variants from a size exclusion column (Fig 2.7). DTNB activity assays were used to determine where catalytically active dimers and inactive tetramers and monomers eluted from the size exclusion column (Fig 2.7). The percentage of TrxR1 existing as tetramers, dimers, and monomers was calculated based on densitometry of the Western Blots (Fig 2.7).

## 2.7.2. Supplementary Figures.

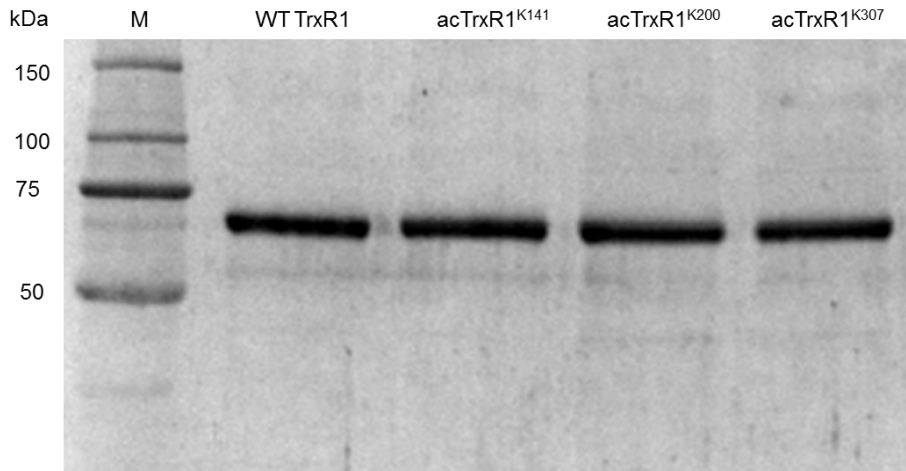


**Figure S2.1. Purified WT and acTrxR1 variants.** His-tagged WT TrxR1 and acTrxR1 variants were visualized on a Coomassie stained SDS gel showing successful purification of full-length (62 kDa) TrxR1 variants (isoform 4). The variants are indicated above each lane, while M represents a molecular weight marker.

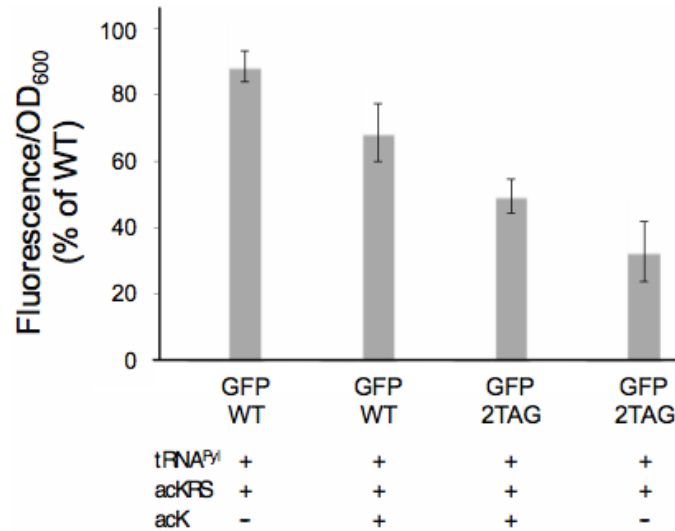


**Figure S2.2. GFP reporter detecting UAG read-through.** Protein expression levels for GFP reporters in *E. coli* ΔRF1. GFP fluorescence levels were measured in an *E. coli* ΔRF1 background strain expressing acKRS and tRNA<sup>Pyl</sup>. Expression of WT GFP and GFP with a UAG codon at position 2 (2TAG) were compared in the presence or absence of acK.



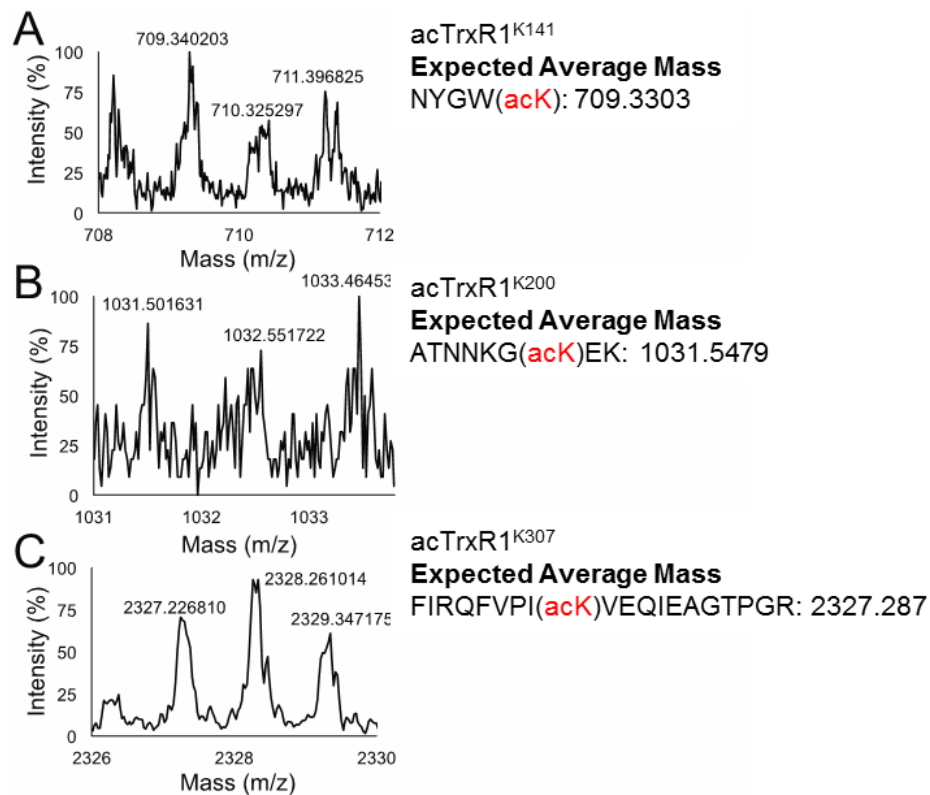


**Figure S2.3. MALDI MS analysis confirms acetylation of acTrxR1 variants.** Peaks for tryptic peptides corresponding to acetylated lysine at position 141 (A), 200 (B), and 307 (C) were observed. The expected average mass reported refers to the monoisotopic mass (all carbons <sup>12</sup>C). Peptides containing 1, or 2, <sup>13</sup>C isotope(s) are also shown, and should have the expected average mass + 1, or +2, respectively.

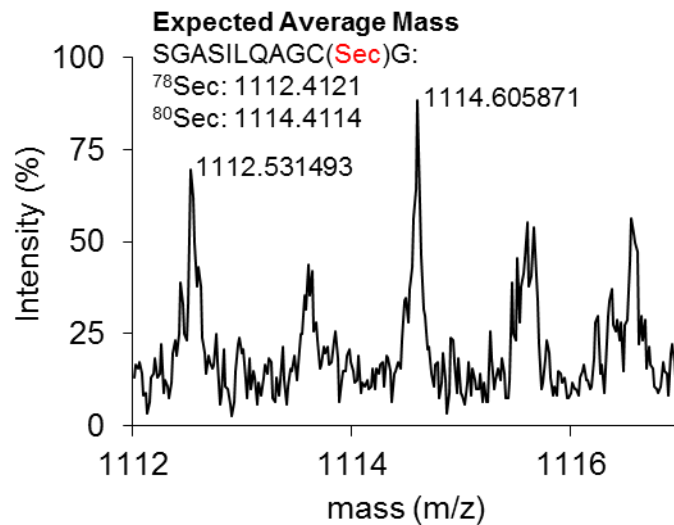


**Figure S2.4. Confirmation of Sec incorporation in WT TrxR1 by MALDI MS analysis of the tryptic digested protein.** Peaks for peptides containing two Se isotopes ( $^{78}\text{Se}$ ,  $^{80}\text{Se}$ ) were observed.

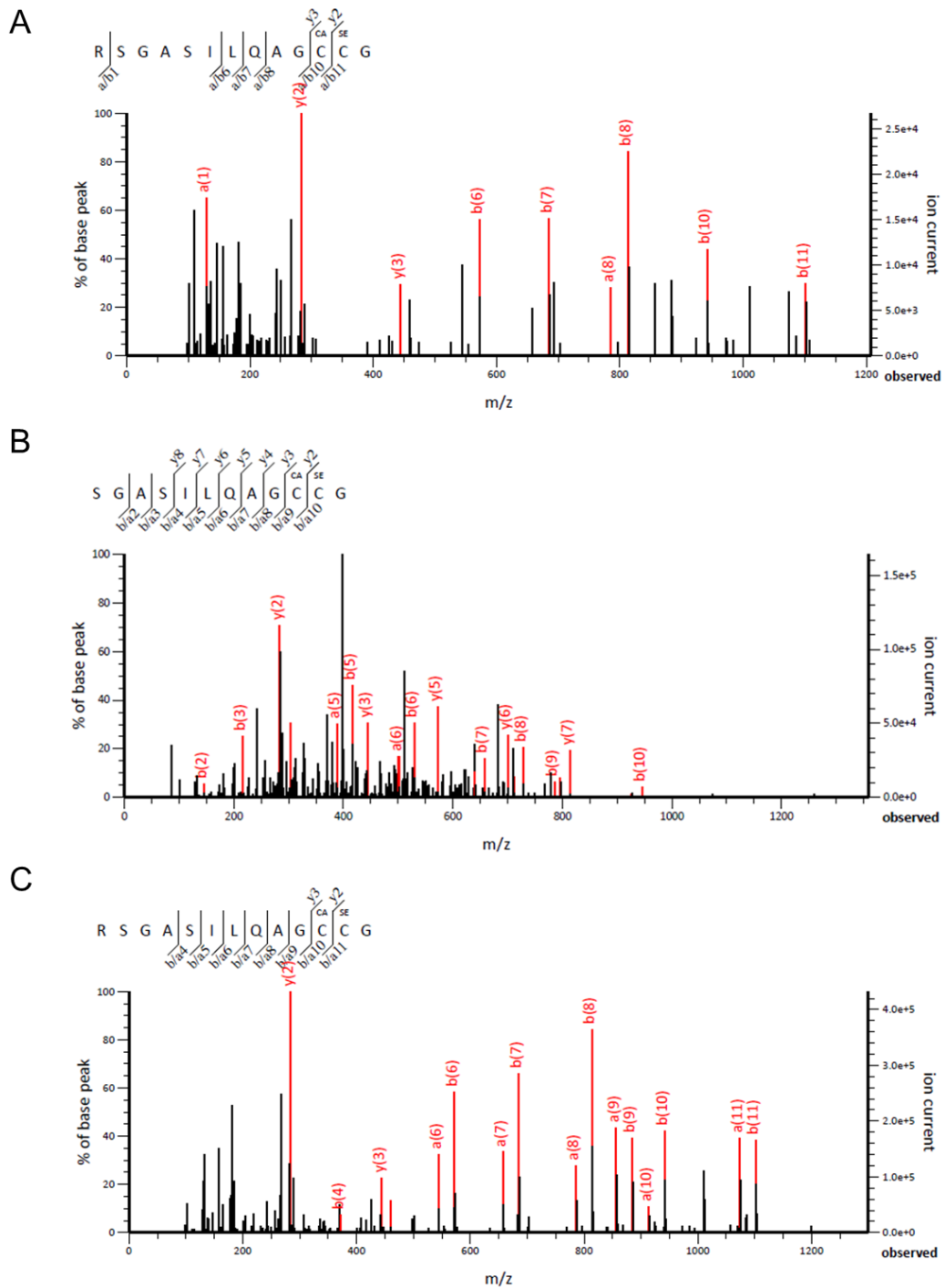


**Figure S2.5. LC-MS/MS confirming Sec incorporation for WT TrxR1, acTrxR1<sup>K141</sup>, and acTrxR1<sup>K307</sup> variants.** Trypsin digested WT and acTrxR1 variants were analyzed by LC-MS/MS. A peptide from trypsin digested TrxR1 demonstrating Sec incorporation for WT TrxR1 (A), acTrxR1<sup>K141</sup> (B), and acTrxR1<sup>K307</sup> (C). Sec is shown as C with Se superscript, while Cysteine is noted as C with CA superscript.

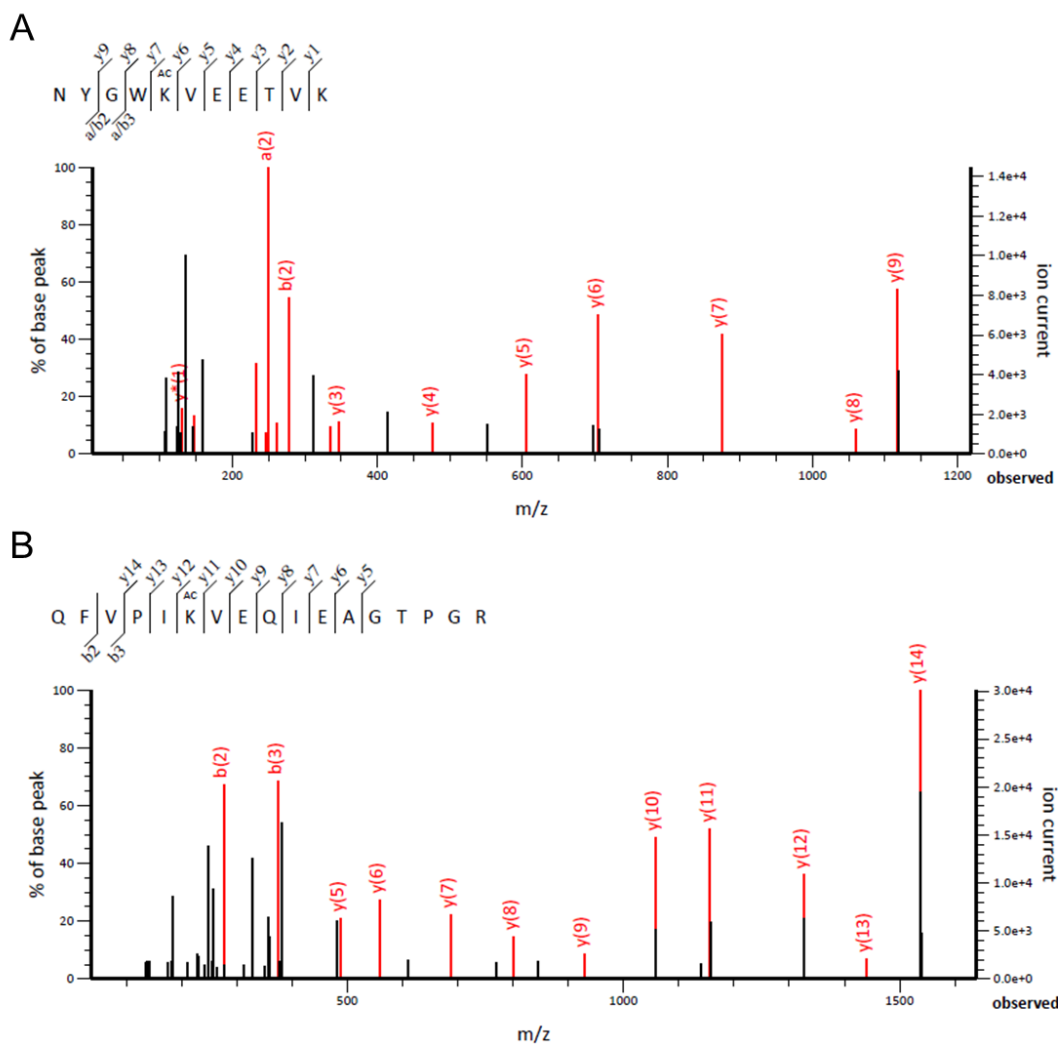


**Figure S2.6. LC-MS/MS confirming genetically encoded acK incorporation into acTrxR1<sup>K141</sup> and acTrxR1<sup>K307</sup>.** Trypsin digested WT and acTrxR1 variants were analyzed by LC-MS/MS. A peptide from trypsin digested TrxR1 demonstrating acK incorporation for acTrxR1<sup>K141</sup> (A), and acTrxR1<sup>K307</sup> (B). Acetylated lysine is indicated by K with AC superscript.

## Chapter 3

### 3. Acetylated Thioredoxin Reductase 1 Resists Oxidative Inactivation

#### 3.1. Introduction

Human cells actively eliminate reactive oxygen species (ROS) and resolve oxidative damage to proteins using multiple pathways, including the glutathione or thioredoxin (Trx) systems [1]. The Trx system includes the selenocysteine-containing protein (selenoprotein) thioredoxin reductase (TrxR1). TrxR1 is a disulfide reductase with specificity for the redox mediator Trx. TrxR reduces a disulfide bond in Trx by catalyzing the oxidation of nicotinamide adenine dinucleotide phosphate (NADPH). The reduced Trx transfers electrons to oxidatively damaged proteins or ROS directly. For example, a pathway that resolves oxidation of methionine residues uses Trx-dependent enzymes to protect the proteome [2]. The resulting oxidized Trx can then be reduced again by TrxR1.

The Trx system is involved in regulating gene expression, embryonic development, cell proliferation, apoptosis, and many other cellular processes [3]. In addition to Trx, TrxR1 can also directly reduce other cellular proteins, such as p53, protein disulfide isomerase, glutathione peroxidase, and NK-lysin [4, 5] as well as low molecular weight ROS, including hydrogen peroxide, lipoic acid, selenite, 15-HPETE, and more [6]. The Trx system provides a defense mechanism against ROS generated during oxidative stress, and consequently, alterations in the Trx system are associated with various diseases. TrxR1 is over-active in many aggressive cancers and is an early diagnostic marker [7, 8]. TrxR1 is also an established anti-cancer drug target [9], and increased TrxR1 production or activity provides chemotherapeutic resistance to treatments that rely on the production of ROS to kill cells [10].

TrxR1 exists in an equilibrium of several different quaternary structures [7, 11-13]. TrxR1 can exist as inactive monomers, or as low active tetramers or higher order oligomers [11-14]. Catalytically competent dimers are the most active form of TrxR1, while inactive cross-linked dimers form because of covalent linkage between opposing subunits in associations between TrxR1 tetramers [11, 12] (Fig 3.1). In cells, oxidative stress generated by Reactivating p53 and Inducing Tumor Apoptosis (RITA) induces TrxR1 tetramerization and covalent linkage, resulting in reduced activity or inactivation of TrxR1 [12]. Thus, as oxidative stress increases, one of the cell's major oxidative stress defense mechanisms is prone to become increasingly ineffective.

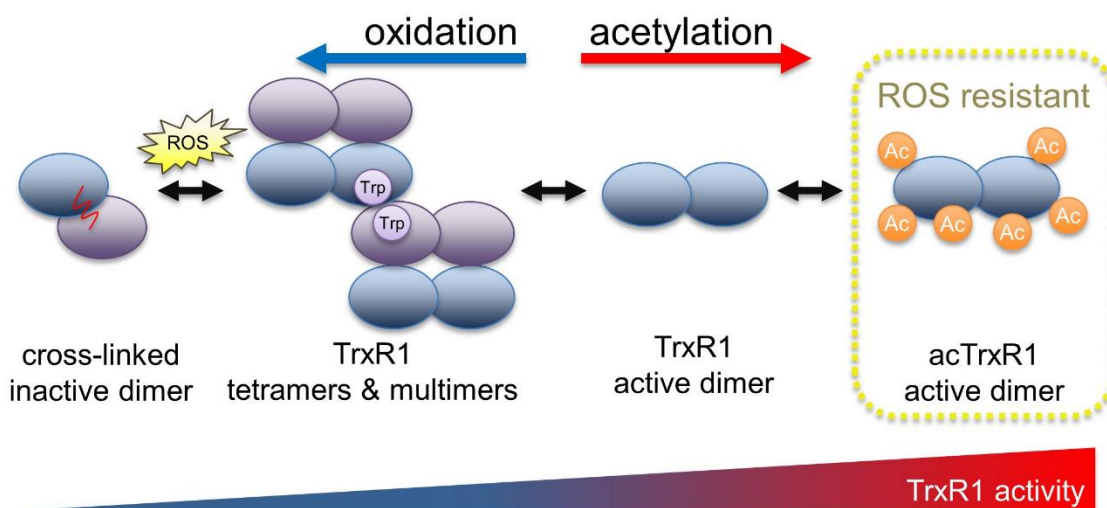


**Figure 3.1. TrxR1 activity is regulated by oxidation and acetylation.** With increasing levels of reactive oxygen species, TrxR1 shows increased propensity to form low activity tetramers and higher order multimers [11]. Oxidation ultimately leads to the formation of a covalent linkage between non-productive TrxR1 monomers, forming inactive cross-linked dimers [12]. Acetylation of TrxR1, on the other hand, is associated with increased TrxR1 activity, reduced cross-linked dimer formation [11], and here we show that acetylated TrxR1 is resistant to oxidation and peroxide-induced multimerization.

Multiple reports document regulation of the Trx system without changes in total protein levels. These studies implicate post-translational modifications as potent regulators of the activity of different Trx system components [15-18]. Three members of the Trx system can be acetylated to increase their activity, including TrxR1 [11], Trx1 [16], and

peroxiredoxin (Prx) [19]. Acetylation inhibits super-oxidation of Prx, preventing its oligomerization into higher molecular weight complexes with low peroxidase activity [19]. In the context of disease, TrxR1 acetylation levels correlated positively with the level of oxidized cellular proteins in a mouse model of cardiomyopathy [15]. The oxidative stress generating anti-cancer compound RITA reduces TrxR1 activity in cell cultures by altering the oligomerization status of TrxR1 and increasing levels of inactive and cross-linked dimers [12]. These reports suggest a relationship between acetylation, oligomerization, and oxidative damage in components of the Trx system. Although TrxR1 is known to be acetylated in response to oxidative stress [15], the function of TrxR1 acetylation under oxidizing conditions is unknown.

Proteomic studies in Jurkat T lymphocytes, A549 cells and related non-small cell lung cancer cell lines have identified acetylation of TrxR1 at five distinct sites [12, 17, 20]. We showed that single acetylation at three of these sites in TrxR1 resulted in a 1.5 to 3-fold increase in enzyme activity [11]. Because acetylated TrxR1 shows increased activity, we hypothesized that the acetylation of TrxR1 may serve as a mechanism to maintain TrxR1 activity under oxidizing conditions associated with increased ROS levels. To test this hypothesis, we used protein biochemistry to precisely measure the activity of acetylated TrxR1 variants over a broad range of peroxide concentrations that models the relevant range of ROS levels encountered by cells. We also generated non-specifically acetylated TrxR1 using aspirin as a model acetyl donor. Together our findings suggest that acetylation is a potent mechanism to regulate TrxR1 activity that also allows the enzyme to evade oxidative inactivation.

## 3.2. Materials and Methods

### 3.2.1. Plasmids and Strains.

The plasmid pET-pylT-TrxR1 contains a His-tagged Human TrxR1 (isoform 4) with an in-frame UGA codon (Sec551) followed by the *Escherichia coli* selenocysteine insertion sequence (SECIS) RNA-hairpin loop (derived from the *E. coli* FdhF gene) in the 3' untranslated region (UTR), which directs Sec-insertion at the UGA551 codon in recombinantly produced human TrxR1 variants from *E. coli* (Fig 3.2) [11]. UAG stop codons inserted at positions 141, 200, or 307 in the TrxR1 gene allows for site-specific insertion of *N*<sub>ε</sub>-acetyl-L-lysine (acK) when co-expressed with plasmids bearing a pyrrolysyl-tRNA synthetase mutant specific for acK (acKRS) [21] and an optimized [22] UAG-decoding tRNA<sup>Pyl</sup> (pTech-acKRS-tRNA<sup>Pyl-opt</sup>) (Fig 3.2) [11].

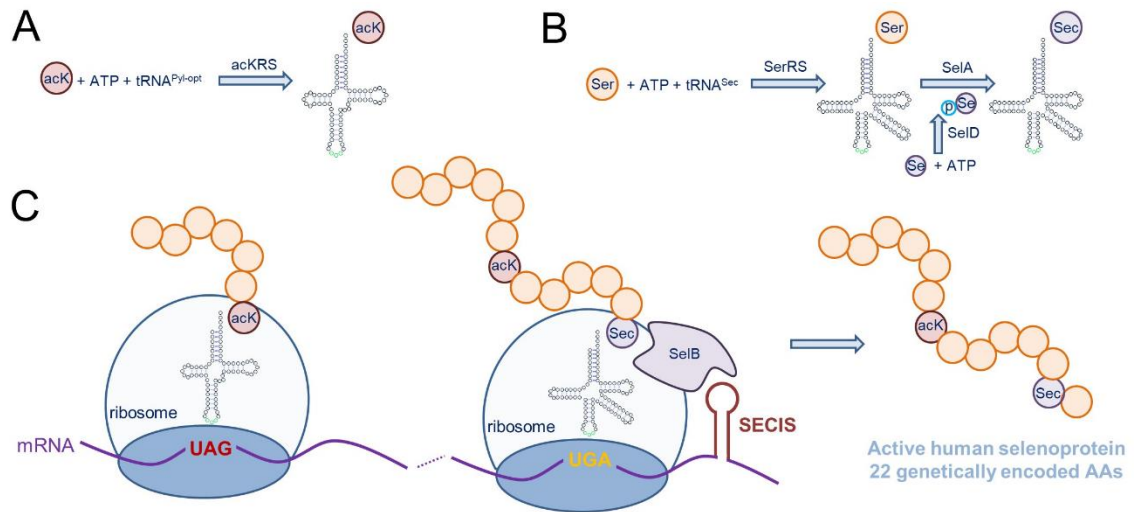


**Figure 3.2. Genetic code expansion to incorporate acK and Sec in TrxR1.** Expressed from a plasmid in *E. coli*, (A) acKRS ligates the UAG-decoding tRNA<sup>Pyl-opt</sup> with acK, (C) allowing insertion of acK at UAG codons. (B) In the endogenous Sec incorporation pathway (reviewed in [23]) in *E. coli*, SerRS ligates tRNA<sup>Sec</sup> with Ser, selenophosphate synthetase (SelD) produces selenophosphate (pSe), and selenocysteine synthase (SelA) uses the products of these reactions to convert Ser-tRNA<sup>Sec</sup> to Sec-tRNA<sup>Sec</sup>. An endogenous *E. coli* elongation factor (SelB) recruits Sec-tRNA<sup>Sec</sup> to a UGA codon by also binding to a selenocysteine insertion sequence (SECIS) included in the 3' untranslated region of the TrxR1 mRNA, allowing Sec incorporation at a specific UGA codon (C). Together the acK and Sec systems can be used to produce active human TrxR1 protein with 22 genetically encoded amino acids.



### 3.2.2. TrxR1 and acTrxR1 Protein Purification.

*E. coli* BL21 (DE3) (Invitrogen) was co-transformed with pET and pTech vectors. Preparative cultures (1 l) for each transformed strain were incubated with shaking at 37 °C in lysogeny broth (LB) supplemented with 5 mM acK (A4021-5G Sigma), 10 µM sodium selenite (10102-18-8, AlfaAesar), and appropriate antibiotics (100 µg/ml ampicillin (BP1760-25, Fisher) for pET and 34 µg/ml chloramphenicol (02930-100G, Ampresco) for pTech). We employed a previously optimized protocol for production of the selenoproteins in *E. coli* [11]. At  $A_{600} = 1.2$ , the temperature was reduced to 20 °C. At  $A_{600} = 1.5$ , 1 mM isopropyl  $\beta$ -d-1-thiogalactopyranoside (IPTG) (BP1755-10, Fisher) was added and the cells then produced protein for a further 16 to 24 hours. Cells were harvested by centrifugation and stored at -80°C until further use. TrxR1 variants were purified as previously [11]. Briefly, cell pellets were resuspended in 30 mL phosphate buffer (100 mM potassium phosphate (PB0445, Biobasic), pH 7.2, 10% glycerol (CA97063-892, VWR)) supplemented with lysozyme (1 mg/ml) (12650-88-3, Biobasic) and disrupted by sonication. Following centrifugation at  $6250 \times g$ , cell lysate was purified by affinity chromatography using Ni<sup>2+</sup>-Nitrilotriacetic acid (NTA) resin (HisPur™ Ni-NTA Resin, PI88222, Fisher), as previously [11]. Purified TrxR1 variants were stored in 100 mM potassium phosphate, pH 7.2, 50% glycerol at -80 °C until use.

### 3.2.3. TrxR1 Activity Assays.

TrxR1 activity was assessed using 5,5-dithio-bis-(2-nitrobenzoic acid) (DTNB) (D8130-5G, Sigma) also known as Ellman's reagent to detect the rate and level of reductive activity from TrxR1. The colorimetric reaction is followed by measuring reduction of DTNB to 2-nitro-5-thiobenzoate (TNB), which absorbs at 412 nm ( $A_{412}$ ). Each reaction contains 250 nM TrxR1, 300 µM nicotinamide adenine dinucleotide phosphate (NADPH) (N5130-25MG, Sigma) and 5 mM DTNB in buffer containing 100 mM potassium phosphate, 1

mM Ethylenediaminetetraacetic acid (EDTA) (E4378-25G, Sigma), pH 7.0. Reactions were started by the addition of DTNB to a solution containing TrxR1 and NADPH, for a final volume of 100  $\mu$ l in a 96 well plate. Measurements were taken in a Biotek Synergy H1 microplate reader every 1 minute over a one-hour time course. All assays were performed using three independent enzyme reactions for each condition tested.

### **3.2.4. Peroxide and Aspirin Incubations.**

TrxR1 variants were also incubated with increasing concentrations of peroxide and then assessed as above for activity. Each TrxR1 and acTrxR1 enzyme variant (1  $\mu$ M) was incubated in phosphate buffer (100 mM potassium phosphate, 1 mM EDTA, pH 7.0) with increasing peroxide concentrations (0  $\mu$ M to 500  $\mu$ M H<sub>2</sub>O<sub>2</sub> (16911-250ML-F, Sigma)) for 1 hour in a total volume of 200  $\mu$ l at 37 °C. To generate non-site-specifically acetylated TrxR1, 500 nM TrxR1 was incubated with increasing concentrations (0 to 15 mM) of aspirin (A5376-250G, Sigma) in phosphate buffer for 1 hour at 37 °C. Activity assays with aspirin-treated and untreated TrxR1 were conducted exactly as above.

### **3.2.5. Western Blotting.**

Purified protein samples were suspended in 1  $\times$  sodium dodecyl sulfate (SDS) loading buffer (250 mM Tris-HCl pH 6.8, 40% glycerol (v/v), 10% SDS (w/v) (SB0485, Biobasic), 0.05% bromophenol blue (w/v) (0449-25G, Amresco), 5% 2-mercaptoethanol (M6250-100ML, Sigma)) and heated for 5 minutes at 95°C. Samples were then loaded in 15% SDS-polyacrylamide gels and electrophoresed. Following this, a polyvinylidene difluoride (PVDF) membrane was soaked in methanol for 1 minute. Both the SDS gel and membrane were soaked in transfer buffer (0.025M Tris-HCl (TRS001.5, Bioshop Canada), pH 9.5, 0.192M Glycine (56-40-6, Fisher), 20% (v/v) Methanol (CA71007-742, VWR), 0.5% (w/v) SDS) for 15 minutes. The blot was carried out with a TransBlot Turbo Transfer

System (BioRad) at 15 V with 1.3 A for 15 min. The membrane was incubated in blocking solution (5% (w/v) skim milk powder (LP0031, Oxoid), 0.1% (v/v) Tween20 (9005-64-5, Ampresco), 1x PBS (137 mM NaCl (BP358-212, Fisher), 0.027 mM KCl (7447-40-7, Anachemia), 10 mM Na<sub>2</sub>HPO<sub>4</sub> (SDB0487, Biobasic), and 2 mM KH<sub>2</sub>PO<sub>4</sub>) for 1 hour, shaking, at room temperature. Then the membrane was incubated overnight with the primary antibody (anti-acetyl Lysine antibody from rabbit, Abcam ab80178; or anti-TrxR1 antibody, Santa Cruz Biotechnology sc28321) at 1:1000 in blocking solution at 4 °C overnight. Three 10-minute washes with wash solution (0.5% (w/v) skim milk powder, 0.1% Tween20, 1x PBS) were conducted, shaking, at room temperature, followed by a 2 hour incubation with a secondary antibody (Rabbit IgG HRP Linked F(ab')<sub>2</sub>, GENA9340; Sigma) at 1:5000 in wash solution at room temperature shaking. Next, three 10-minute washes with PBS-tween (0.1% (v/v) Tween20, 1x PBS) were conducted, followed by a final wash with 1x PBS, shaking at room temperature. Clarity Western ECL Substrate (1705061; Biorad) was used for signal detection and chemiluminescent imaging was performed on a Chemidoc XRS+ (Biorad).

### **3.2.5. Mass Spectrometry.**

For the MS/MS analysis of the aspirin acetylated and untreated TrxR1, gels were loaded with 0.31 µg of purified TrxR1 protein. Following SDS-polyacrylamide gel electrophoresis (SDS-PAGE), a 1 mm circular slice was picked from the gel using an Ettan Robotic Spot-Picker and submitted for proteolytic digestion (Trypsin) and peptide extraction at the Functional Proteomics Facility at the University of Western Ontario. Liquid chromatography and tandem mass spectrometry (LC-MS/MS) analyses of TrxR1 and aspirin-acetylated TrxR1 were performed at the Biological Mass Spectrometry Laboratory at The University of Western Ontario. Gel slices were de-stained with 50 mM ammonium bicarbonate (09830, Sigma) and 50% acetonitrile (00687, Sigma). The protein samples were reduced with 10 mM dithiothreitol (BP25641, Fisher), alkylated with 55 mM

acrylamide (BP1406-1, Fisher), and digested with 5 ng/μl trypsin (Promega). LC-MS/MS was performed using a Q-ToF Micro mass spectrometer (Waters) equipped with a Z-spray source in positive ion mode (+0.1% formic acid) or using Thermo Scientific LTQ-Orbitrap XL mass spectrometer. The data were analyzed and visualized using PEAKS software (Bioinformatic Solutions, Inc, Waterloo, Ontario).

### **3.2.6. Statistical Analysis.**

All activity assays were conducted in at least three independent enzyme reactions, including enzymes from independent preparations. A no enzyme (-TrxR1) control was subtracted from all reactions. All error bars represent one standard deviation, and p-values were calculated from a one-way analysis of variance.

## **3.3. Results**

### **3.3.1. Purification of acK and Selenocysteine-Containing TrxR1 Variants.**

We used genetic code expansion to produce TrxR1 variants in *E. coli* with 22 different genetically encoded amino acids, including the non-canonical amino acids (ncAAs) N<sub>ε</sub>-acetyl-lysine (acK) and selenocysteine (Sec) (Fig 3.2). We previously described purification, biochemical characterization and mass spectrometry analysis of each of TrxR1 variants to determine activity and verify incorporation of acK at K141, K200, or K307 as well as Sec incorporation at the key active residue Sec550 [11]. Briefly, we used a genetic code expansion system based on a PylRS mutant with activity for ligating acK to tRNA<sup>Pyl</sup>, which decodes amber (UAG) stop codons. Thus, by placing a UAG codon at the positions 141, 200 or 307 in our expression construct (Fig 3.2), we generated site-specifically acetylated TrxR1 variants.

Our TrxR1 expression construct also has a *E. coli* SECIS appended to the 3'-untranslated region of our recombinant human TrxR1 gene. The SECIS element recruits the endogenous Sec-incorporation machinery to recode a UGA codon at position 551 from stop to Sec (Fig 3.2). Bacterial cultures must be supplemented with sodium selenite to enable Sec formation (see Materials and Methods). The data generated below are based on multiple independent enzyme preparations, of which representative purified samples were visualized by SDS-PAGE (Fig S3.1).

### **3.3.2. Resistance of Site-Specifically Acetylated TrxR1 to Oxidative Damage.**

Because our work showed increased activity of site-specifically acetylated TrxR1 [11] and previous studies implicated increased TrxR1 acetylation as a response to oxidative damage [15], we hypothesized that acTrxR1 may be more active under oxidizing conditions or even resistant to oxidative damage. In cells, there are many sources of ROS, including superoxide, hydroxy and nitric oxide radicals as well as H<sub>2</sub>O<sub>2</sub>, which is also an important signaling molecule [24].

In mammalian cells, physiological concentrations of H<sub>2</sub>O<sub>2</sub> usually range from 0.1 to 10 μM, while cell stress responses are associated with greater peroxide concentrations in range of 10 to 500 μM [25]. In apoptotic or necrotic human melanoma cells, peroxide levels can rise to more than 500 μM [26]. To mimic oxidative damage that occurs in cells, we designed a series of experiments to measure the activity and initial velocity of purified TrxR1 and acTrxR1 variants under a range of peroxide concentrations (0 to 500 μM) encountered by normal as well as stressed cells. We first measured the catalytic activity of site-specifically acetylated TrxR1 (acTrxR1) variants as well as the wild-type (WT) TrxR1 (Fig 3.3). As previously [11], we found that under normal conditions (0 μM H<sub>2</sub>O<sub>2</sub>), each of the acTrxR1 variants showed substantially more activity (~1.5-fold) than the un-

modified TrxR1 (Fig 3.3). Increased activity of acTrxR1 variants is evident in both the maximal level of DTNB reduced (Fig 3.3) as well as the initial velocity observed during the reaction time course (Fig 3.4).

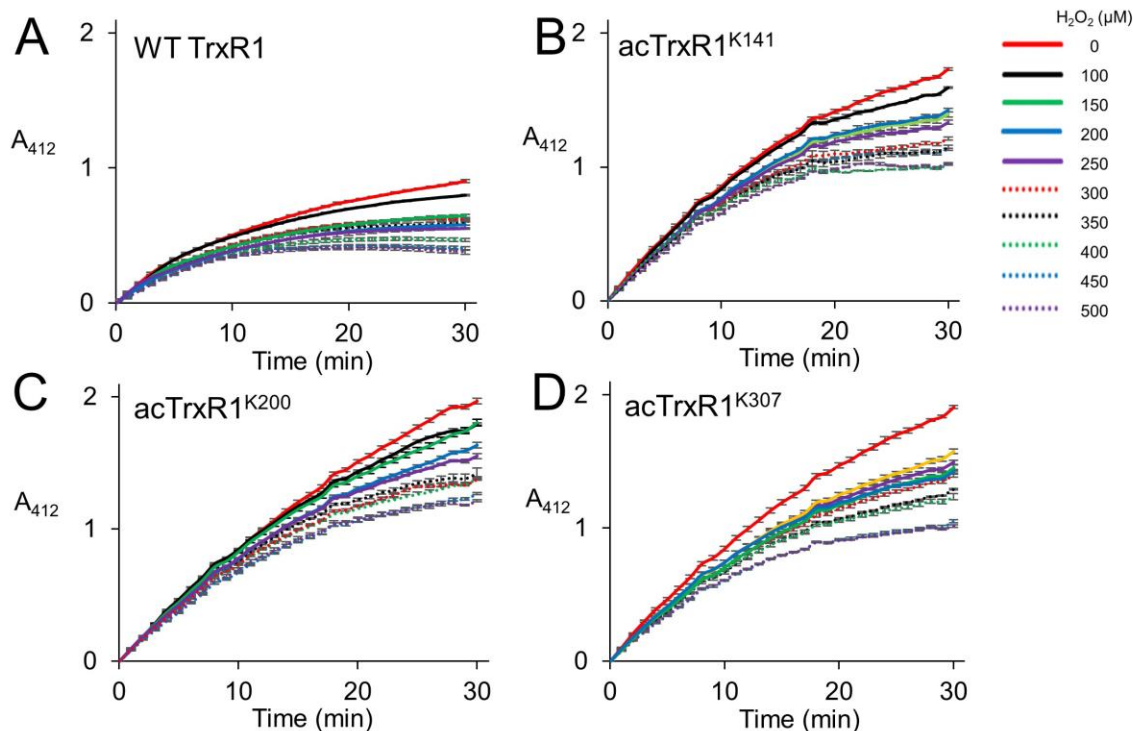


**Figure 3.3. Activity of un-modified TrxR1 and acTrxR1 variants with increasing peroxide levels.** Purified TrxR1 variants were incubated with varying concentrations of buffer or  $H_2O_2$  ranging from 0 to 500  $\mu M$  for 1 hour at 37°C. Following incubation, enzyme activity with the TrxR1 substrate DTNB was determined by following absorbance at 412 nm ( $A_{412}$ ). Activity was measured for (A) wild-type (WT) TrxR1 and site-specifically acetylated variants (B) acTrxR1<sup>K141</sup>, (C) acTrxR1<sup>K200</sup>, and (D) acTrxR1<sup>K307</sup>. Error bars represent  $\pm 1$  standard deviation about the mean of three independent enzyme reactions.

All TrxR1 variants showed reduced catalytic activity with increasing concentrations of hydrogen peroxide ( $H_2O_2$ ). At all concentrations of  $H_2O_2$ , we observed significantly more absolute activity of each acTrxR1 variant compared to WT TrxR1 (Fig 3.4A). Even at the highest peroxide concentrations, the absolute maximal activity level of acTrxR1 variants was still higher than that we observed for WT TrxR1, even without

peroxide treatment (Fig 3.3). The data suggest that the acTrxR1 variants are resistant to oxidation.

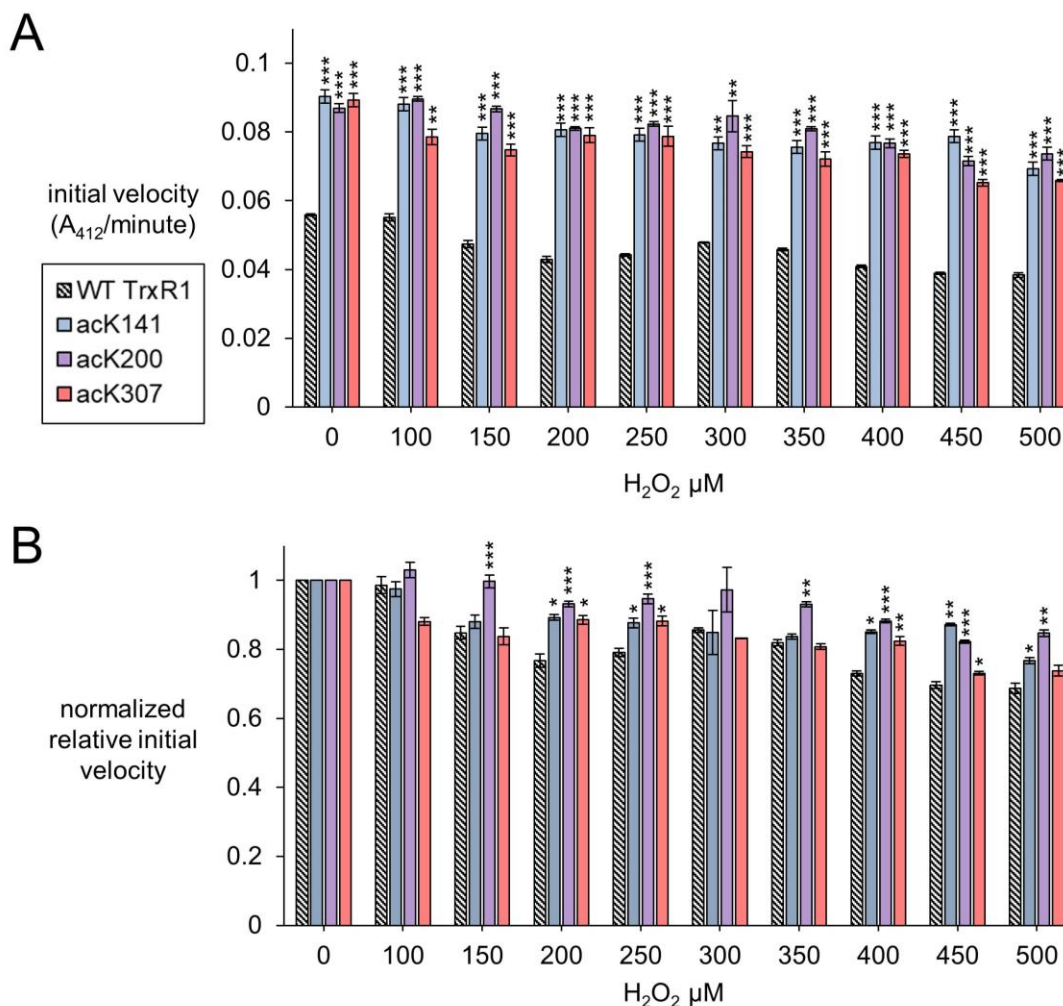


**Figure 3.4. Initial velocity of un-modified and specifically acetylated TrxR1 variants with increasing oxidative damage.** (A) Initial velocity of each TrxR1 variants under the indicated H<sub>2</sub>O<sub>2</sub> concentrations was calculated from the kinetic data (Fig 3.3). (B) To show relative changes in activity, the initial velocities were normalized by the activity of each variant under normal conditions (0 μM H<sub>2</sub>O<sub>2</sub>). Error bars represent ± 1 standard deviation about the mean of three independent enzyme reactions. Significant differences are annotated (\* p < 0.05; \*\* p < 0.01; \*\*\* p < 0.001) to compare activity at each peroxide concentration to the 0 μM condition.

Based on the initial velocity observed in the DTNB reduction reactions, we then calculated the absolute (Fig 3.4A) and relative (Fig 3.4B) reduction in catalytic rate observed in WT compared to acTrxR1 variants with increasing peroxide concentration.

The absolute reaction rates responded to oxidation similarly as noted above. Namely, the acTrxR1s showed reduced initial velocities with increasing peroxide that was always significantly greater than the observed for the wild type TrxR1 (Fig 3.4A). The acTrxR1 variants also show robust or partial resistance to oxidation even when the maximal catalytic rates for TrxR1 and acTrxR1 are both normalized to 1.0. After normalization to WT TrxR1, both acTrxR1<sup>K141</sup> and acTrxR1<sup>K200</sup> showed significantly less relative activity reduction at each peroxide concentration tested (Fig 3.4B). The data demonstrate that acTrxR1<sup>K141</sup> and acTrxR1<sup>K200</sup> are significantly more resistant to oxidation than the un-modified enzyme. For the acTrxR1<sup>K307</sup> variant, we found similar resistance to oxidation in the normalized relative activity rates at about half of the peroxide concentrations tested from 200 – 450  $\mu\text{M}$   $\text{H}_2\text{O}_2$ . The data indicate that site-specific acetylation of TrxR1 is protective against the effects of oxidative damage. Of the acTrxR1 variants, the acTrxR1<sup>K200</sup> variant had the highest level of protection against oxidation induced activity loss compared to the unmodified enzyme, while the acTrxR1<sup>K307</sup> variant had the lowest level of protection against oxidation-induced activity loss compared to the unmodified enzyme (Fig 3.4B)

We also monitored the TrxR1 variants in the above reactions using SDS-PAGE. We visualized the TrxR1 variants under each condition using Coomassie staining and Western blotting with an anti-TrxR1 antibody (Fig S3.2). At the highest peroxide concentration, we observe some degradation of the TrxR1 protein. The western blot revealed the presence of covalently linked high molecular weight TrxR1 oligomers following oxidation with  $\text{H}_2\text{O}_2$  (Fig S3.2, S3.3). For unmodified TrxR1, the high molecular weight complexes are visible already at 100  $\mu\text{M}$  peroxide (Fig S3.2A). Each of the acTrxR1 variants showed less accumulation of the TrxR1 multimers at each peroxide concentration. For the acTrxR1 variants, we observed a similar level of oligomerization to un-modified TrxR1 only at 500  $\mu\text{M}$  peroxide (Fig S3.2B-S3.2D). Quantification of the western blots confirmed that all acTrxR1 variants had a statistically significant reduction in the accumulation of higher molecular weight TrxR1 complexes compared to un-modified



TrxR1 at all peroxide concentrations tested for acTrxR1<sup>K307</sup>, from 100 to 400  $\mu\text{M}$  H<sub>2</sub>O<sub>2</sub> for acTrxR1<sup>K200</sup>, and from 200 to 400  $\mu\text{M}$  H<sub>2</sub>O<sub>2</sub> for acTrxR1<sup>K141</sup> (Fig S3.3).

### **3.3.3. Aspirin Acetylates TrxR1 and Provides Robust Resistance to Oxidative Damage.**

Protein acetylation can occur specifically in cells resulting from the activity of acetyltransferases, but also non-specifically through interactions with acetyl donors including acetyl-CoA or certain drugs, such as aspirin [27]. We hypothesized that like specific or programmed acetylation of TrxR1, general or non-specific acetylation of the enzyme may also provide resistance to oxidative damage.

A previous report used incubated HeLa cells with a range of aspirin concentrations from 0.5 mM to 20 mM to generate aspirin-mediated and non-specific acetylation of many cellular proteins, including TrxR1 [27]. Thus, we used western blotting to detect acetylation of purified TrxR1 resulting from incubation with aspirin over a similar concentration range (Fig 3.5). To estimate the level of acetylated TrxR1, we used our site-specifically modified acTrxR1<sup>K141</sup> as control. The untreated and un-modified TrxR1 showed no reactivity with an anti-acK antibody, while robust detection was evident with the acetylated control sample (acTrxR1<sup>K141</sup>). Lower concentrations of aspirin did not lead to detectable acetylation, but at higher concentrations significant acTrxR1 is clearly present in the blot (Fig 3.5A). We then used the Coomassie stained gel to normalize the amount of protein loaded and determined the relative intensity of bands in the anti-acK immunoblot. We showed previously that acTrxR1<sup>K141</sup> has stoichiometric incorporation of acK at the 141 site [11]. Thus, based on comparison to the control, the relative level of acetylation following aspirin incubation reached a level ~65% of that observed in acTrxR1<sup>K141</sup> (Fig 3.5B).

We next compared the activity of TrxR1 and non-specifically acetylated TrxR1 following incubation with aspirin. In contrast to site-specifically acTrxR1 variants, aspirin incubation results in a slight decrease to ~70% of WT TrxR1 activity that was significantly lower only at the highest aspirin concentrations (> 5 mM) (Fig 3.6B). Controls lacking enzyme (-TrxR1) and with or without aspirin showed no ability to catalytically reduce DTNB (Fig 3.6A). To test the ability of non-specifically acetylated TrxR1 to resist oxidative damage, unmodified TrxR1 was incubated with or without aspirin, followed by a second incubation of 1 hour with increasing peroxide concentrations (0 to 500  $\mu$ M H<sub>2</sub>O<sub>2</sub>) before DTNB reduction activity assays were conducted. In contrast to un-treated TrxR1, TrxR1 incubated with aspirin showed no statistically significant decrease in relative activity in response to any of the H<sub>2</sub>O<sub>2</sub> concentrations tested (Fig 3.6C). The data suggest that aspirin mediated TrxR1 acetylation provides robust resistant to oxidative damage.

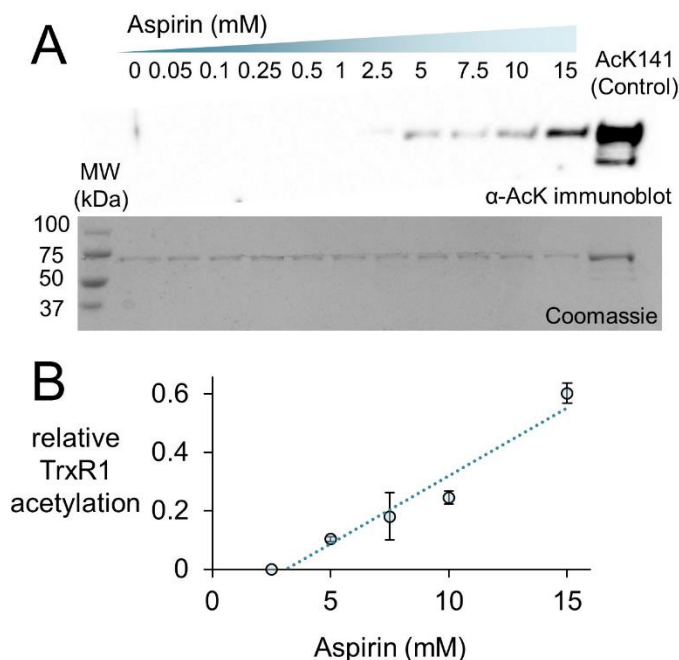


**Figure 3.5. Aspirin acetylates TrxR1.** TrxR1 was incubated with varying concentrations of aspirin (0 to 15 mM) for 1 hour at 37°C. Following incubation, 0.31  $\mu$ g of protein samples were separated on a 15% SDS-PAGE and visualized (A) after immunoblotting with an anti-acetyl-lysine antibody ( $\alpha$ -acK) or staining with Coomassie blue dye. The acTrxR1<sup>K141</sup> produced with genetic code expansion served as a positive control. Based on these data, we calculated the relative level of TrxR1 acetylation compared to the acTrxR1<sup>K141</sup> control (B), which increased linearly with increasing aspirin concentration.

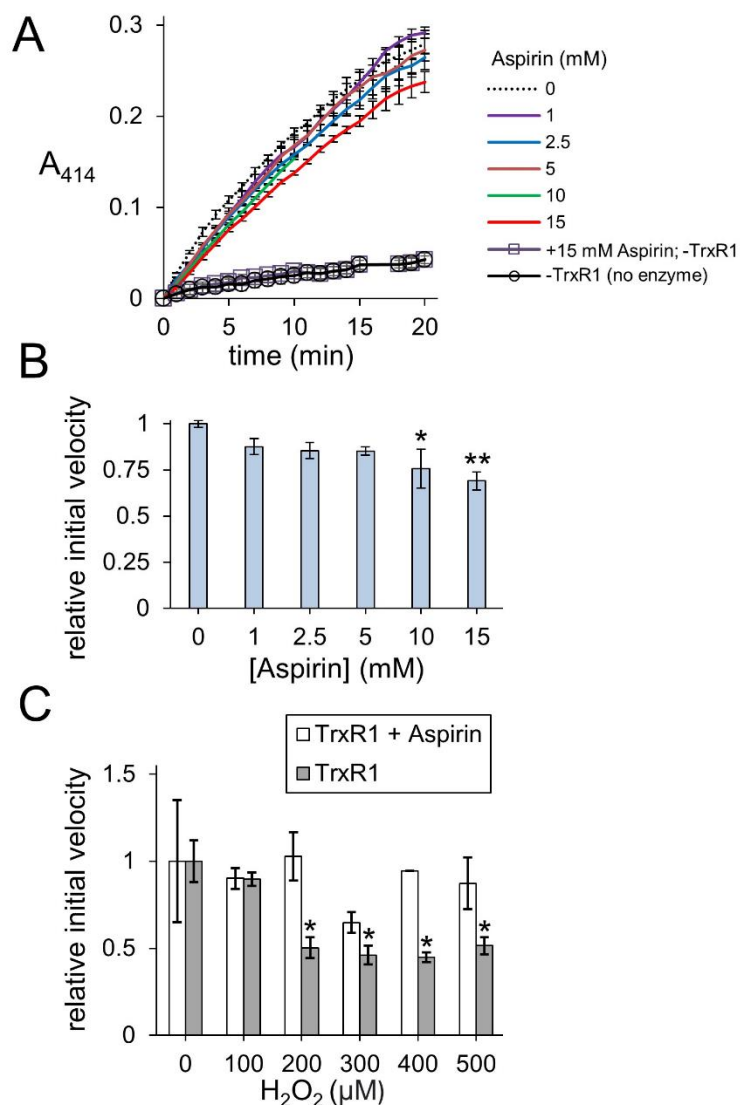


**Figure 3.6. TrxR1 activity following aspirin incubation.** (A) TrxR1 was incubated with 0 to 15 mM aspirin for 1 hour at 37°C, followed by TrxR1 activity assays using DTNB. Negative controls containing no TrxR1 (-TrxR1) with 0 or 15 mM aspirin was also incubated for 1 hour at 37°C, followed by the DTNB assay. (B) Initial velocity was calculated for TrxR1 activity based on the data in (A). Statistical analysis comparing the activity at each aspirin concentration (B) to the untreated enzyme showed significant reductions in activity only at 10 and 15 mM aspirin (\* p < 0.05; \*\* p < 0.005). (C) TrxR1 was incubated with 15 mM aspirin for 1 hour at 37°C, followed by incubation with 0 to 500 μM H<sub>2</sub>O<sub>2</sub> for 1 hour at 37°C. Following incubations, the initial velocity of TrxR1 activity was determined from TrxR1 activity assays and normalized to the initial velocity with 0 μM H<sub>2</sub>O<sub>2</sub>. Statistical analysis comparing the activity at each peroxide concentration show significant reductions in activity in the un-modified TrxR1 only and not in the aspirin treated enzyme (\* p < 0.05). Error bars represent ± 1 standard deviation about the mean of three independent enzyme reactions.

### **3.3.4. Location of TrxR1 Acetylation Sites Following Aspirin Treatment.**

We used tandem mass spectrometry to identify acetylation sites in purified WT TrxR1 following incubation with or without aspirin. Following incubation, the purified protein samples were digested with trypsin and analyzed by LC-MS/MS. We searched the spectra for the possibility of multiple modifications, including lysine acetylation. In the un-treated sample, we identified acetylation only at K307 according to a single peptide hit (Table S3.1), perhaps due to acetylation by acetyl-phosphate in *E. coli* [28]. Based on our observations in the acK immunoblot (Fig 3.5), we can conclude that the untreated TrxR1 has low levels of acetylation at this site.

In contrast, mass spectrometry on aspirin treated TrxR1 identified many new and different lysine acetylation sites supported with multiple, high quality peptides hits to the spectra (Fig 3.7, S3.4, Table S3.1). These data provide strong evidence that aspirin incubation with TrxR1 leads to acetylation at K28, K31, K52, K88, K176, K307, K351, and K360 (Figs 3.7A, S3.4, Table S3.1).

## **3.4. Discussion**

### **3.4.1. Interplay Between Acetylation and Oxidation in the Trx System.**

Many proteins are acetylated or hyper-acetylated in conditions of oxidative stress characterized by elevated levels of ROS [29]. Increased acetylation of lysine residues is a common response to oxidative stress documented in diverse proteins, including histones [30], FoxO [31] and zinc-finger [32] transcription factors, tRNA synthetases [33], and superoxide dismutase [34]. The acetylation status of the Trx system in conditions of oxidative stress is not yet completely characterized, however, increased acetylation of TrxR1 has been linked to oxidative stress in a mouse model of cardiomyopathy [15].

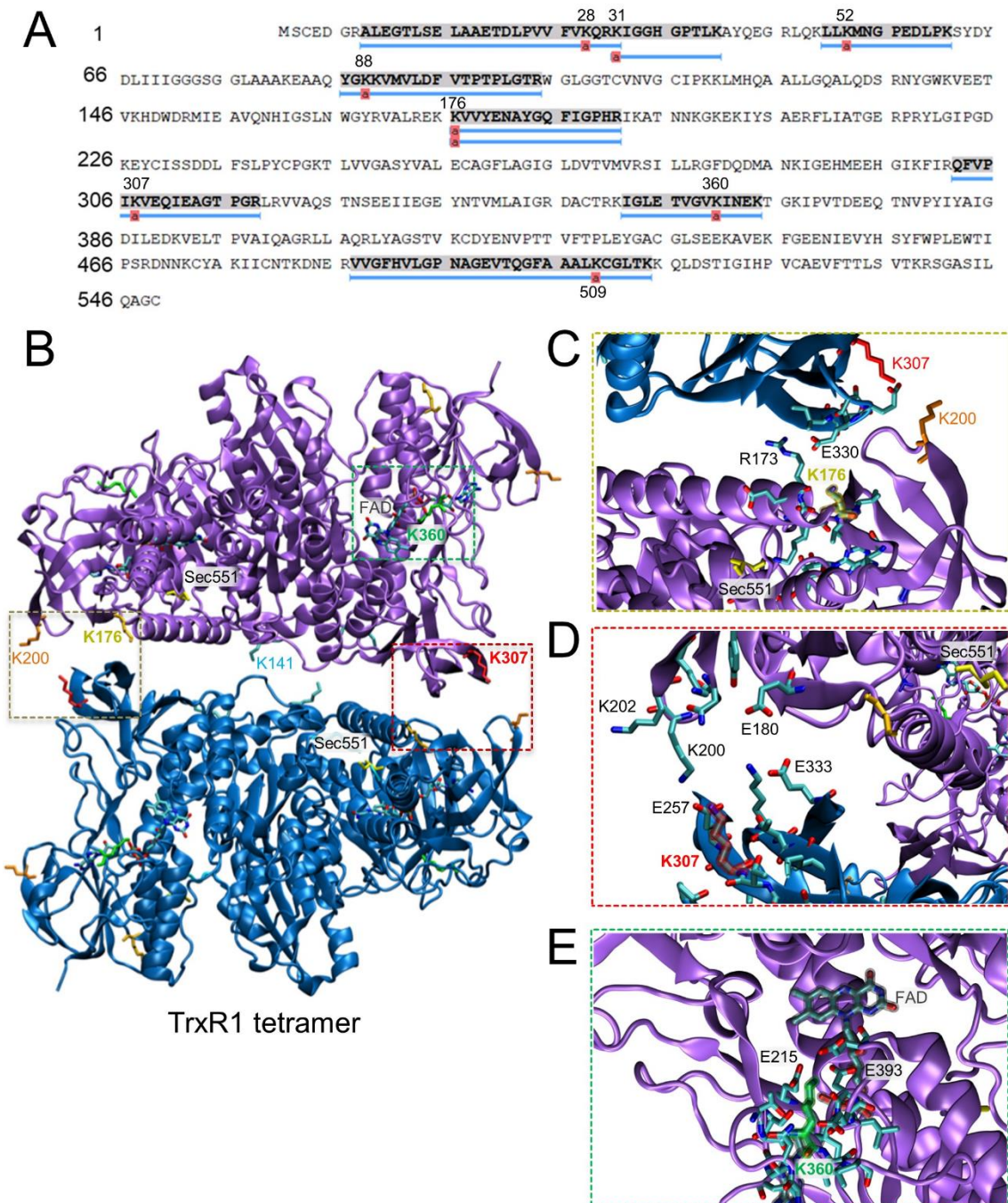


**Figure 3.7. Mapping acetylation sites in TrxR1 to the quaternary structure.** (A) Coverage map showing acetylation sites identified by LC-MS/MS following incubation of TrxR1 with the non-specific acetyl donor aspirin. (B) Lysine acetylation sites were mapped onto the TrxR1 tetramer structure (PDB codes 4KPR and 3EAN [12],): K176 (gold), K307 (red), K360 (green), and K307 (red). Sec551 (yellow) was modeled based on data from the structure 3ean [13]. The FAD co-factor is highlighted (grey). Close-up views show interactions with (C) K176, (D), K307 (E), and K360. Structures were drawn using VMD [35].

Different components of the Trx system, including TrxR1, Trx and Prx are acetylated at multiple lysine residues in mammalian cells [12, 17, 20]. We and others have found that acetylation increases the activity of TrxR1 [11], Trx1 [16], and Prx1 [19]. Data from these studies suggest an emerging theme for how acetylation regulates the activity of the Trx system. Our work documented the ability of site-specific acetylation to increase TrxR1 activity by reducing oligomerization [11], and here we found acetylation also provided robust resistance to oxidative damage and peroxide-induced TrxR1 oligomer formation.

In studies of Trx, TrxR1, and Prx [19], oxidation leads to the formation of low activity oligomers [12, 19], while acetylation provide resistance to oxidative damage and oligomerization [11, 19]. Trx acetylation was linked to increased Trx activity in post-mortem diabetic retinas [16]. Much like Prx and TrxR1, Trx oligomerization is induced by oxidation, whereby Trx forms inactive dimers [36]. The potential for Trx acetylation to counteract oxidation is not yet known. Acetylation of Prx prevents overoxidation and oligomerization [19], while TrxR1 acetylation also provides resistance to oxidative inactivation (Figs 3.4, 3.5) and prevents oligomerization (Figs S3.2, S3.3) [11]. Thus, acetylation may play a similar for Trx, which is an interesting area of future study.

The peroxiredoxins, Prx1 and Prx2, are both acetylated by histone acetyltransferase (HAT) *in vitro*, leading to increased activity and resistance to oxidation [19]. Human prostate cancer cells (LAPC4) readily acetylate Prx1 as Lys197, and these cells as well as another prostate line (LNCaP4) exposed to 25  $\mu\text{M}$  to 100  $\mu\text{M}$   $\text{H}_2\text{O}_2$  produced increasing amounts of high molecular mass Prx oligomers [19], which are associated with reduced Prx peroxidase activity [37]. In order to measure the ability of the acetylated enzyme to resist oxidative stress, the activity of acetylated recombinant Prx1 was measured in up to 2 mM  $\text{H}_2\text{O}_2$ . In the presence of 100  $\mu\text{M}$   $\text{H}_2\text{O}_2$ , a 20% increase in Prx1 activity was associated with acK197 compared to the unmodified enzyme. Compared to our measurements with

TrxR1 at the same peroxide concentration, we found 60-70% increased rate of activity in the acTrxR1 variants compared to the unmodified enzyme.

Here, we presented novel biochemical evidence that acetylation prevents TrxR1 activity loss in response to oxidative damage. Similarly to findings regarding Prx [19], our studies suggest that site-specific acetylation increases TrxR1 activity [11] and regulates TrxR1 oligomerization to prevent oxidative inactivation due to covalently linked multimer formation. TrxR1 forms these inactive cross-linked dimers due to oxidation at Trp114 in the dimer-dimer interface [12]. Taken together, these studies highlight acetylation as a potent regulatory mechanism for Trx system activity that may provide protection against oxidative damage in cells at a time when the Trx system is most in need. The crosstalk between acetylation and oxidation is an open area of research for future work in the Trx system and beyond.

### **3.4.2. Non-Specific Acetylation of Proteins in the Context of Oxidative Stress.**

We also demonstrated acetylation by the non-specific acetyl-donor aspirin provides TrxR1 with resistance to oxidative damage. We did not detect non-specific acetylation at the K141 or K200 sites, indicating these sites may not be accessible to aspirin. We previously found that acK307 reduces the formation of low activity tetramers and cross-linked inactive dimers [11]. K176 is also in the dimer-dimer interface and participates in interactions with E300 of the opposing subunit (Fig 3.7C). K307 is localized close to K176 and in the dimer-dimer interface (Fig 3.7D). Both K176 and K307 participate in salt bridge interactions with the opposing subunit, and acetylation of these sites will weaken or eliminate key interactions that stabilize the TrxR1 tetramers. Other aspirin-mediated acetylation sites, K351 and K360, are located near the Flavin adenine dinucleotide (FAD) cofactor binding site close to the active site of TrxR1 (Fig 3.7). Acetylation of K351 may disrupt interactions

with the FAD co-factor, while acetylation of K360 may disrupt salt bridge interactions between K360 and E215 and E393, which are in the vicinity of the FAD co-factor (Fig 3.7E). Because the position and environment of FAD is critical for TrxR1 function, acetylation at K351 and K360 may be responsible for the marginal loss of TrxR1 activity we observed at high aspirin concentrations (Fig 3.6B).

Various metabolic compounds can non-enzymatically acetylate proteins, including acetyl-CoA [38]. Mitochondrial proteins show increased non-enzymatic acetylation by acetyl-CoA produced alongside energy metabolism [39]. In addition to metabolites, certain drugs, such as aspirin, can lead to acetylation of many proteins [27]. Indeed, the ability of aspirin to reduce inflammation and relieve pain is due to acetylation of the cyclooxygenases COX-1 and COX-2 in their active sites [40]. Studies in mammalian cells demonstrated aspirin-mediated acetylation of p53 and many other cellular proteins using radiolabeled aspirin and immunodetection [41]. These studies provide a direct link between non-enzymatic acetylation of proteins under conditions that generate ROS or in response to certain medications. Non-enzymatic acetylation may play an important role in TrxR1 and other proteins that maintain the balance between oxidative damage and antioxidant defense.

### **3.4.3. Relevance of Trx System Acetylation to Disease.**

Resistance to oxidative damage is of particular interest in cancer biology and therapeutics [42]. The Trx system is overactive in many cancer cells [7, 8, 10]. The reductive power of the Trx system provides resistance to certain chemotherapies relying on the generation of oxidative stress [10]. For example, the anti-cancer agent RITA induces oxidative stress in HCT116 colon cancer cells leading to increased TrxR1 tetramer and cross-linked dimer formation [12]. Newly developed direct inhibitors of TrxR1 have shown efficacy in combination with the cancer chemotherapeutic cisplatin in colon cancer cells [43]. Various other small compounds targeting TrxR1 activity are also of interest for cancer treatments



[44]. Fascinatingly, pre-treatment of the cells with a ROS scavenger and acetate source [45], N-acetyl-L-cysteine, reduced ROS generation, cell death and deoxyribonucleic acid (DNA) damage associated with TrxR1 inhibition.

Higher levels of TrxR1 in the serum correlates with shortened overall survival in patients with non-small cell lung cancer [46]. Proteomic studies of similar cell lines have consistently identified acTrxR1 in Henrietta Lacks (HeLa) cells, A549 cells and related non-small cell lung cancer cell lines [12, 17, 20, 28]. Together our data and other studies suggest that TrxR1 acetylation is a potential mechanism to maintain higher Trx system activity. These findings have relevance for the role of TrxR1 acetylation in cancers with poor survival [46] as well as chemotherapeutic resistance [47, 48].

### **3.5. Conclusion**

We demonstrated both site-specific and non-specific acetylation of TrxR1 provides robust resistance to oxidative damage even under oxidizing conditions that represent the full range of ROS experienced by TrxR1 in cells. Because TrxR1 plays a vital role in resolving oxidative damage on Trx and other target proteins, TrxR1 and the activity of the Trx system activity is most important to the cell under conditions of oxidative stress or chemotherapeutic assault. Acetylation of TrxR1 provides a route to increase redox activity, enabling TrxR1 to resist oxidative damage associated with the very reactive oxygen species that the enzyme is tasked to resolve.

### **3.6. Conflict of Interest**

*The authors declare that the research was conducted in the absence of any commercial or financial relationships that could be construed as a potential conflict of interest.*

### **3.7. Author Contributions**

D.W. and N.P. performed experiments and collected data. D.W. and P.O. designed the study, analysed the data, and wrote and edited the manuscript.

### **3.8. Funding**

This work was supported from the Natural Sciences and Engineering Research Council of Canada [04282 to P.O.]; Canada Research Chairs [232341 to P.O.]; and the Canadian Institutes of Health Research [165985 to P.O.].

### **3.9. Acknowledgements**

We are grateful to Ilka Heinemann for critical discussions. We are also grateful to Victoria Clarke and Paula Pittock for assistance with mass spectrometry, sample preparation and analysis.

### 3.10. References

1. Schweizer, U. and N. Fradejas-Villar, *Why 21? The significance of selenoproteins for human health revealed by inborn errors of metabolism*. FASEB J, 2016. **30**(11): p. 3669-3681.
2. Kim, H.Y. and V.N. Gladyshev, *Methionine sulfoxide reductases: selenoprotein forms and roles in antioxidant protein repair in mammals*. Biochem J, 2007. **407**(3): p. 321-9.
3. Lu, J. and A. Holmgren, *Thioredoxin system in cell death progression*. Antioxid Redox Signal, 2012. **17**(12): p. 1738-47.
4. Mustacich, D. and G. Powis, *Thioredoxin reductase*. Biochem J, 2000. **346 Pt 1**: p. 1-8.
5. Arner, E.S., L. Zhong, and A. Holmgren, *Preparation and assay of mammalian thioredoxin and thioredoxin reductase*. Methods Enzymol, 1999. **300**: p. 226-39.
6. Arner, E.S., *Focus on mammalian thioredoxin reductases--important selenoproteins with versatile functions*. Biochim Biophys Acta, 2009. **1790**(6): p. 495-526.
7. Selenius, M., et al., *Selenium and the selenoprotein thioredoxin reductase in the prevention, treatment and diagnostics of cancer*. Antioxid Redox Signal, 2010. **12**(7): p. 867-80.
8. Dong, C., et al., *Role of thioredoxin reductase 1 in dysplastic transformation of human breast epithelial cells triggered by chronic oxidative stress*. Sci Rep, 2016. **6**: p. 36860.
9. Wang, L., et al., *Ethaselen: a potent mammalian thioredoxin reductase 1 inhibitor and novel organoselenium anticancer agent*. Free Radic Biol Med, 2012. **52**(5): p. 898-908.
10. Roh, J.L., et al., *Targeting of the Glutathione, Thioredoxin, and Nrf2 Antioxidant Systems in Head and Neck Cancer*. Antioxid Redox Signal, 2017. **27**(2): p. 106-114.
11. Wright, D.E., et al., *Acetylation Regulates Thioredoxin Reductase Oligomerization and Activity*. Antioxid Redox Signal, 2018. **29**(4): p. 377-388.
12. Wu, Q., et al., *Suberoylanilide hydroxamic acid treatment reveals crosstalks among proteome, ubiquitylome and acetylome in non-small cell lung cancer A549 cell line*. Sci Rep, 2015. **5**: p. 9520.
13. Rengby, O., et al., *Highly active dimeric and low-activity tetrameric forms of selenium-containing rat thioredoxin reductase 1*. Free Radic Biol Med, 2009. **46**(7): p. 893-904.
14. Shu, N., et al., *Inhibition and crosslinking of the selenoprotein thioredoxin reductase-1 by p-benzoquinone*. Redox Biol, 2020. **28**: p. 101335.
15. Banerjee Mustafi, S., et al., *Aggregate-prone R120GCRYAB triggers multifaceted modifications of the thioredoxin system*. Antioxid Redox Signal, 2014. **20**(18): p. 2891-906.
16. Folami Lamoke, C.S., Annamaria Maraschi, Frances Fan, Annalisa Montemari, Dennis M. Marcus, Pamela M. Martin, Manuela Bartoli, *Epigenetic Regulation of Endogenous Antioxidants in the Diabetic Retina*. Investigative Ophthalmology & Visual Science, 2011. **52**(14).

17. Choudhary, C., et al., *Lysine acetylation targets protein complexes and co-regulates major cellular functions*. Science, 2009. **325**(5942): p. 834-40.
18. Lamoke, F., et al., *Epigenetic Regulation of Endogenous Antioxidants in the Diabetic Retina*. Investigative Ophthalmology & Visual Science, 2011. **52**(4448): p. -.
19. Parmigiani, R.B., et al., *HDAC6 is a specific deacetylase of peroxiredoxins and is involved in redox regulation*. Proc Natl Acad Sci USA, 2008. **105**(28): p. 9633-8.
20. Hornbeck, P.V., et al., *PhosphoSitePlus, 2014: mutations, PTMs and recalibrations*. Nucleic Acids Res, 2015. **43**(Database issue): p. D512-20.
21. Guo, L.T., et al., *Polyspecific pyrrolysyl-tRNA synthetases from directed evolution*. Proc Natl Acad Sci USA, 2014. **111**(47): p. 16724-9.
22. Fan, C., et al., *Rationally evolving tRNAPyl for efficient incorporation of noncanonical amino acids*. Nucleic Acids Res, 2015. **43**(22): p. e156.
23. Serrao, V.H.B., et al., *The unique tRNA(Sec) and its role in selenocysteine biosynthesis*. Amino Acids, 2018. **50**(9): p. 1145-1167.
24. Bae, Y.S., et al., *Regulation of reactive oxygen species generation in cell signaling*. Mol Cells, 2011. **32**(6): p. 491-509.
25. Sies, H., *Hydrogen peroxide as a central redox signaling molecule in physiological oxidative stress: Oxidative eustress*. Redox Biol, 2017. **11**: p. 613-619.
26. Clement, M.V., A. Ponton, and S. Pervaiz, *Apoptosis induced by hydrogen peroxide is mediated by decreased superoxide anion concentration and reduction of intracellular milieu*. FEBS Lett, 1998. **440**(1-2): p. 13-8.
27. Tatham, M.H., et al., *A Proteomic Approach to Analyze the Aspirin-mediated Lysine Acetylation*. Mol Cell Proteomics, 2017. **16**(2): p. 310-326.
28. Weinert, B.T., et al., *Lysine succinylation is a frequently occurring modification in prokaryotes and eukaryotes and extensively overlaps with acetylation*. Cell Rep, 2013. **4**(4): p. 842-51.
29. Santo-Domingo, J., L. Dayon, and A. Wiederkehr, *Protein Lysine Acetylation: Grease or Sand in the Gears of beta-Cell Mitochondria?* J Mol Biol, 2020. **432**(5): p. 1446-1460.
30. Gu, X., et al., *Oxidative stress induces DNA demethylation and histone acetylation in SH-SY5Y cells: potential epigenetic mechanisms in gene transcription in Abeta production*. Neurobiol Aging, 2013. **34**(4): p. 1069-79.
31. Daitoku, H., J. Sakamaki, and A. Fukamizu, *Regulation of FoxO transcription factors by acetylation and protein-protein interactions*. Biochim Biophys Acta, 2011. **1813**(11): p. 1954-60.
32. Wu, C.C., et al., *Upregulation of Znf179 acetylation by SAHA protects cells against oxidative stress*. Redox Biol, 2018. **19**: p. 74-80.
33. Cao, X., et al., *Acetylation promotes TyrRS nuclear translocation to prevent oxidative damage*. Proc Natl Acad Sci USA, 2017. **114**(4): p. 687-692.
34. Ozden, O., et al., *Acetylation of MnSOD directs enzymatic activity responding to cellular nutrient status or oxidative stress*. Aging (Albany NY), 2011. **3**(2): p. 102-7.
35. Humphrey, W., A. Dalke, and K. Schulten, *VMD: visual molecular dynamics*. J Mol Graph, 1996. **14**(1): p. 33-8, 27-8.

36. Ren, X., et al., *Mutagenesis of structural half-cystine residues in human thioredoxin and effects on the regulation of activity by selenodiglutathione*. *Biochemistry*, 1993. **32**(37): p. 9701-8.
37. Moon, J.C., et al., *Oxidative stress-dependent structural and functional switching of a human 2-Cys peroxiredoxin isotype II that enhances HeLa cell resistance to H<sub>2</sub>O<sub>2</sub>-induced cell death*. *J Biol Chem*, 2005. **280**(31): p. 28775-84.
38. Weinert, B.T., et al., *Acetylation dynamics and stoichiometry in *Saccharomyces cerevisiae**. *Mol Syst Biol*, 2014. **10**: p. 716.
39. Wagner, G.R. and R.M. Payne, *Widespread and enzyme-independent Nepsilon-acetylation and Nepsilon-succinylation of proteins in the chemical conditions of the mitochondrial matrix*. *J Biol Chem*, 2013. **288**(40): p. 29036-45.
40. Loll, P.J., D. Picot, and R.M. Garavito, *The structural basis of aspirin activity inferred from the crystal structure of inactivated prostaglandin H<sub>2</sub> synthase*. *Nat Struct Biol*, 1995. **2**(8): p. 637-43.
41. Alfonso, L.F., K.S. Srivenugopal, and G.J. Bhat, *Does aspirin acetylate multiple cellular proteins? (Review)*. *Mol Med Rep*, 2009. **2**(4): p. 533-7.
42. Klaunig, J.E., *Oxidative Stress and Cancer*. *Curr Pharm Des*, 2018. **24**(40): p. 4771-4778.
43. Zhang, T., et al., *Curcuminoid WZ26, a TrxR1 inhibitor, effectively inhibits colon cancer cell growth and enhances cisplatin-induced cell death through the induction of ROS*. *Free Radic Biol Med*, 2019. **141**: p. 93-102.
44. Zhang, J., et al., *Targeting the Thioredoxin System for Cancer Therapy*. *Trends Pharmacol Sci*, 2017. **38**(9): p. 794-808.
45. Raftos, J.E., et al., *Kinetics of uptake and deacetylation of N-acetylcysteine by human erythrocytes*. *Int J Biochem Cell Biol*, 2007. **39**(9): p. 1698-706.
46. Chen, G., et al., *The serum activity of thioredoxin reductases 1 (TrxR1) is correlated with the poor prognosis in EGFR wild-type and ALK negative non-small cell lung cancer*. *Oncotarget*, 2017. **8**(70): p. 115270-115279.
47. Raninga, P.V., et al., *TrxR1 inhibition overcomes both hypoxia-induced and acquired bortezomib resistance in multiple myeloma through NF- $\kappa$ B inhibition*. *Cell Cycle*, 2016. **15**(4): p. 559-72.
48. Iwasawa, S., et al., *Upregulation of thioredoxin reductase 1 in human oral squamous cell carcinoma*. *Oncol Rep*, 2011. **25**(3): p. 637-44.

### 3.11. Chapter 3 Appendix – Supplementary Tables and Figures

#### 3.11.1. Supplementary Tables.

**Table S3.1. MS/MS identified peptides showing lysine acetylation sites in TrxR1.**

<b>Residue number</b>	<b>Peptide identified</b>	<b>-10logP</b>	<b>observed m/z</b>
TrxR1 + aspirin			
28	ALEGTLSELAAETDLPVVFVK(+42.01)QRK(+21.98)	67.56	1339.7255
31	K(+42.01)IGGHGPTLK	68.67	525.3088
52	LLK(+42.01)M(+15.99)NGPEDLPK	82.5	706.8766
88	YGK(+42.01)KVM(+15.99)VLDFVTPPLGTR	63.00	727.3947
176	K(+42.01)VVY(+42.01)ENAYGQFIGPHR	68.26	654.6655
176	K(+42.01)(+43.99)VVYENAYGQFIGPHR	75.22	655.3327
176	K(+57.02)(+42.01)VVYENAYGQFIGPHR	78.52	659.6704
307	QFVPIK(+42.01)VEQIEAGTPGR	81.28	637.6832
351	K(+27.99)(+42.01)IGLETVGVK	60.77	557.3230
360	IGLETVGVK(+42.01)INEK	64.32	721.4198
TrxR1 (un-modified)			
307	K(+57.02)(+42.01)VVYENAYGQFIGPHR	70.47	659.6697

### 3.11.2. Supplementary Figures.

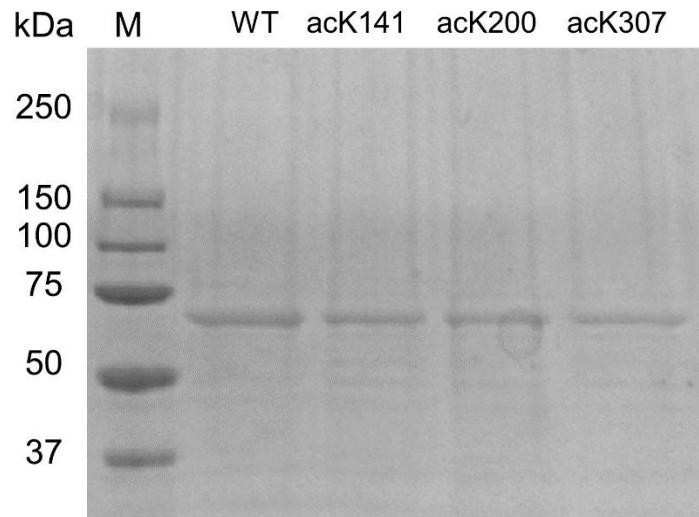


**Figure S3.1. Purified TrxR1 and site-specifically acetylated TrxR1 variants.** Unmodified and acetylated TrxR1 (acTrxR1) variants were purified by nickel column and run on a 15% SDS PAGE, followed by staining with Coomassie. Lanes labels: M indicates a molecular weight marker; wild-type TrxR1 (WT), acTrxR1<sup>K141</sup> (acK141), acTrxR1<sup>K200</sup> (acK200), and acTrxR1<sup>K307</sup> (acK307).

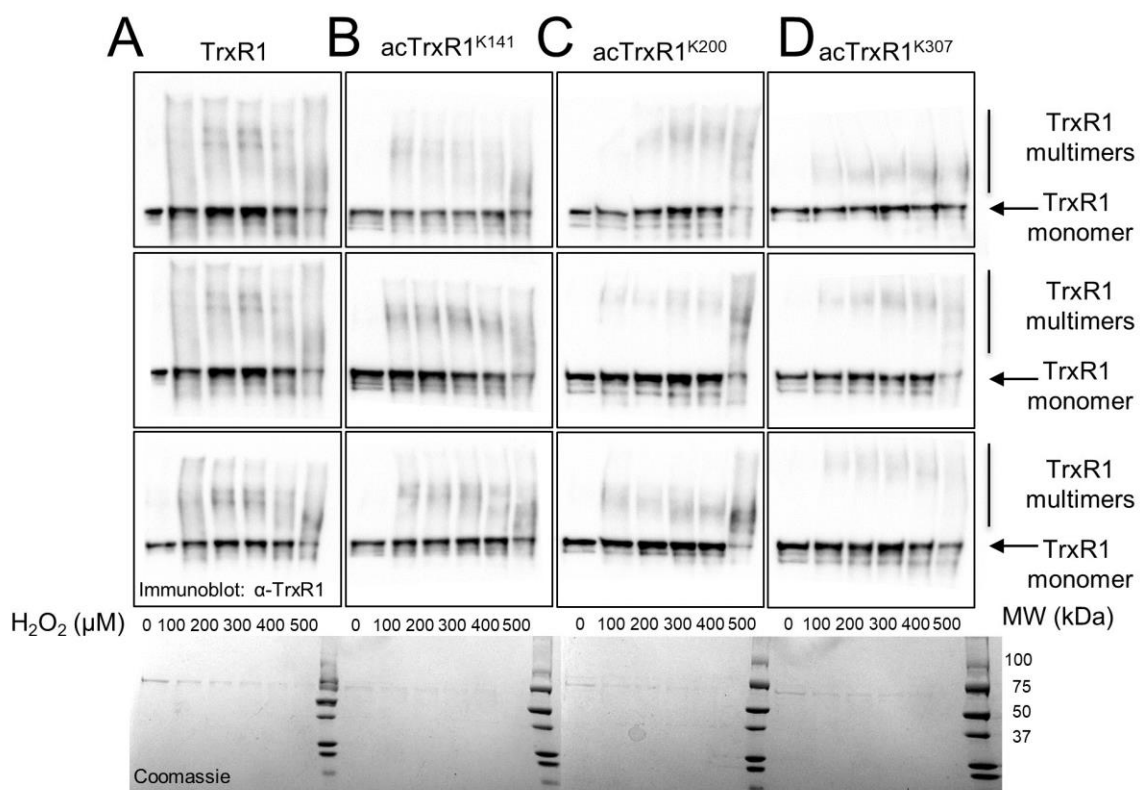


**Figure S3.2. Oxidation of TrxR1 and site-specifically acetylated TrxR1 variants.** Purified (A) unmodified TrxR1 or (B-D) acetylated TrxR1 variants were incubated with buffer or buffer containing increasing concentrations of H<sub>2</sub>O<sub>2</sub> ranging from 0 to 500 μM for 1 hour at 37°C. Following incubation, the proteins were visualized by SDS-PAGE followed by Western blotting (anti-TrxR1, above) or Coomassie staining (below). Annotations indicate the molecular weight of TrxR1 monomers and peroxide-induced multimers.



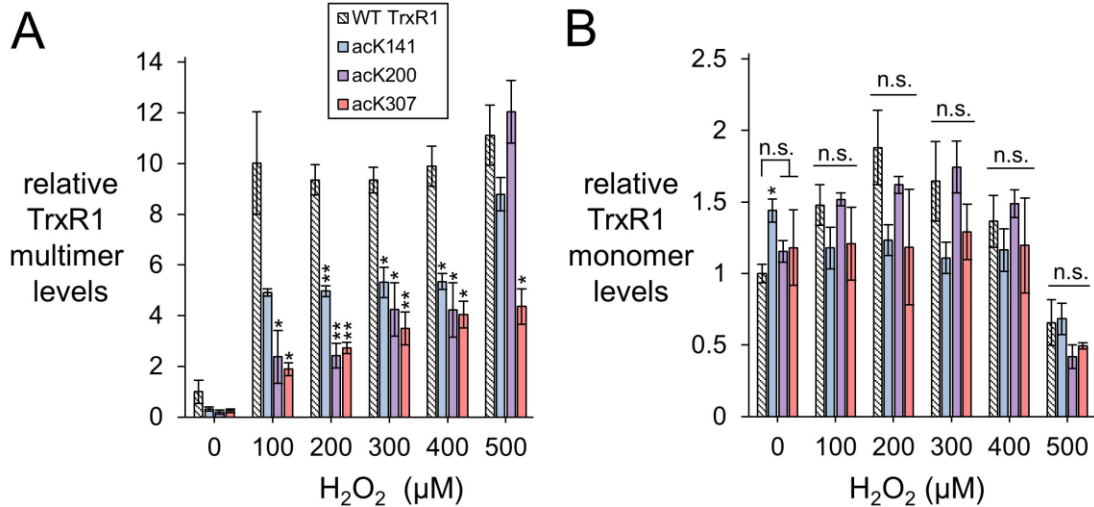


**Figure S3.3. Quantification of TrxR1 western blot.** The anti-TrxR1 blots (Fig. S2) were used to quantify the level of TrxR1 (A) high molecular multimeric complexes or (B) monomers for wild type (WT) and acTrxR1 variants incubated with 0 to 500  $\mu\text{M}$   $\text{H}_2\text{O}_2$ . Densitometry from the anti-TrxR1 western blot was normalized by the level observed for wild type TrxR1 (A) multimer or (B) monomer. Error bars represent  $\pm 1$  standard deviation about the mean of three independent enzyme incubations. Statistical analysis (ANOVA) comparing the amount of protein for each acTrxR1 variant to wild-type TrxR1 at nearly all  $\text{H}_2\text{O}_2$  concentrations demonstrated consistent and significant reductions (by 2 to 5- fold) in high molecular weight complexes (A) for acTrxR1 variants compared to unmodified TrxR1. At 500  $\mu\text{M}$  peroxide, only the acTrxR1<sup>K307</sup> remains resistant to significant multimerization. Except for a modest and less than 1.5-fold increase in the level of monomeric acTrxR1<sup>K141</sup> at 0  $\mu\text{M}$  peroxide, the level of monomer observed was not significantly different between wild type and acTrxR1 at each peroxide concentration tested. Significant differences are annotated (\*  $p < 0.05$ ; \*\*  $p < 0.005$ ; n.s. – not significant).

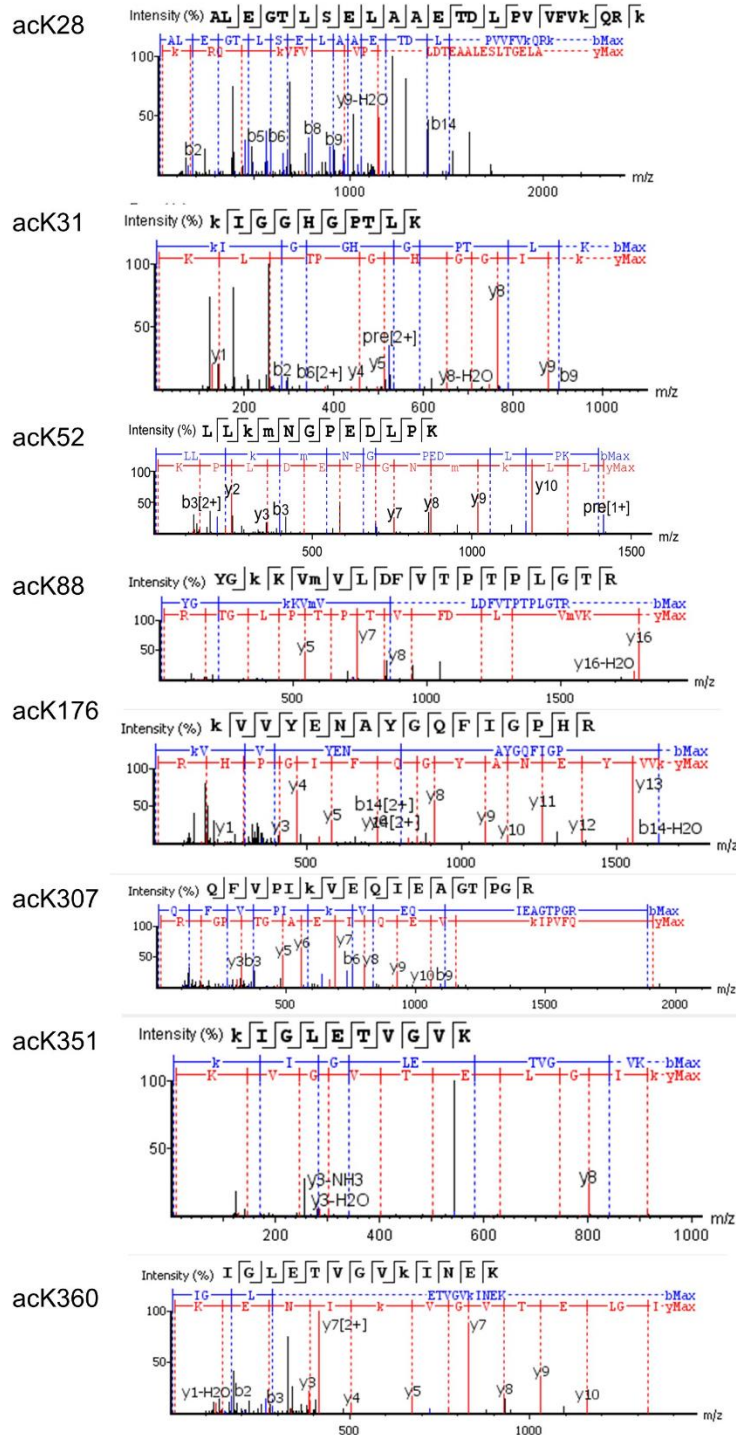


**Figure S3.4. MS/MS spectra of representative TrxR1 peptides showing lysine acetylation following aspirin incubation.** Unmodified TrxR1 was incubated with 15 mM aspirin and then the digested with trypsin and analyzed by LC-MS/MS. These spectra are representative of the complete list of high confidence acetylated peptides identified (Table S3.1).

## Chapter 4

### 4. Delivery of the Selenoprotein

#### Thioredoxin Reductase 1 to Mammalian Cells

##### 4.1. Introduction

Mammalian thioredoxin reductases (TrxRs) are an important enzyme family that helps to protect cells from damage caused by reactive oxygen species (ROS) [1] and serves critical roles in redox signaling [2]. TrxR1 is the most abundant member of the TrxR family and is expressed in the cytosol [1]. TrxR1 is also a validated cancer target, and several efforts are underway to generate new inhibitors of TrxR1 that can compromise the rapid growth of cancer cells [3, 4]. For example, recent work on compounds with a 4,5-dichloropyridazinone core structure were identified as irreversible TrxR1 inhibitors that displayed potent toxicity in a series of cancer cells [5].

TrxR1 is a selenoprotein [6], and its activity relies on the efficient incorporation of selenocysteine (Sec, U) in response to the UGA codon at position 550. TrxR1 is a complex enzyme that catalyzes the transfer of electrons from a bound nicotinamide adenine dinucleotide phosphate (NADPH) cofactor, with the aid of a second flavin adenine dinucleotide (FAD) cofactor, to a disulfide N-terminal active site. From there, TrxR1 transfers electrons to the C-terminal selenylsulfide active site (GCUG). The enzyme then reduces the selenylsulfide to selenolthiol that subsequently acts to reduce oxidized substrates in the cell. Thus, the Sec residue forms a critical part of the TrxR1 active site and is necessary for its enzymatic reduction of the oxidized thioredoxin (Trx), a major TrxR1 substrate [7]. The reduced Trx1 is then able to resolve oxidative damage in cellular proteins [8]. TrxR1 itself is also able to directly reduce protein disulfide substrates [9] and small molecule ROS, including hydrogen peroxide ( $H_2O_2$ ) [10], lipoic acid [11], selenite [12], and quinones [13].

Because of the vital role of TrxR1 in human biology and applications in medicine, there is a continuing need to generate mammalian cells with precise levels of TrxR1 activity. Applications of these cell lines will provide insight into how TrxR1 activity regulates redox biology in human cells and provide a critical platform to screen new inhibitors of TrxR1. One roadblock in this area involves the challenges of generating mammalian cell lines that over-express TrxR1. Unfortunately, normal approaches to genetically over-express TrxR1 in mammalian cells lead to increased cell death. Over-expression of TrxR1 by stable transfection produced a > 2-fold increase in cell death in Michigan cancer foundation-7 (MCF-7) cells compared to empty vector control [14]. A form of TrxR1 that stops at the UGA550 codon, and lacks the C-terminal Sec-Gly dipeptide, is toxic and induces cell death in human A549 cells [15]. In human embryonic kidney (HEK) 293T cells, one recent report generated a stable cell line over-expressing TrxR1, yet no experiments were provided to demonstrate incorporation of Sec in TrxR1 or to evaluate apoptosis [16]. Direct lipid-mediated transfection of TrxR1 protein lacking the two C-terminal residues caused a significant increase in cell death, while transfection of the full-length and Sec-containing TrxR1 showed no change in cell toxicity [15]. These observations may result from selenium compromised thioredoxin reductase-derived apoptotic proteins (SecTRAPs) [17]. Indeed, inhibition of genetically encoded TrxR1 in mammalian cells can also produce SecTRAPs and induce apoptosis [18].

We previously developed a genetic code expansion approach with Sec to generate recombinant human TrxR1 from *Escherichia coli* containing stoichiometric incorporation of Sec at position 550 (Fig 4.1) [7, 19, 20]. Here we used the same approach and produced a novel form of recombinant human TrxR1 that also contains a N-terminal cell penetrating peptide (CPP) tag derived from the human immunodeficiency virus (HIV) Trans-Activator of Transcription (TAT) protein [21-23]. The TAT protein binds to the HIV promoter to recruit transcription complexes and is essential for transcription of viral genes and HIV replication [24]. TAT is also excreted from infected cells and can cross the plasma

membrane of various eukaryotic cells to alter their gene expression and cellular function [25], which can help HIV to spread to neighboring cells and contributes to the development of comorbidities associated with HIV infection, such as the development of acquired immunodeficiency syndrome, cancers, accelerated aging, cardiovascular diseases, and neurocognitive disorders [26]. A small basic domain allows the TAT protein to penetrate cellular membranes, permitting cellular uptake, and this basic TAT domain has since been widely used as a CPP to allow for transduction of recombinant proteins other than TAT into various mammalian and plant cells [25].

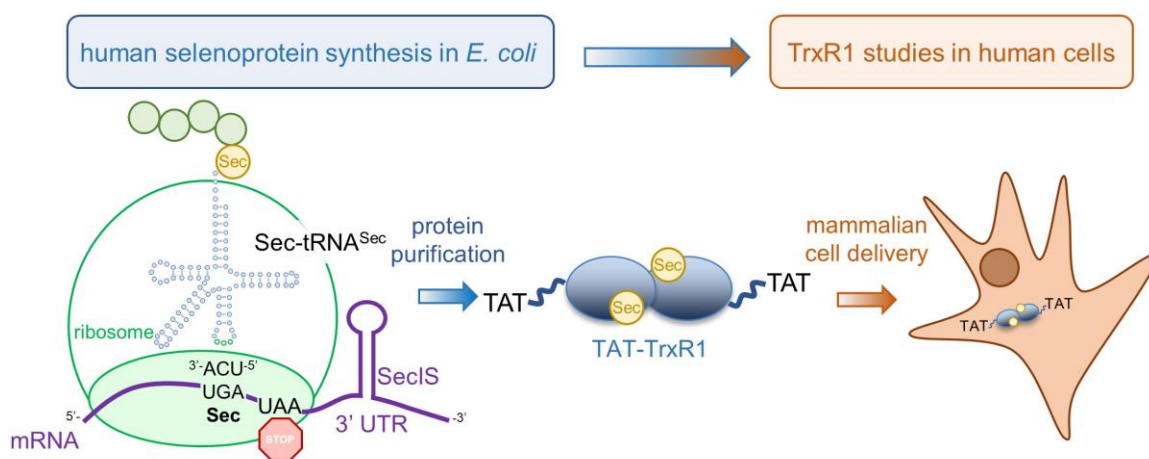


**Figure 4.1. Production of recombinant selenocysteine containing TrxR1 in *E. coli* and delivery to mammalian cells.** Recombinant production of human TrxR1 containing Sec550 was accomplished by fusing a bacterial Sec insertion sequence (SecIS) hairpin to the 3' untranslated region of the human TrxR1 gene [20]. We have previously confirmed that the approach leads to the stoichiometric installation of Sec and the production of abundant and active human TrxR1 from bacterial cells [7, 19, 20]. The construct used here also contains an N-terminal TAT peptide fusion (YGRKKRRQRRRPQ) that enables efficient delivery of purified recombinant TAT-TrxR1 to mammalian cells.

CPPs, such as the TAT peptide, include a diverse and growing catalog of small peptide tags that can be used to deliver proteins [27], mRNAs [28], and small molecules [29], including pharmaceutical compounds, directly to mammalian cells [30]. We used a CPP tag to circumvent the need to genetically over-express TrxR1 due to the pitfalls associated with expressing TrxR1 in mammalian cells. Using a genetically encoded red

fluorescent TrxR1 activity reporter (redox sensitive red fluorescent protein (RFP) fused to Trx1 (TrxRFP1)) [31], we found that TAT-dependent uptake was rapid and led to robust TrxR1 activity in mammalian cells. The TAT-tag provides a greatly needed platform to study TrxR1 biology and our technology will enable future studies to identify novel TrxR1 inhibitors for applications in cancer and other human diseases.

## **4.2. Materials & Methods**

### **4.2.1. Plasmids and Molecular Cloning.**

Wild-type (WT) TrxR1 was expressed in *E. coli* from the plasmid pET-TrxR1, previously described [7], that contains N-terminally His<sub>6</sub>-tagged human TrxR1 (isoform 4) with a UGA codon at residue Sec550. The TrxR1 gene is followed by selenocysteine insertion sequence (SecIS) RNA hairpin loop, which is derived from the *E. coli fdhF* gene, in the 3' untranslated region (UTR) [7, 19, 20]. Site-specific insertion of Sec at the UGA550 codon depends on recruitment of the native *E. coli* Sec insertion machinery that decodes the UGA550 codon as Sec due to the adjacent SecIS in the 3' UTR, as previously [7, 19, 20].

The bacterial expression vector pTAT-HA, a kind gift from Steven Dowdy (Addgene plasmid #35612), was used to produce TAT fused TrxR1 protein. The pTAT-HA vector includes an N-terminal His<sub>6</sub>-tag upstream of the adjacent TAT peptide sequence (YGRKKRRQRRR) [32]. The TrxR1 gene including the 3'UTR SecIS was polymerase chain reaction (PCR) amplified using primers with *Nco*I and *Eco*RI restriction sites on the 5' and 3' ends, respectively. Following digestion of the pTAT-HA vector and TrxR1 insert, T4 DNA ligase (New England Biolabs, Ipswich, MA, USA) was used to clone TrxR1 into the *Nco*I and *Eco*RI sites in the pTAT-HA vector. The resulting construct was verified by DNA sequencing (Azenta Life Sciences, New Jersey, USA). Sequences of the TrxR1 and TAT-TrxR1 gene constructs are available in the Appendix.

#### **4.2.2. TrxR1 Protein Purification.**

*E. coli* strain BL21 (DE3) was transformed with pET-TrxR1 or pTAT-TrxR1 plasmid. Following selection on lysogeny broth (LB) agar plates containing 100 µg/mL ampicillin, at least 3 independent single colonies were inoculated into separate overnight 10 mL pre-cultures in LB with 100 µg/mL ampicillin. The pre-cultures were then used to inoculate preparative 1 L cultures in LB containing 100 µg/mL ampicillin and 10 µM sodium selenite and were incubated with shaking at 37 °C. We followed a previously optimized protocol for the production of selenoproteins in *E. coli* [7, 19, 20]. At  $A_{600} = 1.2$ , the temperature was decreased to 20 °C. At  $A_{600} = 1.5$ , 1 mM isopropyl β-d-1-thiogalactopyranoside (IPTG) was added to the culture with shaking for 18 hours to induce protein production. Cell pellets were harvested by centrifugation and stored at -80 °C until purification. TrxR1 proteins were purified as previously described [7]. Briefly, cell pellets were resuspended in 30 mL phosphate buffer (100 mM potassium phosphate, pH 7.2, 10% glycerol), supplemented with lysozyme (1 mg/mL), and disrupted by sonication with 70% amplification. After centrifugation at  $6250 \times g$  for 1 hour, clear cell lysates were purified by affinity chromatography using Ni<sup>2+</sup>-Nitrilotriacetic acid (NTA) resin (HisPur Ni-NTA Resin, PI88222, ThermoFisher Scientific, Mississauga, ON, Canada) as detailed before [7]. Purified TrxR1 proteins were kept in storage buffer containing 100 mM potassium phosphate pH 7.2 and 50% glycerol at -80 °C until use.

#### **4.2.3. TrxR1 *in vitro* Activity Assays.**

TrxR1 activity was monitored, as we did before [7], using 5,5-dithio-bis-(2-nitrobenzoic acid) (DTNB) to detect the level of reductive activity from TrxR1 and TAT-TrxR1. Active TrxR1 reduces DTNB to 2-nitro-5-thiobenzoate (TNB<sup>2-</sup>), which absorbs at wavelength 414 nm ( $A_{414}$ ). Each reaction mixture contained 50 nM or 100 nM TrxR1, 300 µM Nicotinamide adenine dinucleotide phosphate (NADPH) and 5 mM DTNB in buffer

containing 100 mM potassium phosphate, 1 mM Ethylenediaminetetraacetic acid (EDTA) pH 7.0. Protein concentration was assessed by the Bradford protein assay (Catalog #5000006; Bio-Rad) at 595 nm according to the manufacturer's instructions. Reactions were initiated in a 96 well micro-plate by the addition of DTNB to the reaction mixture containing TrxR1 (at 50 nM or 100 nM, as indicated) and NADPH in a final volume of 100  $\mu$ L. Measurements were taken in a Biotek Synergy H1 microplate reader every 1 minute for an 80 min time course. All assays were performed in triplicate using three independent enzyme reactions for each condition tested.

#### **4.2.4. Endogenous TrxR1 Activity in Live Cells and Fluorescence Microscopy.**

TrxR1 activity biosensor (TrxRFP1) was used to monitor the TrxR1 activity in live cells by measuring the changes in red fluorescence of the reporter [31]. The pcDNA3-TrxRFP1 was a kind gift from Huiwang Ai (Addgene plasmid # 98996). HEK 293T cells were cultured in Dulbecco's Modified Eagle Medium (Cellgro DMEM, ThermoFisher Scientific) containing 10% fetal bovine serum and 1% penicillin/streptomycin in 5% CO<sub>2</sub> at 37 °C. Equal numbers of HEK 293T cells were seeded onto a 6 well culture plates containing media and transfected with Lipofectamine 2000 (Invitrogen) and 2  $\mu$ g/mL plasmid DNA bearing the TrxRFP1 reporter according to manufacturer's instructions. In three biological and three technical replicates, un-transfected cells and transfected cells were monitored by fluorescent microscopy (excitation  $542 \pm 20$  nm, emission  $593 \pm 40$  nm) using an EVOS FL Cell Imaging System (ThermoFisher Scientific). At 24 hours after transfection, cell images were acquired every 1 min for a 60 min time course. At the 10 min time point, the TrxR1 inhibitor aurothioglucose (ATG) was added to the media at a concentration of 100  $\mu$ M.



#### **4.2.5. TAT-TrxR1 Delivery and Activity in Live Cells.**

HEK 293T cells were transfected with the plasmid bearing the TrxRFP1 reporter as above. At 24 hours after transfection, cells were incubated with no protein or with 0.5  $\mu\text{M}$  of TrxR1 or TAT-TrxR1 protein. Immediately before addition of the protein and at 30 mins and at 24 hours after incubation with protein or no protein, bright field and fluorescent (excitation  $542 \pm 20$  nm, emission  $593 \pm 40$  nm) cell images for each condition were acquired EVOS FL Cell Imaging System. Fluorescence intensities were analyzed by image J software and statistical analysis was based on 3 biological replicates with 3 technical replicates each using pairwise single factor analysis of variance (ANOVA).

#### **4.2.6. Western Blotting.**

HEK 293T cells were cultured in DMEM (Cellgro) media containing 10% fetal bovine serum and 1% penicillin/streptomycin in 5%  $\text{CO}_2$  at 37  $^\circ\text{C}$ . Equal number of cells were plated onto 6 well culture plates and incubated with buffer only or with 1  $\mu\text{M}$  TrxR1 or TAT-TrxR1 protein. After a 1-hour incubation, cells were washed with phosphate buffered saline (PBS) and cell pellets were collected by centrifugation. Cells were resuspended in lysis buffer containing (50 mM  $\text{Na}_2\text{HPO}_4$ , 1mM  $\text{Na}_4\text{P}_2\text{O}_7$ , 20 mM NaF, 2 mM EDTA, 2 mM ethylene glycol-bis( $\beta$ -aminoethyl ether)-N,N,N',N'-tetraacetic acid (EGTA), 1 mM dithiothreitol, 300  $\mu\text{M}$  phenylmethylsulfonyl fluoride (PMSF), and protease inhibitor tablet (Catalog number 04 693 159 001, Roche Canada, Mississauga, ON, Canada). Pellets were kept on ice for 10 minutes and vortexed every 2 minutes. Supernatant was collected from cells representing three biological replicates by centrifugation at  $15,000 \times g$  for 15 mins at 4  $^\circ\text{C}$ .

Protein concentration was measured by Bradford assay and extracted proteins were diluted to 5  $\mu\text{g}/\mu\text{L}$ , and 50  $\mu\text{g}$  of protein was separated using 10% sodium dodecyl sulfate-poly acrylamide gel electrophoresis (SDS-PAGE). The protein was transferred to a

polyvinylidene difluoride (PVDF) membrane using Turbo-Blot Turbo transfer system (Bio-Rad). The membrane was blocked in PBS with 0.1% (v/v) Tween 20 (PBST) and 5% (w/v) skim milk powder for 1 hour at room temperature. The membrane was immunoblotted with specific anti-TrxR1 (B-2) mouse monoclonal primary antibody (sc-28321, Santa Cruz Biotechnology, Santa Cruz, CA, USA) overnight at 4 °C followed by 3 × 10 minutes washes with agitation in PBST with 1% (w/v) skim milk powder. The membrane was then incubated in fluorescent secondary antibody (Goat-anti-mouse #AQ127, Sigma Aldrich, Oakville, Canada) for 1 hour at room temperature with agitation and washed 3 × 10 minutes in PBST. The membrane was stored in PBS for further analysis and bands were visualized using a LiCor (LiCor Biosciences, Lincoln, Nebraska USA) fluorescence imager (693 nm emission, 700 nm excitation). A glyceraldehyde 3-phosphate dehydrogenase (GAPDH) antibody (#ab8245, abcam, Toronto, Canada) and secondary fluorescent antibody (Goat-anti-mouse #AQ127, Sigma Aldrich, Oakville, Canada) were used to establish loading controls.

In identical and independent experiments, additional western blots were performed by chemiluminescence imaging with the His<sub>6</sub> and Vinculin antibodies. Briefly, the membrane was immunoblotted with specific mouse anti-His antibody (#H1029; Sigma, Oakville, Canada) overnight at 4 °C followed by 3 × 10 minutes washes with agitation in PBST with 1% (w/v) skim milk powder. The membrane was then incubated in sheep anti-mouse immunoglobulin G horseradish peroxidase linked antibody (#GENA931, GE Healthcare, Oakville, Canada) for 1 hour at room temperature with agitation and washed 3 × 10 minutes in PBST. The membrane was stored in PBS for further analysis and chemiluminescent signal detection was performed on a ChemiDoc MP system (BioRad). Mouse anti-vinculin antibody (#sc25336, Santa Cruz Biotechnology, Dallas, Texas, USA) and secondary antibody sheep anti-mouse immunoglobulin G horseradish peroxidase linked antibody (#GENA931 GE Healthcare, Oakville, Canada) were used to establish loading controls.

## 4.3. Results

### 4.3.1. Purification and Activity of TrxR1 and TAT-TrxR1 Variants.

In previous work [7, 19, 20], we developed a facile approach to produce human TrxR1 in *E. coli*. The method involves recombinant expression of the human TrxR1 gene with a bacterial SecIS derived from the *E. coli fdhF* gene was appended to the 3' UTR (Fig 4.1). As we have demonstrated using mass spectrometry (MS) [7, 20], elemental analysis with inductively coupled plasma mass spectrometry (ICP-MS) [7, 20], and biochemical activity [7, 19, 20], our method leads to a yield of ~2 mg/L *E. coli* culture of active TrxR1 with stoichiometrically incorporated Sec at the UGA550 codon [7, 19, 20]. We previously characterized the incorporation of Sec in recombinant TrxR1 using tandem MS/MS analysis to demonstrate Sec incorporation, and we also conducted ICP-MS, which demonstrated quantitative incorporation at a level of 98.5% Sec in the recombinant TrxR1 protein [20]. In independent work, we again provided tandem MS/MS analysis to demonstrate Sec incorporation in TrxR1, and we also performed matrix-assisted laser desorption/ionization (MALDI)-MS analysis to demonstrate Sec incorporation at UGA550 [7]. Finally, we again employed ICP-MS to demonstrate quantitative incorporation of Sec in the recombinant TrxR1 protein [7].

Here, we modified this original TrxR1 construct to include a TAT peptide at the N-terminus of the TrxR1 construct that produces a TAT-TrxR1 protein. Following purification, we confirm similar purity and yield of the TAT-TrxR1 protein compared to the wild-type (WT) TrxR1 enzyme (Fig 4.2A). We previously characterized recombinant TrxR1 activity using Ellman's reagent (5,5'-Disulfaneyldis(2-nitrobenzoic acid, DTNB), 9,10-phenanthroquinone, as well as an insulin linked Trx1 assay [7]. We found that recombinant TrxR1 showed similar and robust activity with each of these substrates [7]. Because of this fact and because reduction of DTNB is a straightforward assay for TrxR1 activity that is monitored at A<sub>414</sub> by the yellow color of the reduced form of DTNB (2-

nitro-5-thiobenzoate anion, TNB<sup>2-</sup>), we chose to characterize the TAT-TrxR1 activity using DTNB.

Thus, to compare the activity of the WT and TAT-tagged TrxR1 enzymes, we measured the DTNB reduction activity of TrxR1 and TAT-TrxR1 at 50 nM and 100 nM concentrations over a time course (Fig 4.2B). In comparing the initial velocity of the reactions at 50 nM or 100 nM TrxR1 or TAT-TrxR1 concentrations, we recorded no significant difference between the wild-type or TAT-tagged TrxR1 proteins (Fig 4.2C). The TAT-TrxR1 has activity that is robust and indistinguishable from the recombinant TrxR1 protein and because the activity of TrxR1 relies critically on Sec550 incorporation, we can confirm the TAT-TrxR1 protein contains the same level of Sec as in TrxR1, which we documented before using multiple mass spectrometry methods [7, 20]. Thus, the TAT-tag does not significantly affect that activity of the TrxR1 enzyme, and the TAT-tagged version of the protein will provide an appropriate model of TrxR1 activity that can be readily delivered to mammalian cells.

#### **4.3.2. Assessing the TrxRFP1 Reporter in Mammalian Cells.**

Before attempting to deliver the TrxR1 or TAT-TrxR1 proteins to mammalian cells, we characterized the response of a live-cell reporter for TrxR1 activity. The TrxRFP1 reporter was engineered and developed previously [31]. We obtained a plasmid that genetically encodes the TrxRFP1 reporter, which is a fusion protein of RFP with the natural substrate of TrxR1, Trx1. In TrxRFP1, Trx1 was fused to the N-terminal of an engineered RFP protein where native cysteine residues (Cys) were replaced in the protein and a new redox coupled pair of Cys residues was introduced near the N- and C-terminus of the RFP domain. Thus, following reduction of the Trx1 domain by TrxR1, the Trx1 moiety can then reduce the engineered Cys redox couple in the RFP domain and eliminate red fluorescence of RFP. Once expressed in mammalian cells, TrxRFP1 fluorescence is inversely correlated with TrxR1 activity. In the reduced form, the Trx1 domain of the reporter disrupts the

normal red fluorescence of the fused RFP, while in the oxidized form of Trx1 the red fluorescence of RFP is restored in proportion to the amount of oxidized Trx1. Because Trx1 is a selective substrate of TrxR1 [31], the system provides a specific and robust biosensor to monitor TrxR1 activity in live cells (Fig 4.3A).

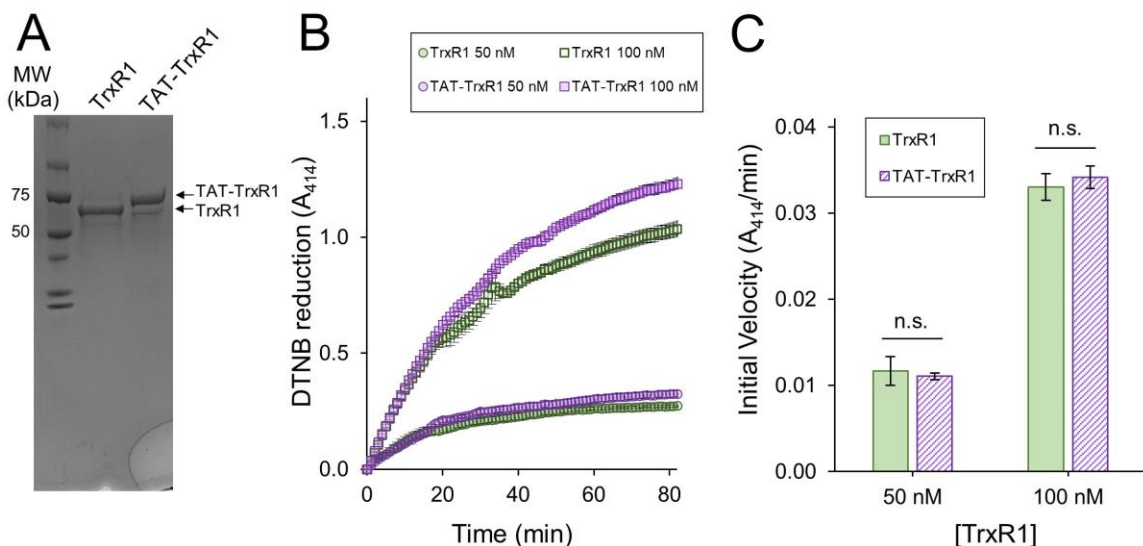


**Figure 4.2. Purity and biochemical activity of TrxR1 and TAT-TrxR1 variants.** The wild-type (WT) TrxR1 and TAT-tagged TrxR1 (TAT-TrxR1) were produced in *E. coli* according to our established approach [7, 19, 20] (Fig 4.1). Both the WT and TAT-TrxR1 variants were produced at high yield (~2 mg/L *E. coli* culture). We used the reduction of Ellman’s reagent (DTNB) monitored by absorbance at 414 nm ( $A_{414}$ ) to assay (B) the activity of the WT (green curves) or TAT-TrxR1 (purple curves) at a concentration of 50 nM or 100 nM enzyme. Based on linear regression to the linear phase of the enzyme reactions, we derived (C) the initial velocity ( $A_{414}/\text{min}$ ) of each reaction and determined that there was no significant different between WT TrxR1 and TAT-TrxR1 activity at 50 nM or 100 nM concentrations. Error bars represent 1 standard deviation of 3 independent enzyme reactions and statistical analysis was based on pairwise single factor ANOVA (n.s. – not significant).

To test the reporter in our hands, we transiently transfected the plasmid bearing TrxRFP1 into HEK 293T cells, and we used cells transfected without plasmid as a control. At 24 hours after transfection, we began monitoring red fluorescence in the control cells and in cells transfected with the TrxRFP1 plasmid. After 10 minutes, we then added the well-established TrxR1 inhibitor aurothioglucose (ATG) [33] to the media at a

concentration of 100  $\mu\text{M}$ . Using fluorescence microscopy, we observed a sharp increase in red fluorescence across 3 biological replicates, only in cells expressing the TrxRFP1 reporter (Fig 4.3B). The data demonstrate inhibition of endogenous TrxR1 in live HEK 293T cells, and in agreement with previous observations [31], confirm the proper function of the TrxRFP1 reporter.

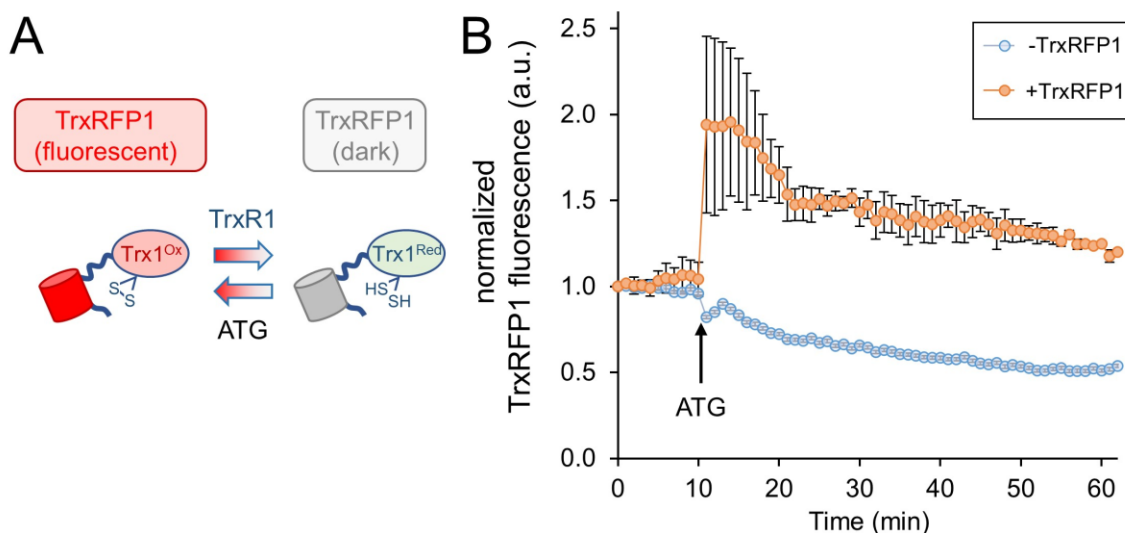


**Figure 4.3. Measurement of endogenous TrxR1 activity in live cells.** HEK 293T cells were transfected with a plasmid expressing a TrxR1 specific activity reporter. (A) The reporter (TrxRFP1) is a fusion of RFP with the TrxR1 substrate protein Trx1 [31]. In the oxidized state ( $\text{Trx1}^{\text{Ox}}$ ) the fused RFP (red cylinder) is fluorescent, while in the reduced state ( $\text{Trx1}^{\text{Red}}$ ) the RFP fluorescence (gray cylinder) is lost in proportion to the amount of TrxR1 activity. (B) The time course begins 24 hours after transfection and records TrxRFP1 fluorescence (excitation  $542 \pm 20$  nm, emission  $593 \pm 40$  nm) in HEK 293T cells transfected with (orange circles) or without (blue circles) the plasmid encoding TrxRFP1. Following application of TrxR1 inhibitor aurothioglucose (ATG) at 10 min after we began recording red fluorescence, cells with the TrxRFP1 reporter show a strong induction of red fluorescence that is proportional to the level of TrxR1 inhibition. Error bars represent  $\pm 1$  standard deviation of three biological replicates.

#### 4.3.3. Delivery of TAT-TrxR1 to Mammalian Cells.

As noted above, genetic approaches to over-express TrxR1 in mammalian cells can lead to substantial cytotoxicity due to the formation of SecTRAPs, and lipid-based protein transfection approaches with TrxR1 [15] or other proteins [34] are of limited efficiency. Furthermore, lipid-based transfection reagents also induce toxicity and immunogenic

reactions in mammalian cells [34], demonstrating the need for an improved approach to deliver active TrxR1 to cells.

In the absence of any transfection reagents, we incubated HEK 293T cells with buffer only, with WT TrxR1, or with TAT-tagged TrxR1. At 1 hour after incubation with the proteins, cells were washed to remove any extracellular protein and analyzed by western blotting with anti-TrxR1 and with anti-GAPDH as a loading control (Fig 4.4A). In the case of TAT-TrxR1, we observed a consistent level of successfully delivered TAT-TrxR1 to cells, as evident by the larger molecular weight of TAT-TrxR1 compared to the endogenous protein.

To confirm selective uptake of the TAT-TrxR1, we also performed western blotting of an identical and independent set of biological triplicate experiments using the anti-His<sub>6</sub> antibody and anti-Vinculin antibody as a loading control. As above, at 1 hour after incubation of HEK 293T cells with buffer only, with WT TrxR1, or with TAT-tagged TrxR1, cells were washed to remove any protein remaining outside of the cells. Both the TAT-TrxR1 and TrxR1 recombinant proteins contain the His<sub>6</sub> tag. We detected only the TAT-TrxR1 as successfully delivered to the interior of the cells (Fig 4.4B).

#### **4.3.4. TAT-tagged Dependent Uptake and Activity of TAT-TrxR1 in Live Cells.**

To determine if the successfully delivered TAT-TrxR1 was active in HEK 293T cells, we conducted a series of experiments using the TrxRFP1 reporter examined above. First, HEK 293T cells were transfected with the plasmid encoding the TrxRFP1 reporter. At 24 hours after transfection, cells were incubated with buffer only, with WT TrxR1, or with TAT-TrxR1. We then monitored the changes in red fluorescence of the TrxRFP1 reporter at 0 min, 30 min, and 24 hours after incubation with the TrxR1 protein variants or with no protein added. At each time point, both brightfield and fluorescent images of the cells were

captured and quantitated (Fig 4.5). As anticipated, in the case of the WT TrxR1 and the no protein control, we found no significant change in the TrxRFP1 fluorescence over the 24-hour time course. In contrast, only the cells incubated with TAT-TrxR1 showed significant and marked decreases in red fluorescence (Fig 4.5).

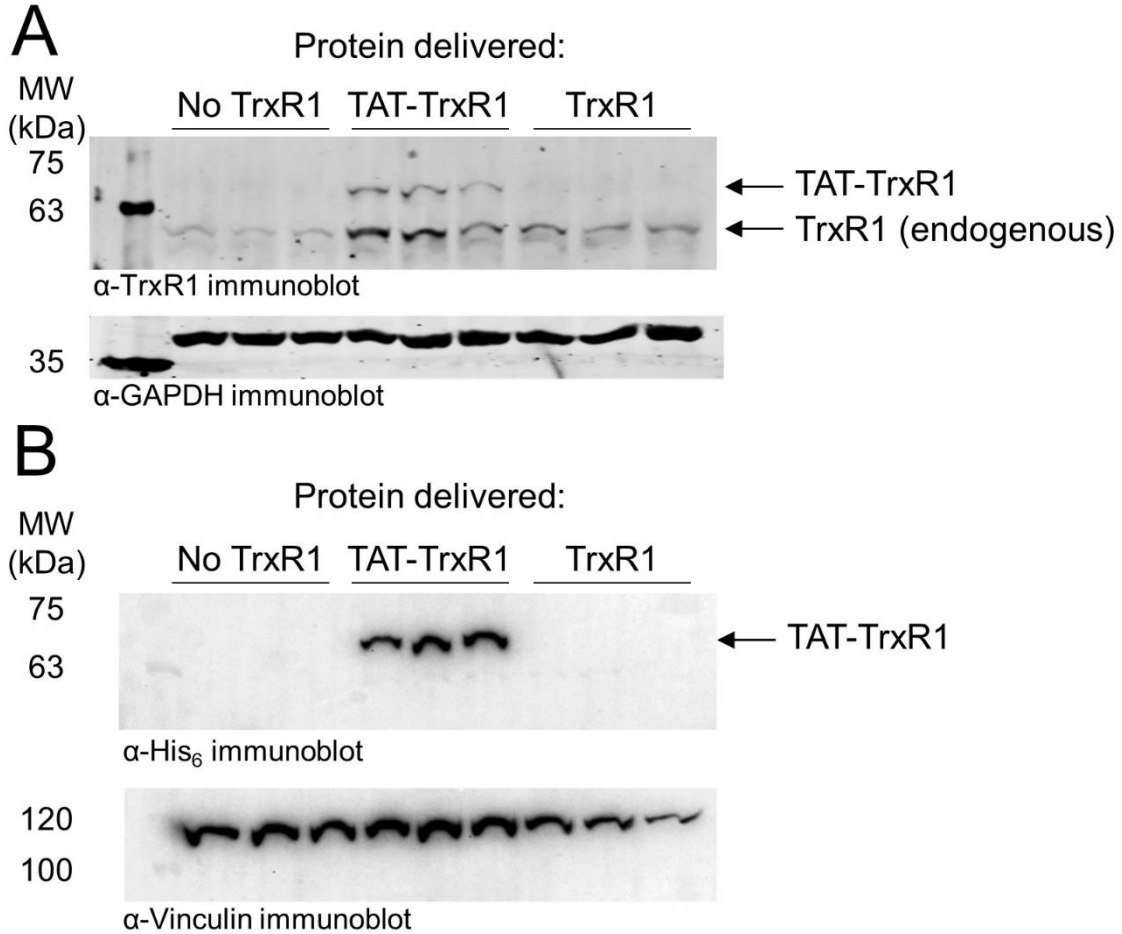


**Figure 4.4. Immunoblotting confirms delivery of TAT-TrxR1 to cells.** (A) Biological triplicates of HEK 293T cells were incubated for 1 hour with buffer only (No TrxR1), with TAT-tagged TrxR1 (TAT-TrxR1), or with TrxR1 lacking the TAT-tag (TrxR1). Following incubation, cells were washed to remove any protein remaining outside of the cells. The location of endogenous TrxR1 and TAT-tagged TrxR1 are indicated in a western blot with anti-TrxR1 antibody (above), and GAPDH was used as a loading control (below). (B) In an independent set of biological triplicates an identical experiment was performed; HEK 293T cell were incubated for 1 hour with buffer only (No TrxR1), with TAT-tagged TrxR1 (TAT-TrxR1), or with TrxR1 lacking the TAT-tag (TrxR1). Following washing of the cells, a western blot was performed with the anti-His<sub>6</sub> antibody as well as the anti-Vinculin antibody as a loading control. Both TAT-TrxR1 and TrxR1 protein contain the His<sub>6</sub> tag, yet only the TAT-TrxR1 protein was imported into the cells.



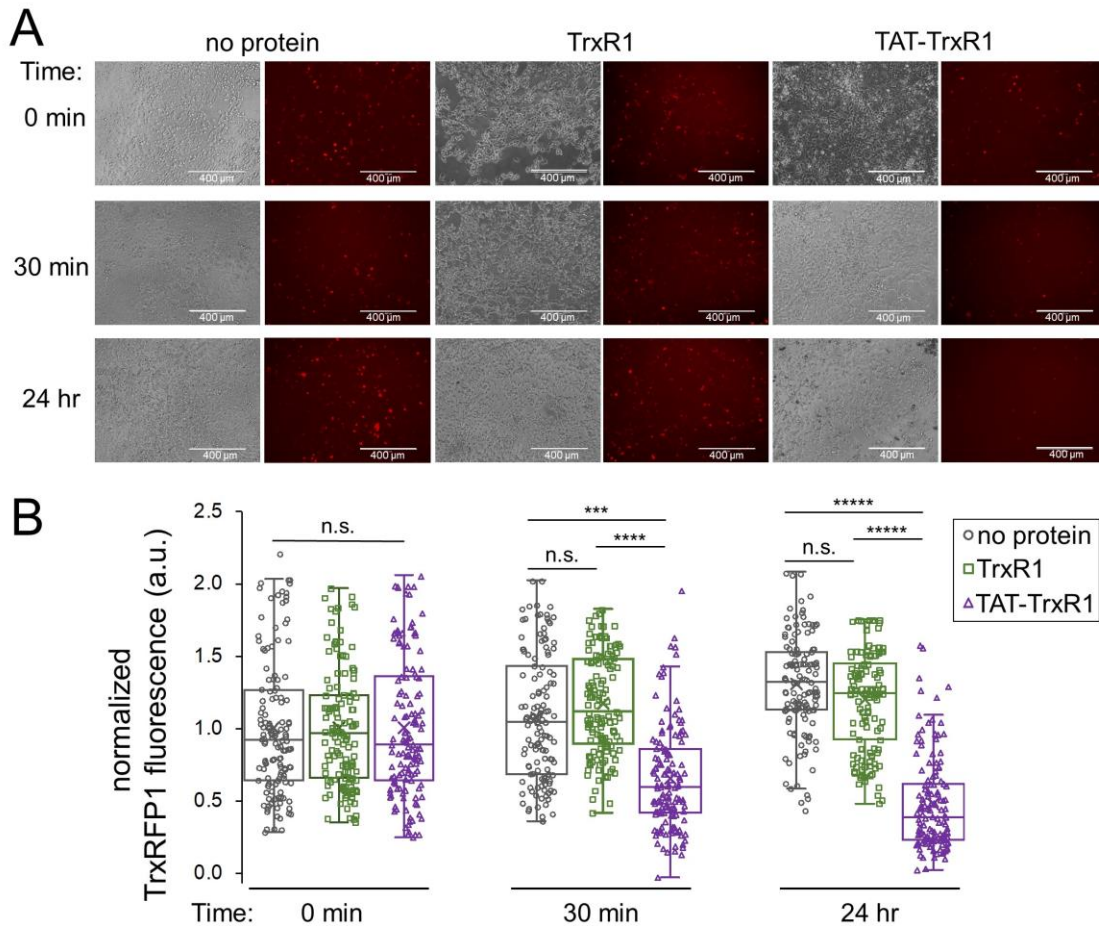


**Figure 4.5. TAT-dependent delivery of active TrxR1 to mammalian cells.** At 24 hours after transfection with a plasmid bearing the TrxRFP1 activity reporter, cells were incubated with buffer only (no protein), with WT TrxR1 lacking the TAT-tag (TrxR1), or with TAT-tagged TrxR1 (TAT-TrxR1). (A) Following addition of protein to the media, brightfield images of the cells and fluorescence images of the TrxRFP1 reporter (excitation  $542 \pm 20$  nm, emission  $593 \pm 40$  nm) were recorded before addition of protein (0 min), at 30 min after, and at 24 hours after, protein delivery. Decreasing red fluorescence demonstrates increased TrxR1 activity inside the cells. (B) At the 0 min time point, the average value of the fluorescence was normalized to 1.0 across each condition. Only the cells incubated with TAT-TrxR1 displayed a time dependent and statistically significant decrease in TrxRFP1 fluorescence during the time course. Data points taken from individual cells treated with no protein (gray circles), TrxR1 (green squares), or TAT-TrxR1 (purple triangles) are shown overlaid with box and whisker plots indicating the mean ( $\bar{x}$ ), median (line), range (bars), and lower and upper quartiles (boxed) of the data. Statistical analysis was based on 3 biological replicates and 3 technical replicates each and pairwise single factor ANOVA (n.s. – not significant; \*\*\*  $p < 0.005$ ; \*\*\*\*  $p < 0.0001$ ; \*\*\*\*\*  $p < 10^{-5}$ ).

These data agree precisely with our findings based on western blotting (Fig 4.4). Because only the TAT-TrxR1 was delivered successfully to the interior of the cells, only cells treated with TAT-TrxR1 and not those treated with WT TrxR1 showed a significant increase in TrxR1-specific activity. Thus, together the data demonstrate that only incubation with TAT-TrxR1 led to robust TrxR1-specific reduction activity inside the live human cells. The TAT-tag, therefore, represents a facile strategy to deliver active human TrxR1 selenoprotein to mammalian cells.

As a first demonstration of the TAT-tagging approach to delivery selenoprotein to human cells, we chose to work with HEK 293T cells. These cells are well established cell biological model systems that display robust growth and high transfection efficiencies [35]. This aspect was important since we relied on the TrxRFP1 live cell reporter to demonstrate the activity from the TAT-TrxR1 protein delivered to the human cells. Furthermore, since HEK 293T cells are derived from kidney cells, where endogenous TrxR1 is abundant and active (see Figs 4.3 and 4.4), these particular cells are also appropriate models systems to study TrxR1 biology [36], including in the context of chemotherapeutics where TrxR1 has been implicated as a major source of adverse effects of cisplatin compounds [37]. In the future, we will apply these approaches to other human and mammalian cell lines.

## **4.4. Discussion**

### **4.4.1. Genetic Code Expansion and Codon Reassignment.**

Genetic code expansion is a cornerstone application in synthetic biology that enables protein production with amino acid building blocks beyond the canonical 20 amino acids that are normally used to make proteins [38]. Here we used a genetic code expansion approach to incorporate the 21<sup>st</sup> amino acid, Sec, into a recombinant human protein produced in *E. coli*. The genetic code expansion method, which we established previously [7, 19, 20], involves expression of a synthetic gene construct where we fused SecIS from

the 3'UTR of an *E. coli* *fdhF* gene to a human TrxR1 gene that we codon optimized for *E. coli*. The resulting protein product is an active TrxR1 enzyme containing 21 different amino acids. As a novel extension of our approach, here we employed the CPP TAT-tag to enable our studies of the recombinant human TrxR1 enzyme in the homologous context of human cells without any engineering steps to otherwise modify the human cells themselves.

Genetic code expansion systems enable site-specific incorporation of non-canonical amino acids (ncAAs) into proteins to introduce 21 [20, 39, 40], 22 [7, 19, 41, 42], or recently, in a few cases, 23 different amino acids into proteins [43, 44]. These approaches, which normally require engineering a new tRNA synthetase and tRNA pair, are powerful in their ability to introduce new chemistry into proteins and functionalities that enable bio-orthogonal protein labeling [45]. Applications include creating new probes for protein function [46, 47] and protein structure [48] as well as protein and peptide pharmaceuticals to provide novel antibiotics [49], vaccines [50], and to treat major human diseases, including cancers [51] and auto-immune disorders [52].

Despite the success of genetic code expansion and its many applications in biology as well as studies of health and disease, the methods often involve re-assignment of a particular codon, normally one or more of the stop codons (UGA, UAA, and UAG), not only in a particular protein of interest but also in every instance of that codon throughout the proteome. Indeed, this situation leads to the extension of many natural proteins beyond their normal termination point [53]. When used in a cell free context [54], or simply in a production host to make proteins for downstream applications, this defect is of less importance. Genetic code expansion approaches, however, were also deployed in the very same cells that are the exact object of study. In one example, expanding the genetic code by reassigning the UAG codon to *N*<sub>ε</sub>-acetyl-lysine in mammalian cells to study the impact of a specific histone modification also caused transcriptome-wide changes in gene expression ranging from 2 to 100-fold [55]. Thus, the engineered cells were substantially

more affected by the codon reassignment than by the insertion of a specific acetylation into histone proteins. The combination of CPPs with genetic code expansion that we demonstrated here allowed engineering in one kind of cell and then subsequent delivery of a protein product of genetic code expansion into otherwise naïve mammalian cells, thus minimizing perturbations associated with expanding the genetic code.

#### **4.4.2. Delivery of ncAA-Containing Proteins with Cell Penetrating Peptides.**

Since genetic code expansion can have such a dramatic impact on the nature of the cell under investigation, we sought to devise a novel approach to deliver proteins containing ncAAs to mammalian cells, eliminating the need to engineer the mammalian cells themselves. CPPs represent a diverse and growing catalog of small peptides that have already demonstrated great utility in facilitating the delivery of proteins [27], mRNAs [28], and small molecules [29] to mammalian cells [30]. The TAT peptide is derived from the HIV TAT protein, which is essential for HIV replication [56]. A chemically synthesized 86 amino acid full-length TAT protein was rapidly taken up by HeLa cells, and the protein delivery activity was localized to the region including residues 37-72 of the synthetic TAT protein [57]. Shortly thereafter, this same region of the TAT protein was chemically cross-linked to several different larger proteins, including beta-galactosidase, horseradish peroxidase, RNase A, and domain III of Pseudomonas exotoxin A that were all shown to be rapidly delivered to several different mammalian cell types in culture [58].

Our work demonstrated a novel approach to deliver an active and full-length human selenoprotein to mammalian cells via fusion with a genetically encoded CPP for the first time. We found that the selenoprotein TAT-TrxR1 was efficiently delivered to cells and already displayed significant activity 30 minutes after incubation of the protein with HEK 293T cells. We found the TAT-TrxR1 continued to display robust and TrxR1-specific

reduction activity in the cells for at least 24 hours after protein delivery. To our knowledge, there are no other examples in the literature using cell penetrating peptides to deliver Sec-containing full-length proteins to mammalian cells. A recent study successfully engineered a Sec-containing small peptide, called PSELT (FQICVSUGYR), and demonstrated efficient delivery of the peptide to human neuroblastoma SH-SY5Y cells [59]. PSELT protected the cells against oxidative damage associated with Parkinson's disease, indicating an important avenue for therapeutic application of Sec-containing peptides.

Indeed, there is just one example of delivering ncAA-containing protein to mammalian cells using a CPP tag. The report demonstrated production of the murine dihydrofolate reductase (DHFR) in *E. coli* containing the ncAA *N*<sub>ε</sub>-propargyloxycarbonyl-lysine [60]. The authors then used click chemistry along with an azide-functionalized TAT peptide to chemically link the TAT-peptide to the DHFR protein, achieving a 90% yield. The DHFR protein was also chemically cyclized to help prevent degradation in HeLa cells. Although the engineered DHFR protein showed relatively efficient delivery to the cells at 1 hour after incubation with the protein, by the 2-hour time point most of the protein was degraded. In the case of the linear or non-cyclized TAT functionalized DHFR, nearly all of the protein was degraded after 2 hours [60]. Thus, our work demonstrates additional novelty in that the TAT-tag was genetically encoded in *E. coli* in the same protein as the ncAA Sec, and no downstream chemical synthetic steps were required. Our simpler approach also showed a longer lasting effect as we observed robust activity of the TAT-TrxR1 protein up to the 24-hour time point.

#### **4.4.3. A New System to Study TrxR1-Dependent Activity in Mammalian Cells.**

Our approach to engineering selenoproteins production in *E. coli* has allowed us to develop a new system to study TrxR1 redox biology in a homologous context of the mammalian

cell without engineering the mammalian cells. Our approach also requires no addition of costly and toxic transfection reagents. Previous work found that lipid-mediated transfection of TrxR1 was achieved but with limited efficiency [15]. Indeed, compared to standard protein transfection reagents, including lipofectamine derivatives, CPPs, including TAT are well tolerated in mammalian cells. While lipofectamine can strongly depress cell viability, induce apoptosis, and generate significant immune responses in human acute monocytic leukemia cells (THP-1), CPPs were found to be neither toxic nor immunogenic [34].

## 4.5. Conclusion

We demonstrated a simple and efficient approach to deliver the active human selenoprotein TrxR1 to mammalian cells. We showed that a genetically encoded TAT-tagged TrxR1 was produced in *E. coli* with similar efficiency and activity to an untagged TrxR1 in *E. coli* that we already demonstrated had stoichiometric incorporation of Sec550 by multiple methods [7, 19, 20]. The TAT-tag enabled rapid delivery of the active selenoprotein to mammalian cells that provided robust Trx1-specific reductive activity for at least 24 hours. Given the complex nature of selenoprotein synthesis in mammalian cells, our approach represents an important step forward to aid studies in the native and homologous context of mammalian cells of other human selenoproteins as well as ncAA-containing proteins produced in engineered cells with expanded genetic codes. Recent breakthroughs also enable site-specific incorporation of Sec at any location in a recombinant protein in *E. coli* [39, 61-64], thus indicating that our approach with CPPs can be applied to other selenoproteins and in combination with other genetic code expansion systems.

Finally, because TrxR1 is an important and validated drug target for cancers [3-5] and other human diseases, including Rheumatoid arthritis [65] and neurodegeneration [66], the system we developed here will not only be a valuable tool for studying TrxR1 biology in human cells, but also represents a novel platform to screen inhibitors of TrxR1. Since

TrxR1 inhibitors have already found application in clinical settings [67, 68], our approach will facilitate applications in developing the next generation of therapeutics to target TrxR1 activity in human diseases.

## **4.6. Conflict of Interest**

The authors declare that the research was conducted in the absence of any commercial or financial relationships that could be construed as a potential conflict of interest.

## **4.7. Author Contributions**

The authors are recognized for the following contributions: designed experiments (D.W., P.O.), performed experiments (D.W., T.S), analysed data (D.W., T.S., P.O), wrote the paper (T.S., I.H., P.O.), edited the paper (T.S., I.H., P.O.).

## **4.8. Funding**

This work was supported from the Natural Sciences and Engineering Research Council of Canada [04282 to P.O.; 04776 to I.U.H]; Canada Foundation for Innovation [229917 to P.O.]; the Ontario Research Fund [229917 to P.O.]; Canada Research Chairs [232341 to P.O.]; and the Canadian Institutes of Health Research [165985 to P.O.]; Ontario Ministry of Research and Innovation [ER-18-14-183 to I.U.H].

## **4.9. Acknowledgments**

We are grateful to Paul Walton for critical discussions and suggestions.

## 4.10. References

1. Mustacich, D. and G. Powis, *Thioredoxin reductase*. *Biochem J*, 2000. **346 Pt 1**: p. 1-8.
2. Ren, X., et al., *Redox Signaling Mediated by Thioredoxin and Glutathione Systems in the Central Nervous System*. *Antioxid Redox Signal*, 2017. **27**(13): p. 989-1010.
3. Arnér, E.S.J., *Targeting the Selenoprotein Thioredoxin Reductase 1 for Anticancer Therapy*. *Adv Cancer Res*, 2017. **136**: p. 139-151.
4. Hasan, A.A., et al., *The Thioredoxin System of Mammalian Cells and Its Modulators*. *Biomedicines*, 2022. **10**(7).
5. Busker, S., et al., *Irreversible TrxR1 inhibitors block STAT3 activity and induce cancer cell death*. *Sci Adv*, 2020. **6**(12): p. eaax7945.
6. Tamura, T. and T.C. Stadtman, *A new selenoprotein from human lung adenocarcinoma cells: purification, properties, and thioredoxin reductase activity*. *Proc Natl Acad Sci USA*, 1996. **93**(3): p. 1006-11.
7. Wright, D.E., et al., *Acetylation Regulates Thioredoxin Reductase Oligomerization and Activity*. *Antioxid Redox Signal*, 2018. **29**(4): p. 377-388.
8. Lee, S., S.M. Kim, and R.T. Lee, *Thioredoxin and thioredoxin target proteins: from molecular mechanisms to functional significance*. *Antioxid Redox Signal*, 2013. **18**(10): p. 1165-207.
9. Lundstrom-Ljung, J., et al., *Two resident ER-proteins, CaBP1 and CaBP2, with thioredoxin domains, are substrates for thioredoxin reductase: comparison with protein disulfide isomerase*. *FEBS Lett*, 1995. **357**(3): p. 305-8.
10. Zhong, L. and A. Holmgren, *Essential role of selenium in the catalytic activities of mammalian thioredoxin reductase revealed by characterization of recombinant enzymes with selenocysteine mutations*. *J Biol Chem*, 2000. **275**(24): p. 18121-8.
11. May, J.M., Z.C. Qu, and D.J. Nelson, *Uptake and reduction of alpha-lipoic acid by human erythrocytes*. *Clin Biochem*, 2007. **40**(15): p. 1135-42.
12. Kumar, S., M. Bjornstedt, and A. Holmgren, *Selenite is a substrate for calf thymus thioredoxin reductase and thioredoxin and elicits a large non-stoichiometric oxidation of NADPH in the presence of oxygen*. *Eur J Biochem*, 1992. **207**(2): p. 435-39.
13. Xia, L., et al., *The mammalian cytosolic selenoenzyme thioredoxin reductase reduces ubiquinone. A novel mechanism for defense against oxidative stress*. *J Biol Chem*, 2003. **278**(4): p. 2141-6.
14. Ma, X., et al., *Regulation of interferon and retinoic acid-induced cell death activation through thioredoxin reductase*. *J Biol Chem*, 2001. **276**(27): p. 24843-54.
15. Anestai, K. and E.S. Arnér, *Rapid induction of cell death by selenium-compromised thioredoxin reductase 1 but not by the fully active enzyme containing selenocysteine*. *J Biol Chem*, 2003. **278**(18): p. 15966-72.
16. Lu, X., et al., *[Construction and identification of a HEK293 cell line with stable TrxR1 overexpression]*. *Nan Fang Yi Ke Da Xue Xue Bao*, 2022. **42**(4): p. 554-560.



17. Anestalt, K., et al., *Cell death by SecTRAPs: thioredoxin reductase as a prooxidant killer of cells*. PLoS One, 2008. **3**(4): p. e1846.
18. Zhang, Y., et al., *Thioredoxin reductase 1 inhibitor shikonin promotes cell necroptosis via SecTRAPs generation and oxygen-coupled redox cycling*. Free Radic Biol Med, 2022. **180**: p. 52-62.
19. Wright, D.E., N. Panaseiko, and P. O'Donoghue, *Acetylated Thioredoxin Reductase 1 Resists Oxidative Inactivation*. Front Chem, 2021. **9**: p. 747236.
20. Brocker, M.J., et al., *Recoding the genetic code with selenocysteine*. Angew Chem Int Ed Engl, 2014. **53**(1): p. 319-23.
21. Han, K., et al., *Efficient intracellular delivery of GFP by homeodomains of Drosophila Fushi-tarazu and Engrailed proteins*. Mol Cells, 2000. **10**(6): p. 728-32.
22. Vives, E., et al., *TAT peptide internalization: seeking the mechanism of entry*. Curr Protein Pept Sci, 2003. **4**(2): p. 125-32.
23. Lichtenstein, M., et al., *TAT for Enzyme/Protein Delivery to Restore or Destroy Cell Activity in Human Diseases*. Life (Basel), 2021. **11**(9).
24. Brigati, C., et al., *HIV Tat, its TARgets and the control of viral gene expression*. FEMS Microbiol Lett, 2003. **220**(1): p. 57-65.
25. Kurnaeva, M.A., et al., *Tat basic domain: A "Swiss army knife" of HIV-1 Tat?* Rev Med Virol, 2019. **29**(2): p. e2031.
26. Ensoli, B., et al., *New insights into pathogenesis point to HIV-1 Tat as a key vaccine target*. Arch Virol, 2021. **166**(11): p. 2955-2974.
27. Kurrikoff, K., B. Vunk, and U. Langel, *Status update in the use of cell-penetrating peptides for the delivery of macromolecular therapeutics*. Expert Opin Biol Ther, 2021. **21**(3): p. 361-370.
28. Yokoo, H., M. Oba, and S. Uchida, *Cell-Penetrating Peptides: Emerging Tools for mRNA Delivery*. Pharmaceutics, 2021. **14**(1).
29. Tian, Y. and S. Zhou, *Advances in cell penetrating peptides and their functionalization of polymeric nanoplatforms for drug delivery*. Wiley Interdiscip Rev Nanomed Nanobiotechnol, 2021. **13**(2): p. e1668.
30. Shoari, A., et al., *Delivery of Various Cargos into Cancer Cells and Tissues via Cell-Penetrating Peptides: A Review of the Last Decade*. Pharmaceutics, 2021. **13**(9).
31. Fan, Y., et al., *Monitoring thioredoxin redox with a genetically encoded red fluorescent biosensor*. Nat Chem Biol, 2017. **13**(9): p. 1045-1052.
32. Nagahara, H., et al., *Transduction of full-length TAT fusion proteins into mammalian cells: TAT-p27Kip1 induces cell migration*. Nat Med, 1998. **4**(12): p. 1449-52.
33. Gromer, S., et al., *Human placenta thioredoxin reductase. Isolation of the selenoenzyme, steady state kinetics, and inhibition by therapeutic gold compounds*. J Biol Chem, 1998. **273**(32): p. 20096-101.
34. Suhorutsenko, J., et al., *Cell-penetrating peptides, PepFects, show no evidence of toxicity and immunogenicity in vitro and in vivo*. Bioconjug Chem, 2011. **22**(11): p. 2255-62.
35. Thomas, P. and T.G. Smart, *HEK293 cell line: a vehicle for the expression of recombinant proteins*. J Pharmacol Toxicol Methods, 2005. **51**(3): p. 187-200.

36. Zhu, J., et al., *Upregulation of Thioredoxin Reductase 1 Expression by Flavan-3-Ols Protects Human Kidney Proximal Tubular Cells from Hypoxia-Induced Cell Death*. *Antioxidants* (Basel), 2022. **11**(7).
37. Cheng, P., et al., *Inhibition of thioredoxin reductase 1 correlates with platinum-based chemotherapeutic induced tissue injury*. *Biochem Pharmacol*, 2020. **175**: p. 113873.
38. O'Donoghue, P., et al., *Upgrading protein synthesis for synthetic biology*. *Nat Chem Biol*, 2013. **9**(10): p. 594-8.
39. Haruna, K., et al., *Engineering the elongation factor Tu for efficient selenoprotein synthesis*. *Nucleic Acids Res*, 2014. **42**(15): p. 9976-83.
40. Bain, J.D., et al., *Ribosome-mediated incorporation of a non-standard amino acid into a peptide through expansion of the genetic code*. *Nature*, 1992. **356**(6369): p. 537-9.
41. Köhrer, C., et al., *A possible approach to site-specific insertion of two different unnatural amino acids into proteins in mammalian cells via nonsense suppression*. *Chem Biol*, 2003. **10**(11): p. 1095-102.
42. Venkat, S., et al., *Genetically Incorporating Two Distinct Post-translational Modifications into One Protein Simultaneously*. *ACS Synth Biol*, 2018. **7**(2): p. 689-695.
43. Dunkelmann, D.L., et al., *Engineered triply orthogonal pyrrolysyl-tRNA synthetase/tRNA pairs enable the genetic encoding of three distinct non-canonical amino acids*. *Nat Chem*, 2020. **12**(6): p. 535-544.
44. Tharp, J.M., et al., *Genetic Encoding of Three Distinct Noncanonical Amino Acids Using Reprogrammed Initiator and Nonsense Codons*. *ACS Chem Biol*, 2021. **16**(4): p. 766-774.
45. Ngo, J.T. and D.A. Tirrell, *Noncanonical amino acids in the interrogation of cellular protein synthesis*. *Acc Chem Res*, 2011. **44**(9): p. 677-85.
46. O'Donoghue, P., I.U. Heinemann, and C. Fan, *Editorial: Synthetic Nucleic Acids for Expanding Genetic Codes and Probing Living Cells*. *Front Bioeng Biotechnol*, 2021. **9**: p. 720534.
47. Courtney, T. and A. Deiters, *Recent advances in the optical control of protein function through genetic code expansion*. *Curr Opin Chem Biol*, 2018. **46**: p. 99-107.
48. Mihaila, T.S., et al., *Enhanced incorporation of subnanometer tags into cellular proteins for fluorescence nanoscopy via optimized genetic code expansion*. *Proc Natl Acad Sci USA*, 2022. **119**(29): p. e2201861119.
49. Vinogradov, A.A. and H. Suga, *Introduction to Thiopeptides: Biological Activity, Biosynthesis, and Strategies for Functional Reprogramming*. *Cell Chem Biol*, 2020. **27**(8): p. 1032-1051.
50. Si, L., et al., *Generation of influenza A viruses as live but replication-incompetent virus vaccines*. *Science*, 2016. **354**(6316): p. 1170-1173.
51. Huang, Y. and T. Liu, *Therapeutic applications of genetic code expansion*. *Synth Syst Biotechnol*, 2018. **3**(3): p. 150-158.
52. Gauba, V., et al., *Loss of CD4 T-cell-dependent tolerance to proteins with modified amino acids*. *Proc Natl Acad Sci USA*, 2011. **108**(31): p. 12821-6.

53. Heinemann, I.U., et al., *Enhanced phosphoserine insertion during Escherichia coli protein synthesis via partial UAG codon reassignment and release factor 1 deletion*. FEBS Lett, 2012. **586**(20): p. 3716-22.
54. Ranji Charna, A., et al., *An efficient cell-free protein synthesis platform for producing proteins with pyrrolysine-based noncanonical amino acids*. Biotechnol J, 2022: p. e2200096.
55. Elsasser, S.J., et al., *Genetic code expansion in stable cell lines enables encoded chromatin modification*. Nat Methods, 2016. **13**(2): p. 158-64.
56. Arya, S.K., et al., *Trans-activator gene of human T-lymphotropic virus type III (HTLV-III)*. Science, 1985. **229**(4708): p. 69-73.
57. Green, M. and P.M. Loewenstein, *Autonomous functional domains of chemically synthesized human immunodeficiency virus tat trans-activator protein*. Cell, 1988. **55**(6): p. 1179-88.
58. Fawell, S., et al., *Tat-mediated delivery of heterologous proteins into cells*. Proc Natl Acad Sci U S A, 1994. **91**(2): p. 664-8.
59. Alsharif, I., et al., *Cell-penetrating, antioxidant SELENOT mimetic protects dopaminergic neurons and ameliorates motor dysfunction in Parkinson's disease animal models*. Redox Biol, 2021. **40**: p. 101839.
60. Bi, X., et al., *Immobilization and Intracellular Delivery of Circular Proteins by Modifying a Genetically Incorporated Unnatural Amino Acid*. Bioconjug Chem, 2018. **29**(7): p. 2170-2175.
61. Welegedara, A.P., et al., *Site-Specific Incorporation of Selenocysteine by Genetic Encoding as a Photocaged Unnatural Amino Acid*. Bioconjug Chem, 2018. **29**(7): p. 2257-2264.
62. Liu, J., et al., *Site-Specific Incorporation of Selenocysteine Using an Expanded Genetic Code and Palladium-Mediated Chemical Deprotection*. J Am Chem Soc, 2018. **140**(28): p. 8807-8816.
63. Thyer, R., et al., *Custom selenoprotein production enabled by laboratory evolution of recoded bacterial strains*. Nat Biotechnol, 2018. **36**(7): p. 624-631.
64. Wang, Y., et al., *Site-Specific Selenocysteine Incorporation into Proteins by Genetic Engineering*. Chembiochem, 2021. **22**(20): p. 2918-2924.
65. Duan, D., et al., *Rheumatoid arthritis drug sinomenine induces apoptosis of cervical tumor cells by targeting thioredoxin reductase in vitro and in vivo*. Bioorg Chem, 2022. **122**: p. 105711.
66. Wang, H., et al., *Selenite Ameliorates Cadmium-induced Cytotoxicity Through Downregulation of ROS Levels and Upregulation of Selenoprotein Thioredoxin Reductase 1 in SH-SY5Y Cells*. Biol Trace Elem Res, 2022.
67. Sachweh, M.C., et al., *Redox effects and cytotoxic profiles of MJ25 and auranofin towards malignant melanoma cells*. Oncotarget, 2015. **6**(18): p. 16488-506.
68. Zhang, H., et al., *Ethaselen synergizes with oxaliplatin in tumor growth inhibition by inducing ROS production and inhibiting TrxR1 activity in gastric cancer*. J Exp Clin Cancer Res, 2021. **40**(1): p. 260.

## 4.11. Chapter 2 Appendix – Supplementary Data

### 4.11.1. DNA and Protein Sequences for TrxR1 Constructs.

#### Human His6-TrxR1 (*E. coli* codon optimized) DNA sequence in pET-TrxR1 vector

[1]

```
ATGGGCAGCAGCCATCACCATCATCACCACAGCCAGGATCCGAATTCGTCTCGCAAGACGGTCCG
TGCGCTGGAAGGCACCCTGTCCGAACTGGCTGCAGAAACGGACCTGCCGGTGGTATTTGTTAAAC
AGCGTAAAATCGGCGGCCACGGTCCGACTCTGAAAGCGTACCAGGAGGGTTCGTCTGCAGAAACTG
CTGAAAATGAACGGCCCCGGAAGATCTGCCGAAATCTTACGATTACGATCTGATCATCATCGGCGG
TGGTTCGGTGGCCTGGCAGCCGCAAAGGAGGCAGCACAGTATGGCAAAAAGTAATGGTACTGG
ACTTCGTTACCCCGACCCCACTGGGTACCCGTTGGGGCCTGGGTGGTACCTGCGTTAACGTAGGT
TGCATTCCGAAAAAAGTATGCACCAGGCTGCCCTGCTGGGCCAGGCTCTGCAGGACTCCCGTAA
CTACGGTTGGAAGTGAAGAAACGGTTAAACATGATTGGGACCGCATGATCGAGGCGGTTCAAA
ACCACATCGGTAGCCTGAACTGGGGCTACCGCGTTGCACTGCGCGAGAAAAAGTTGTATATGAA
AACCGGTACGGTCAGTTCATTGGCCCCGACCGTATCAAAGCGACTAACAACAAAGGCAAGGAAAA
AATTTACAGCGCAGAACGTTTCCCTGATCGCGACCGGCGAACGTCCGCGTTACCTGGGTATCCCGG
GCGATAAAGAATACTGTATCAGCTCCGATGACCTGTTTTCTCTGCCGTACTGCCCTGGCAAACT
CTGGTCGTGGGTGCATCCTACGTCGCTCTGGAGTGTGCAGGTTTCTGGCAGGTATTGGCCTGGA
CGTTACCGTTATGGTGCCTTCTATTTCTGCTGCGTGGTTTTCGACCAAGATATGGCGAACAAAATCG
GTGAACACATGGAAGAACACGGTATTAAATTCATCCGTCAGTTCGTTCCGATCAAAGTAGAACAG
ATTGAAGCCGGTACCCCGGGCCGTCTGCGTGTGGTAGCTCAGTCCACCAACAGCGAGGAAATTAT
CGAAGGCGAATACAACACTGTTATGCTGGCGATCGGTGCGGATGCTTGTACCCGTAAAATTGGCC
TGGAAACGGTAGGCGTTAAAATCAATGAAAAAACCGGTAATAATCCAGTAACCGACGAAGAACAG
ACCAACGTTCCGTATATCTATGCAATTGGTGATATCCTGGAGGATAAAGTTGAACTGACCCCTGT
TGCTATCCAGGCTGGCCGCTGCTGGCACAGCGTCTGTATGCCGGTAGCACCGTGAAGTGCGACT
ACGAAAACGTGCCGACCACGGTTTTCCACCCCTCTGGAATATGGCGCATGCGGTCTGTCTGAAGAG
AAAGCCGTAGAAAAATTCGGCGAAGAAAACATTGAAGTGTATCACTCTTATTTCTGGCCGCTGGA
ATGGACTATTCCGTCTCGTGACAACAACAATGCTACGCTAAAAATTATCTGCAACACGAAAGATA
ACGAACGTGTGGTTGGCTTCCACGTGCTGGGCCCGAATGCGGGTGAAGTGAAGTCAAGGTTTCGCG
GCTGCCCTGAAATGCGGCCTGACGAAAAAGCAGCTGGATTCTACCATCGGTATCCATCCGGTGTG
TGCTGAAGTTTTACCACTCTGTCTGTACCAAACGTAGCGGTGCGTCCATCCTGCAAGCAGGAT
GCTGAGGC TAA TAA ATCGGTTGCAGGTCTGCACCAATCG
```

TGA codon = Sec

TAA stop codon

*E. coli* fdhF SecIS

## Human His6-TrxR1 protein sequence

MGSSHHHHHSQDPNSSCEDGRALEGLSELAETDLPVVFVKQRKIGGHGPTLKAYQEGRLQKL  
LKMNGPEDLPKSYDYDLIIIGGGSGGLAAAKEAAQYGKKVMVLDVFTPTPLGTRWGLGGTCVNVG  
CIPKKLMHQAALLGQALQDSRNYGWKVEETVKHDWDRMIEAVQNHIGSLNWGYRVALREKKVVYE  
NAYGQFIGPHRIKATNNKGKEKIYSAERFLIATGERPRYLGI PGDKEYCISDDLFSLPYCPGKT  
LVVGASYVALECAGFLAGIGLDVTVMVRSILLRGFDQDMANKIGEHEEHGIKFI RQFVPIKVEQ  
IEAGTPGRLRVVAQSTNSEEIIEGEYNTVMLAIGRDACTRKIGLETVGVKINEKTGKI PVTDEEQ  
TNVPYIYAIGDILEDKVELTPVAIQAGRLLAQRLYAGSTVKCDYENVPTTVFTPLEYGACGLSEE  
KAVEKFGEENIEVYHSYFWPLEWTIPSRDNNKCYAKI ICNTKDNERVVGFHVLGPNAGEVTQGFA  
AALKCGLTKKQLDSTIGIHPVCAEVFTTLSVTKRSGASILQAGCUG

U = Sec residue

## Human His6-TAT-TrxR1 (*E. coli* codon optimized) DNA sequence in pTAT-HA

### vector [2]

ATGCGGGTTCTCATCATCATCATCATGGTATGGCTAGCATGACTGGTGGACAGCAAATGGG  
TCGGGATCTGTACGACGATGACGATAAGGATCGATGGGGATCCAAGCTTGGC **TACGGCCGCAAGA**  
**AACGCCGCCAGCGCCGCGC**GGTGGATCCACCATGTCGGCTATCCATATGACGTCCCAGACTAT  
GCTGGCTCCATGGCCTCCTGCGAAGACGGTTCGTGCGCTGGAAGGCACCCTGTCCGAACTGGCTGC  
AGAAACGGACCTGCCGGTGGTATTTGTTAAACAGCGTAAAATCGGGCGCCACGGTCCGACTCTGA  
AAGCGTACCAGGAGGGTTCGTCTGCAGAACTGCTGAAAATGAACGGCCCCGGAAGATCTGCCGAAA  
TCTTACGATTACGATCTGATCATCATCGGCGGTGGTTCTGGTGGCCTGGCAGCCGCAAAGGAGGC  
AGCACAGTATGGCAAAAAAGTAATGGTACTGGACTTCGTTACCCCGACCCCACTGGGTACCCGTT  
GGGGCCTGGGTGGTACCTGCGTTAACGTAGGTTGCATTCCGAAAAAACTGATGCACCAGGCTGCC  
CTGCTGGGCCAGGCTCTGCAGGACTCCCGTAACTACGGTTGGAAGTGAAGAAACGGTTAAACA  
TGATTGGGACCGCATGATCGAGGCGGTTCAAACCACATCGGTAGCCTGAACTGGGGCTACCCGC  
TTGCACTGCGCGAGAAAAAGTTGTATATGAAAACGCGTACGGTCAGTTCATTGGCCCGCACCGT  
ATCAAAGCGACTAACAACAAGGCAAGGAAAAAATTTACAGCGCAGAACGTTTCTGATCGCGAC  
CGGCGAACGTCCGCGTTACCTGGGTATCCCGGGCGATAAAGAATACTGTATCAGCTCCGATGACC  
TGTTTTCTCTGCCGTACTGCCCTGGCAAACTCTGGTTCGTGGGTGCATCCTACGTCGCTCTGGAG  
TGTGCAGTTTTCTGGCAGGTATTGGCCTGGACGTTACCGTTATGGTGCCTTCTATTCTGCTGCG  
TGGTTTTCGACCAAGATATGGCGAACAAAATCGGTGAACACATGGAAGAACACGGTATTAATTTCA  
TCCGTCAGTTTCGTTCCGATCAAAGTAGAACAGATTGAAGCCGGTACCCCGGGCCGTCTGCGTGTG  
GTAGCTCAGTCCACCAACAGCGAGGAAATTATCGAAGGCGAATACAACACTGTTATGCTGGCGAT  
CGGTCGCGATGCTTGTACCCGTAATAATTGGCCTGGAAACGGTAGGCGTTAAATCAATGAAAAAA  
CCGGTAAATTTCCAGTAACCGACGAAGAACAGACCAACGTTCCGTATATCTATGCAATTGGTGTAT  
ATCCTGGAGGATAAAGTTGAACTGACCCCTGTTGCTATCCAGGCTGGCCGCCTGCTGGCACAGCG  
TCTGTATGCCGGTAGCACCGTGAAGTGGGACTACGAAAACGTGCCGACCACGGTTTTACCCCTC  
TGGAATATGGCGCATGCGGTCTGTCTGAAGAGAAAAGCCGTAGAAAAATTCGGCGAAGAAAACATT  
GAAGTGTATCACTCTTATTTCTGGCCGCTGGAATGGACTATTCCGTCTCGTGACAACAACAATG  
CTACGCTAAAATTATCTGCAACACGAAAGATAACGAACGTGTGGTTGGCTTCCACGTGCTGGGCC  
CGAATGCGGGTGAAGTGACTCAAGTTTTCGCGGCTGCCCTGAAATGCGGCCTGACGAAAAAGCAG  
CTGGATTCTACCATCGGTATCCATCCGGTGTGTGCTGAAGTTTTACCACTCTGTCTGTCACCAA  
ACGTAGCGGTGCGTCCATCCTGCAAGCAGGATGC **TGAGGC** **TAA**TA **ATCGGTTGCAGGTCTGCACC**  
**AATCG**

TAT DNA sequence

TGA codon = Sec

TAA stop codon

*E. coli* fdhF **SecIS**

## Human His6-TAT-TrxR1 protein sequence

MRGSHHHHHGMASMTGGQQMGRDLYDDDDKDRWGSKLG~~YGRKKRRQRRR~~GGSTMSGYPYDVDPDY  
AGSMASCEDGRALEGLSELAAETDLPVVFVKQRKIGGHGPTLKAYQEGRLQKLLKMNGPEDLPK  
SYDYDLIIIGGGSGGLAAAKEAAQYGKKVMVLDFVTPPLGTRWGLGGTCVNVGCI PKKLMHQAA  
LLGQALQDSRNYGWKVEETVKHDWDRMIEAVQNHIGSLNWGYRVALREKKVVYENAYGQFIGPHR  
IKATNNKGKEKIYSAERFLIATGERPRYLGI PGDKEYCISDDLFSLPYCPGKTLVVGASYVALE  
CAGFLAGIGLDVTVMVRSILLRQFDQDMANKIGEHMEEHGIKFI RQFVPIKVEQIEAGTPGRLRV  
VAQSTNSEEIIIEGEYNTVMLAIGRDACTRKIGLETVGVKINEKTGKI PVTDEEQTNVPYIYAIGD  
ILEDKVELTPVAIQAGRLLAQRLYAGSTVKCDYENVPTTVFTPLEYGACGLSEEKAVEKFGEENI  
EYVHSYFWPLEWTIPSRDNNKCYAKI ICNTKDNERVVG FHVLPNAGEVTQGF AAALKCGLTKKQ  
LDSTIGIHPVCAEVFTTLSVTKRSGASILQAGCUG

U = Sec residue

TAT peptide

#### 4.11.2. Appendix References

1. Wright, D.E., et al., *Acetylation Regulates Thioredoxin Reductase Oligomerization and Activity*. *Antioxid Redox Signal*, 2018. **29**(4): p. 377-388.
2. Nagahara, H., et al., *Transduction of full-length TAT fusion proteins into mammalian cells: TAT-p27Kip1 induces cell migration*. *Nat Med*, 1998. **4**(12): p. 1449-52.



# Curriculum Vitae

## David Ernest Wright

### Post-Secondary Education

University of Western Ontario 2016 - Present  
London, Ontario, Canada  
PhD Candidate – Biochemistry  
Supervisor: Dr. P. O'Donoghue

University of Western Ontario 2012 - 2016  
London, Ontario, Canada  
Honors Bachelor of Sciences (BSc)  
Honors Specialization: Genetics and Biochemistry

### Awards and Honors

NSERC Post Graduate Scholarship – Doctoral (2019)  
Ontario Graduate Scholarship (2019) (Awarded, but not accepted)  
Ontario Graduate Scholarship (2018)  
Ontario Graduate Scholarship (2016)  
UWO in-Course Scholarships Year IV (2015)  
Dean's Honor List (2015)  
Dean's Honor List (2014)  
Dean's Honor List (2013)  
Dean's Honor list (2012)  
The Western Scholarship of Excellence (2012)

### Related Work Experience

Teaching Assistant  
Biochemistry 2280  
University of Western Ontario  
2018

## Mentoring

Nikolaus Panaseiko, Undergraduate Student, Sept 2020 – April 2021

Jasmine Fuentes, Highschool co-op student, Feb 2018 – May 2018

Katherine Deanna Van Belois, Undergraduate Student, May 2018 – Dec 2018

Sabrina Wang, Highschool co-op student, May 2017 – Aug 2017

Stephanie Anagnostou, Undergraduate Student, Sept 2016 – April 2017

## Publications

**Wright, D.E.**, Siddika, T., Heinemann, I. U., and O'Donoghue, P. *Delivery of the selenoprotein thioredoxin reductase 1 to mammalian cells*. *Front Mol Biosci*, 2022. **9**: p. 1031756.

Rozik, P., Szabla, R., Lant, J. T., Kiri, R., **Wright, D. E.**, Junop, M., and O'Donoghue, P., *A novel fluorescent reporter sensitive to serine misincorporation*. *RNA Biol*, 2022. **19**(1): p. 221-233.

**Wright, D.E.**, N. Panaseiko, and P. O'Donoghue, *Acetylated Thioredoxin Reductase 1 Resists Oxidative Inactivation*. *Front Chem*, 2021. **9**: p. 747236.

**Wright, D.E.** and P. O'Donoghue, *The Molecular Architecture of Unnatural Amino Acid Translation Systems*. *Structure*, 2019. **27**(8): p. 1192-1194.

**Wright, D.E.**, Altaany Z., Bi Y., Alperstein Z., and O'Donoghue P., *Acetylation Regulates Thioredoxin Reductase Oligomerization and Activity*. *Antioxid Redox Signal*, 2018. **29**(4): p. 377-388.

## **Presentations**

**Wright, D.E.** (2019). Genetic Code Expansion: Acetylation Regulates TrxR1 Activity. Fall Graduate Student symposium. London, Ontario, Canada. (Poster Presentation)

**Wright, D.E.** (2019). Genetic Code Expansion: Acetylation Regulates TrxR1 Activity. Synthetic Biology Symposium 4.0. Waterloo, Ontario, Canada. (Oral Presentation)

**Wright, D.E.** (2019). Acetylation Regulates TrxR1 activity. London Health Research Day. London, Ontario, Canada. (Poster Presentation)

**Wright, D.E.** (2018). Acetylation Regulates TrxR1 activity. Fall Graduate student symposium. London, Ontario, Canada. (Poster Presentation)

**Wright, D.E.** (2018). Acetylation Regulates TrxR1 activity. London Health Research Day. London, Ontario, Canada. (Poster Presentation)

**Wright, D.E.** (2018). Acetylation Regulates TrxR1 Activity. Synthetic Biology Symposium 3.0. London, Ontario, Canada. Poster Presentation.

**Wright, D.E.,** Altaany Z., Bi Y., Alperstein Z., and O'Donoghue P. (2017). Regulation of TrxR1 by Acetylation. International Selenium Conference, Se2017. Stockholm, Sweden. (Poster Presentation).

**Wright, D.E.** (2017). Acetylation Regulates TrxR1 Activity. Synthetic Biology Symposium 2.0. London, Ontario, Canada. (Poster Presentation)

**Wright, D.E.** (2016). Acetylation Regulates TrxR1 activity. Fall Graduate student symposium (2016). London, Ontario, Canada. (Poster Presentation)

**Wright, D.E.** (2015). Recoding the Genetic Code. Fall Graduate student symposium. London, Ontario, Canada. (Poster Presentation)